ANL/CT–76–2

Final Report
DEVELOPMENT OF SELF-ACTUATED SHUTDOWN SYSTEMS FOR LMFBR PLANTS

(ANL Work Project 3194)

by

J. Josephson (Proj. Coord.), P. R. Huebotter, E. S. Sowa, J. B. van Erp, P. A. Pizzica, W. P. Barthold, R. B. Turski, J. F. Schumar, E. D. Parr, and D. Eggen

Any holder of this d ny further distribution to third foreign governments, foreig or foreign divisions of U.S. companies, ctor, Division of Reactor Developme gy Commission.

NO ACCESS RESTRICTIONS

This document is not considered OUO-Applied Technology. It was reviewed for Export Controlled Information and found to be suitable for unlimited access and reproduction.

This label reflects Applied Technology instructions issued April 13, 2006, by the the Department of Energy Office of Nuclear Energy. Additional guidance has also been provided by DOE in 2016 and 2018 memos, as well as from NNSA.

Paul Betten, ANL — 4/24/2019 Date

MASTER

From the
ARGONNE NATIONAL LABORATORY
9700 S. Cass Avenue
Argonne, Illinois 60439

[redacted]

August 1975

DISCLAIMER

This report was prepared as an account of work sponsored by an agency of the United States Government. Neither the United States Government nor any agency Thereof, nor any of their employees, makes any warranty, express or implied, or assumes any legal liability or responsibility for the accuracy, completeness, or usefulness of any information, apparatus, product, or process disclosed, or represents that its use would not infringe privately owned rights. Reference herein to any specific commercial product, process, or service by trade name, trademark, manufacturer, or otherwise does not necessarily constitute or imply its endorsement, recommendation, or favoring by the United States Government or any agency thereof. The views and opinions of authors expressed herein do not necessarily state or reflect those of the United States Government or any agency thereof.

DISCLAIMER

Portions of this document may be illegible in electronic image products. Images are produced from the best available original document.

The facilities of Argonne National Laboratory are owned by the United States Government. Under the terms of a contract (W-31-109-Eng-38) between the U. S. Energy Research and Development Administration, Argonne Universities Association and The University of Chicago, the University employs the staff and operates the Laboratory in accordance with policies and programs formulated, approved and reviewed by the Association.

MEMBERS OF ARGONNE UNIVERSITIES ASSOCIATION

The University of Arizona
Carnegie-Mellon University
Case Western Reserve University
The University of Chicago
University of Cincinnati
Illinois Institute of Technology
University of Illinois
Indiana University
Iowa State University
The University of Iowa
Kansas State University
The University of Kansas
Loyola University
Marquette University
Michigan State University
The University of Michigan
University of Minnesota
University of Missouri
Northwestern University
University of Notre Dame
The Ohio State University
Ohio University
The Pennsylvania State University
Purdue University
Saint Louis University
Southern Illinois University
The University of Texas at Austin
Washington University
Wayne State University
The University of Wisconsin

NOTICE

This report was prepared as an account of work sponsored by the United States Government. Neither the United States nor the United States Energy Research and Development Administration, nor any of their employees, nor any of their contractors, subcontractors, or their employees, makes any warranty, express or implied, or assumes any legal liability or responsibility for the accuracy, completeness or usefulness of any information, apparatus, product or process disclosed, or represents that its use would not infringe privately-owned rights. Mention of commercial products, their manufacturers, or their suppliers in this publication does not imply or connote approval or disapproval of the product by Argonne National Laboratory or the U. S. Energy Research and Development Administration.

ANL/CT-76-2

Final Report

DEVELOPMENT OF SELF-ACTUATED SHUTDOWN SYSTEMS FOR LMFBR PLANTS

(ANL WORK PROJECT 3194)

by

J. Josephson (Proj. Coord.), P. R. Huebotter, E. S. Sowa, J. B. van Erp, P. A. Pizzica, W. P. Barthold, R. B. Turski, J. F. Schumar, E. D. Parr, and D. Eggen

NOTICE

This report was prepared as an account of work sponsored by the United States Government. Neither the United States nor the United States Energy Research and Development Administration, nor any of their employees, nor any of their contractors, subcontractors, or their employees, makes any warranty, express or implied, or assumes any legal liability or responsibility for the accuracy, completeness or usefulness of any information, apparatus, product or process disclosed, or represents that its use would not infringe privately owned rights

Argonne National Laboratory

9700 S. Cass Avenue

Argonne, Illinois 60439

August 1975

[redacted]

TABLE OF CONTENTS

	Page
NOMENCLATURE	1
ABSTRACT	2
I. INTRODUCTION	3
II. BACKGROUND	5
III. MAGNETIC HOLD SELF-ACTUATED SHUTDOWN SYSTEM	7
A. Selection of Conceptual Design	7
B. Design Requirements	11
1. Introduction	11
2. Functional Requirements	12
3. Desirable Design Requirements	13
C. Description of Magnetic Hold Conceptual Design Variations	15
1. Six Face Horizontal Hold Design	17
2. Two Face Horizontal Hold Design	21
3. Snap Ring Vertical Hold Design	23
4. Movable Cam Vertical Hold Design	25
5. Comparison of Magnetic Hold Conceptual Design Characteristics	26
D. Results of Analysis of Conceptual Design	29
1. Magnetic Analysis	29
2. Thermal-Hydraulic Analysis	33
IV. SASS TEST RIG AND EXPERIMENTAL PROGRAM	36
A. Purpose of Tests	36
B. Basis for Experimental Procedure and Design of Test Assembly	36
1. Radial Vane Design	36
2. Basic Requirements for Tests	37
3. Analysis of Heating Time for the Radial Vane Design	41
C. Description of Test Apparatus and Operation	41
D. Instrumentation	44
E. Experimental Plan	45

TABLE OF CONTENTS

		Page
	F. Discussion of Test Results	46
	1. Bench Test Breakaway Force Measurement	46
	2. Modification of Test Assembly	46
	3. Measurement of Breakaway Force in Test Rig	47
	4. Immersion Tests in High Temperature Sodium	48
	5. Conclusions and Recommendations	49
V.	ACCIDENT ANALYSIS IN SUPPORT OF SASS DESIGN	51
	A. Description of Accident Analyses	51
	B. Results and Conclusions	51
VI.	REACTOR PHYSICS ANALYSIS OF SASS	67
	A. ISA and CRBR Control Assembly Absorber Worths	67
	B. Impact of SASS on Core Performance	72
	C. Alnico Magnet Heating Rate	73
	D. Fissile Source Heating Rate	75
	E. Results and Conclusions	75
VII.	MATERIALS ASPECTS OF SASS DESIGN	80
	A. Radiation and Temperature	80
	B. Corrosion and Erosion	81
	C. Self-Welding and Pickup of Debris on Magnet	82
	D. Cladding of Magnetic Materials	83
	E. Fissile Source Materials	83
	F. Structural Properties of Materials	84
	1. Alnico	84
	2. Low Carbon Steel	84
	3. High Nickel Alloys	85
	G. Stability of Materials	85
	1. Alnico	85
	2. Low Carbon Steel and Nickel-Iron Alloys	85
	H. Recommendations	86

TABLE OF CONTENTS

	Page
VIII. CONCLUSIONS AND RECOMMENDATIONS	87
ACKNOWLEDGMENT	89
APPENDICES	
I. Magnetic Circuit Analysis	90
II. Thermal-Hydraulic Analysis	120
III. Reactor Physics Analysis	154
IV. Preliminary System Design Description (SDD) of a Self-Actuated Shutdown (SASS) for Use in LMFBRs	164
REFERENCES	181

LIST OF FIGURES

No.		Page
1.	Conceptual Design of Curie Temperature Magnetic Holding Device	10
2.	Six-Face Horizontal Hold SASS Conceptual Design	18
3.	Two-Face Horizontal Hold SASS Conceptual Design	22
4.	Snap Ring Vertical Hold SASS Conceptual Design	24
5.	Movable Cam Vertical Hold SASS Conceptual Design	27
6.	Cross-Section of Magnet and Yoke Used in Experimental Rig	38
7.	Magnet Assembly Detached from Yokes	39
8.	Magnet Assembly	40
9.	Calculated Temperature Response of Yoke After Sodium Immersion	42
10.	Sketch of SASS Test Fixture	43
11 - 21.	Accident Analysis Computer Runs	56 - 66
22.	Specific ISA Worth versus B-10 Mass per Assembly	69
23.	ISA Worth versus B-10 Mass per Assembly	70
24.	Possible ISA Positions in Core	71
25.	Axial Blanket Flux Depressions Due to ISA	74
26.	Fissile Source (UO_2) Heating Rate vs Axial Position in Core and Enrichment	76
27.	Fissile Source Radial Adjustment Factor	77
28.	Optimum Placement of ISAs in CRBR	78
I-1.	Equivalent Magnetic Circuit - Curie Point Holding Device	94
I-2.	Temperature Dependence of Magnetization (M_s/M_o) and Holding Power (F/F_o) Below the Curie Temperature, T_c	97
I-3.	Permeability of Low Carbon Steel at Room Temperature	98
I-4.	Equivalent Magnetic Circuit Diagram	103
I-5.	Demagnetization Curve and Hysteresis Loop of a Permanent Magnet Material	104

LIST OF FIGURES

No.		Page
I-6.	Alnico V Demagnetization Curve	105
I-7.	Steel Demagnetization Curves	108
I-8.	Temperature Response in Carbon Steel at Parting Plane to Increase in Sodium Temperature	114
II-1.	Six-Face Horizontal Hold SASS Conceptual Design Showing Elevations for Hydraulic Analysis Calculations	125
II-2.	One-Twelfth Segment of Fuel Channel of ISA	134
II-3.	Nodal Mockup of Magnet Assembly	139
II-4.	Response of ISA to Exponential Flux Rise	146
II-5.	Split Magnet Cooling Arrangement for Holding Magnet	150
III-1.	CRBR Model	157
III-2.	CRBR Cross-Section	158
III-3.	CRBR Control Assembly Positions	160

LIST OF TABLES

No.		Page
1.	Comparison of Magnetic Hold Conceptual Designs	28
2.	List of Accident Analyses Performed	52
3.	Results of Accident Analyses - Maximum Fuel Centerline and Coolant Temperature	53
4.	Results of Accident Analyses - Limits to Avoid Fuel Centerline Melting	53
5.	Results of Accident Analysis - Limits to Avoid Coolant Boiling	58
6.	Results of Accident Analyses - Limits to Avoid Coolant Temperature > 750°C	58
7.	Results of Accident Analyses - Limits to Avoid Coolant Temperature > 800°C	63
8.	ISA Worths versus Position in Core	68
I-1.	Properties of Alnico V	107
I-2.	Flux and Holding Force Response to Step in Sodium Temperature from 1000°F to 1500°F	118
II-1.	Summary of Geometric Parameters	137
II-2.	Three-Node Model Steady-State Temperatures	142
II-3.	Temperature Rise in Magnet Due to Internal Heating	152
III-1.	Summary of CRBR Heavy Metal Masses	156
III-2.	CRBR Control Rod B-10 Masses Per Assembly	159
III-3.	CRBR Control Rod Worths	161

NOMENCLATURE

See NOMENCLATURE in Appendices I and II.

ABSTRACT

The further development during FY 1975 of the Self-Actuated Shutdown System (SASS) for LMFBR plants carried out at ANL is presented in this report.

A ferromagnetic Curie temperature permanent magnet holding device has been selected as the basis for the design of the Inherent Shutdown Assembly (ISA) of the SASS. The self-actuated self-contained device operates such that accident conditions, resulting in increased coolant temperature or neutron flux reduce the magnetic holding force by raising the temperature of the trigger mechanism above the Curie point. Boron carbide absorber is then inserted into the core, under gravity, terminating the accident.

Several possible designs of the selected concept are presented. All of the proposed designs derive the magnetic holding force from an Alnico V permanent magnet which drives the magnetic holding flux through the parting plane of a carbon steel magnetic circuit.

Magnetic and thermal-hydraulic analyses have been performed which show the feasibility of the concept with respect to response time, holding force, and coolability.

ISA absorber worths have been estimated in the physics analysis. These have been shown to be sufficient to protect against severe reactor transients such as loss of flow and fast reactivity excursions in an accident analysis. The presence of the absorber material in the upper axial blanket region of a CRBR type core has been shown to have a minimal impact upon core performance. Fissile source and radiation induced heat generation calculations were also carried out in the physics analysis.

An experimental program has also been performed which has demonstrated proof of principle of the selected Curie point magnetic hold device. As part of this program, experiments were carried out in air and in static sodium.

Several of the materials aspects of the SASS design have been examined and discussed particularly with respect to the possible problem areas.

I. INTRODUCTION

The purpose of this report is to present a summary of the progress made during FY 1975 in the development of a "Self-Actuated Shutdown System (SASS)" for LMFBR plants.

The work carried out in this effort utilized discretionary Argonne National Laboratory funding provided by the Associate Laboratory Director for Engineering Research and Development. During FY 1975 this project, designated Work Project 3194, was active from September 1, 1975 to June 30, 1975.

The effort was initiated in January, 1974, with the intention of obtaining support for the Development of Self-Actuated Shutdown Systems (SASS) for LMFBR Plants from the U.S. Atomic Energy Commission, Division of Reactor Research and Development. A proposal with this title was issued to the USAEC in April 1974.[1] The other major document preceding this final report for FY 1975, was a FY 1974 final report for effort funded under ANL Work Project 3134.[2]

Although efforts to obtain direct AEC funding for SASS development were unsuccessful, ANL management felt that the SASS concept was promising and that the work should be continued through FY 1975. However, the funding was at a much lower level than originally proposed.

The SASS development was continued through FY 1975 as a multi-divisional project as it has been since its inception. This enabled bringing into play the diverse, in-depth technical skills available at ANL which are required for a project of this scope.

The divisions of ANL involved in the project, and the contributors to this final report are listed below:

J. Josephson (Project Coordinator)	Components Technology
P. R. Huebotter	Components Technology
E. S. Sowa	Reactor Analysis & Safety
J. B. van Erp	Reactor Analysis & Safety
P. A. Pizzica	Reactor Analysis & Safety
W. P. Barthold	Applied Physics
R. B. Turski	Applied Physics
J. F. Schumar	Materials Science
E. D. Parr	Engineering
D. Eggen (Consultant)	Northwestern University

It is assumed that the reader is familiar with, or has access to, the material presented in the initial proposal[1] and the final report for FY 1974.[2] However, portions of these reports have been repeated in this text whenever necessary, in order to preserve the continuity of the presentation, and to render the report as self-contained as possible.

The main body of the report contains descriptions, discussions, and results of the several investigations. The details of the analyses and calculations upon which they are based are presented in appendices.

II. BACKGROUND

Because of the much lower level of funding of the SASS project, it was evident that meaningful progress could be made only by a substantial truncation of the effort proposed as Phase I - Concept Definition and Selection as set forth in the original project schedule.[1] Therefore, a specific concept for an Inherent Shutdown Assembly (ISA) was selected from among the many options and defined for focused development in FY 1975. The reasons for the choice of the concept are detailed in Section III.

Once the design concept was chosen, the interfaces with the reactor core and blanket, that is the dimensional and mechanical aspects of the design, could be investigated. The concept then became the basis for thermal-hydraulic design analyses, both static and transient. Specific physics analyses and accident analyses were carried out to assess the adequacy of the design as a self-actuated shutdown system and the impact on reactor performance, and to refine the performance requirements. For convenience and internal consistency, the Clinch River Breeder Reactor Plant (CRBRP) was chosen as the "host" reactor for the ISA, even though it was recognized that the first actual application would probably be in the first commercial LMFBRs.

Specific design problems related to the type of design chosen were also addressed. Magnet and magnetic circuit designs and analyses were required for the magnetic Curie temperature point device selected. The behavior and stability of the materials utilized in the device were examined, particularly with an eye to possible problem areas. This is an important consideration because of the high temperature and intense radiation environment in which the system is expected to operate over

long periods of time. In addition, proof-of-principle type laboratory tests were performed.

All of these activities were carried out in FY 1975 with the following goals achieved:

(1) A conceptual design of an ISA, the main hardware component of the SASS, has been developed and refined.

(2) Accident analyses have been completed and performance requirements for reactivity and time response selected.

(3) The number and position of ISAs have been chosen and their impact on reactor performance assessed.

(4) Laboratory tests of a simulated ISA, in air and static sodium, have been successfully completed.

III. MAGNETIC HOLD SELF-ACTUATED SHUTDOWN SYSTEM

The following terminology has been adopted for the discussion of the designs which follow. Self-Actuated Shutdown System (SASS) includes the assembly which can be substituted for a standard fuel assembly (containing fuel pins, ducting and flow channels, and the movable absorber section) and any in-reactor and ex-reactor ancillary equipment needed, e.g., for testing, inspection, and recocking. The assembly itself, which is externally identical to fuel, blanket, and conventional control assemblies, will be referred to as the Inherent Shutdown Assembly (ISA).

A. Selection of Conceptual Design

At the conclusion of the FY 1974 effort on the development of the self-actuated shutdown system, several options appeared to be available based upon system function and system types. As explained in detail in the FY 1974 final report,[2] the ISA must contain components to provide three essential system functions:

(1) Sensing Function

(2) Triggering Function

(3) Locking and Release Function

In that report three attractive system types are discussed. They are:

(1) Thermally Fusible Links

(2) Thermal Expansion

(3) Ferromagnetic Curie Point Permanent Magnet Devices

One viable concept would be to utilize a device combining the three system functions above, since mechanically this would be the simplest (designated Concept IV in Ref. 2). This concept should be compared to

another promising concept, also discussed in Ref. 2, where-in the sensing and triggering functions are combined, but the locking-release function is separate (Designated Concept II). This latter concept is considered to be disadvantageous because it is less simple and because of the possibility of failure of the sensor-trigger or locking-release mechanisms. One of the drawbacks of Concept IV, which consolidates the system functions, is its tendency to exhibit longer time constants than Concept II. The sensing-triggering function mechanism can be made very small through the use of various principles of mechanical advantage. However, Concept IV must be generally of greater bulk since it must hold or lock the full assembly load. After a selection had been made, calculations indicated that the Concept IV system, which was chosen, could yield time constants of an order of magnitude compatible with requirements placed on the system by the accident analysis.

If a Concept IV system is considered desirable, the Curie temperature magnet holding device is a leading contender. (This device was actually selected.) A component depending upon the principle of thermal expansion (e.g., a bimetallic device) could only with difficulty be of the Concept IV type. Thermally fusible links (melting point devices) have, as a principal disadvantage,* the tendency to plastic creep at the reactor operation temperature, limiting the lifetime of the fuse and inviting spurious actuation. The French have experienced some difficulty with this in their design. The details on these devices are covered in the FY 1974 final report.[2] For the reasons above, a Concept IV device, combining the three shutdown system functions, based upon a ferromagnetic Curie point temperature magnet effect, was selected.

---

*Another disadvantage is the difficulty of testing the ISA nondestructively.

The configuration of the Curie point temperature magnet holding device, as presented in the FY 1974 final report[2] (Figure 10 of ANL/CT-74-19), is reproduced in Figure 1 of this report.

The selection of additional parameters for the preferred design is summarized below. The selected option, among the alternatives considered, is underlined.

Reactivity change:	fuel removal, <u>absorber insertion</u>
Trigger:	fusible links, thermal expansion, <u>magnetic effects</u> (Curie point)
Absorber materials:	<u>boron carbide</u>, tantalum, europium oxide
Insertion mode:	<u>gravity</u>, spring assist, pneumatic assist, hydraulic or explosive assist
Absorber form:	solid block, <u>rod bundle</u>, balls or shot
Kinematic approach:	<u>combine sensing triggering and locking functions</u>, combine sensing and triggering with separate locking system

More details on the selection process are covered in Ref. 3

It should be noted that all ISA concepts considered rely upon a temperature change in the material of the device for triggering. This would be brought about by an increase in the temperature of the sodium flowing past two rows of prototypic fuel pins in the ISA, due to an accident condition, and through or around the device. The trigger would be placed at or near the top of the core. For the selected concept, heat would flow from the sodium into the trigger assembly raising its temperature toward or above the ferromagnetic Curie point thus reducing the holding force and dropping the absorber bundle. This action would provide protection against a loss-of-flow type of incident. However, the device would be much too slow

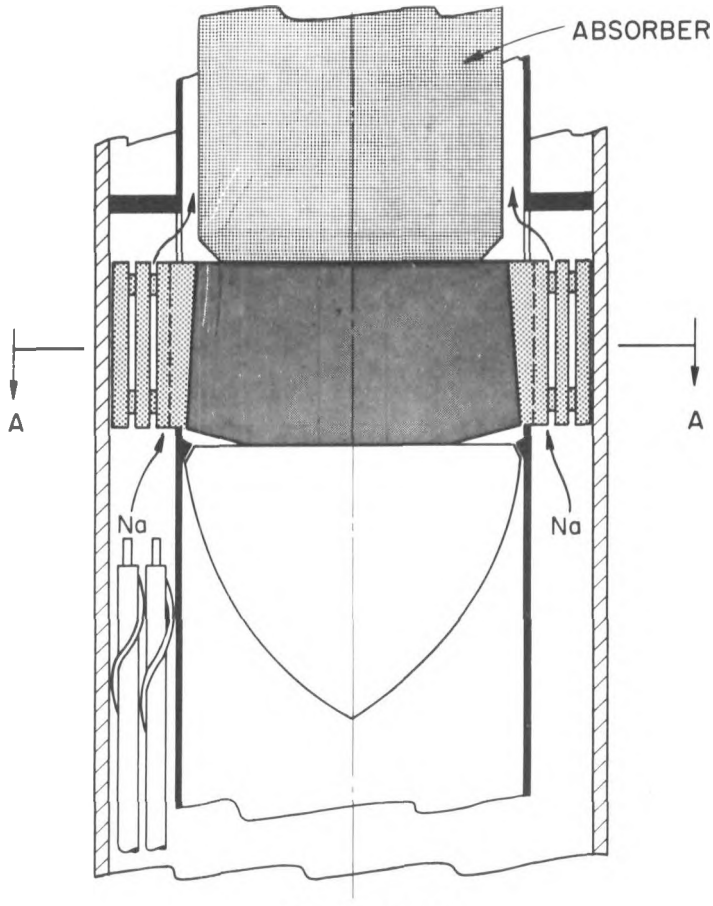

SECTION B-B

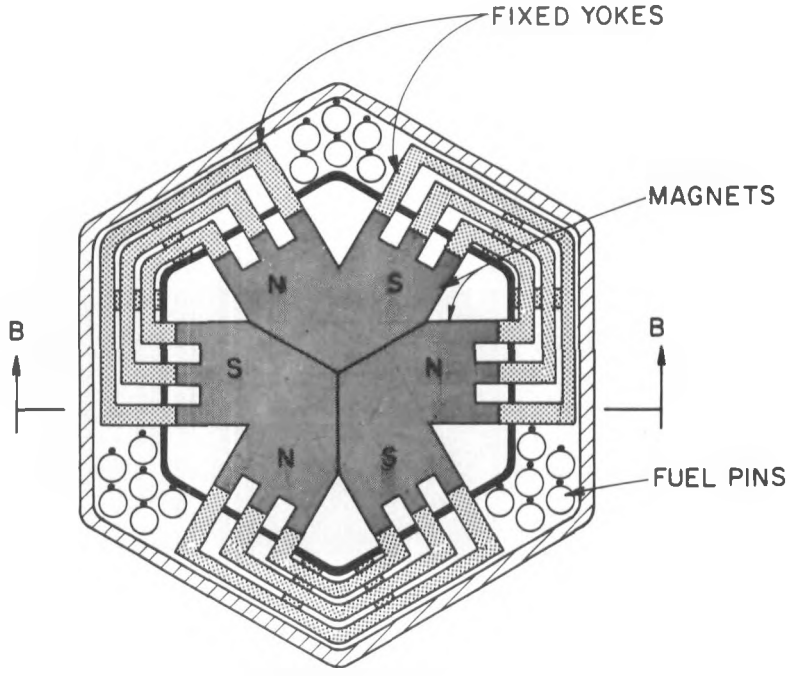

SECTION A-A

FIGURE 1: Conceptual Design of Curie Temperature Magnetic Holding Device

for the detection of a fast reactivity-increase transient. A large neutron flux increase could occur, with substantial fuel melting, before a significant change in the core coolant temperature would be produced. For this reason a fissionable material imbedded in the trigger of the device is proposed to provide a heat source which begins to respond instantaneously to change in the neutron flux at its location. The design and disposition of this fissile source is discussed in several places in this report.

B. Design Requirements

1. Introduction

Various design requirements for a Self-Actuated Shutdown System (SASS) are discussed in detail in the original proposal.[1] Some of this material will be reviewed here, particularly as it applies to the self-actuated shutdown system selected for development in the FY 1975 program.

There appears to be general agreement that a high degree of shutdown reliability can be obtained for LMFBRs by utilizing a self-actuated shutdown system. At the present time, the CRBR demonstration plant project plans to attain high reliability for plant protection by the utilization of a primary shutdown system and an alternate shutdown system, neither of which is self-actuated. Both systems depend upon an external signal, transmission of that signal to a transducer, and the triggering of an electro-mechanical or hydraulic system by the electrical signal. There are substantial differences in the CRBR shutdown systems so that additional safety due to a high degree of diversity can be claimed However, the degree of reliability is yet to be determined.

Because of the high level of reliability which has been called for recently by the AEC regulatory staff[4] (now the NRC) for light water reactors, it would appear that there would be advantages in developing another shutdown system approach for LMFBRs should it be needed.

The SASS is proposed either as a substitute for the alternate shutdown system or as a third system, acting in this latter mode more as an engineered safeguard, in the extremely unlikely event that both of the shutdown systems, primary and alternate, fail. Because the SASS depends only upon natural phenomena occurring solely within the core and blanket and is propelled into the core by gravity it bears the characteristics of an inherent mechanism, hence the name Inherent Shutdown Assembly (ISA).

The self-actuated shutdown system approach pursued by ANL has several attractive characteristics. These are brought out in the following list of requirements originally set forth in Ref. 1 and which are met by the selected SASS concept.

2. Functional Requirements

(a) The SASS shall be wholly contained within the reactor. [No subsystems or components of the selected design are outside the primary system boundary.]

(b) The SASS shall insert negative reactivity sufficient to counteract typical severe reactor transients.

[It is shown in this report that a single assembly of the selected concept has been designed to contain sufficient absorber in the form of enriched boron to counteract the effects of severe reactivity insertion or loss of flow transients.]

(c) The SASS time response and reactivity insertion rate shall be such that all transients considered shall be checked within Part 100 guidelines (that is, without a breach of the containment as a minimum requirement).

[It is shown in this report that the time constant and insertion rate of the selected design are sufficient to protect against severe reactivity insertion and loss of flow transients with at worst minimal core damage.]

(d) The SASS shall be self-actuated by the inherent effects of the transients being considered.

[The SASS concept selected operates through a change of state (demagnetization above the ferromagnetic Curie point) brought about by a temperature rise in the ferromagnetic material due to a coolant temperature increase or an increase in neutron flux.]

(e) The design of the SASS shall be such that it is not rendered inoperable by gross geometric distortion or buildup of crud.

[Clearances have been maintained as large as possible in the designs.]

(f) The design of the SASS shall be such that the triggering and insertion of negative reactivity are achieved by "natural phenomena".

[This has been accomplished by utilizing the temperature dependent ferromagnetic Curie point for detection and triggering. The neutron absorber is inserted by gravity.]

3. Desirable Design Requirements

In addition to the functional requirements outlined above, the chosen SASS design also meets most of the additional desirable design features listed in Section II-C of Reference 1. Several of the more important items are discussed below.

(a) The SASS should be testable.

[This provision has not been addressed in the current design but it could be achieved since the Curie point effect is a reversible and reproducible phenomenon.]

(b) Rapid identification of a spuriously tripped ISA has not been addressed in the current design, but could be provided.

(c) The fissile trigger should be at or near the core mid-plane and mechanisms based on coolant overheating should be located at or near the top of the core.

[The latter requirement has been met. However, the fissile trigger has also been located at the top of the core. It is shown in Section V that this placement of the fissile trigger meets the requirements of the accident analysis.]

The following features have been met in the design:

(d) The SASS should be completely interchangeable with a fuel assembly.

(e) Fuel provided in the SASS should be essentially similar to that of the standard fuel elements.

(f) The SASS should produce negative reactivity by the insertion of an absorber of conventional materials.

(g) The bottom of the absorber section during normal operation should be at or slightly above the core.

(h) When tripped, the bottom of the absorber section should be at or slightly below the bottom of the core.

(i) The absorber release should be triggered by a single mechanism responding to high coolant temperature or high fission rate.

(j) The absorber material should occupy the highest possible fraction of the area within the SASS duct, consistent with the provision of generous clearances around the periphery of the absorber section. An adequate amount and distribution of coolant flow area should be provided such that the absorber operates at temperatures within the design limits for that same absorber material in the conventional control assemblies.

(k) The absorber section should possess a mass and geometric configuration such that fluid drag forces do not retard the insertion of the absorber into the core by more than 0.2 g.

C. Description of Magnetic Hold Conceptual Design Variations

The specific conceptual design, based upon a permanent magnet ferromagnetic Curie point trigger, as conceived at the end of FY 1974, is shown in Figure 1 (Figure 10 of Reference 2). Two questions arose immediately after this concept was selected as the basis for the reference ISA: First considered was the availability of the magnet and yoke and their materials. From whom could a complex magnet and yoke design of this type be obtained? Second, it appeared to be undesirable to take up the annulus containing the fuel pins with magnetic yoke material.

At this point is was decided to solicit an industrial magnet designer to obtain expert information on the design and availability of magnets for this type of application. The Arnold Engineering Company in Marengo, Illinois was approached.* They showed interest in our effort and suggested a magnetic circuit design which was largely adopted.

---

* The Arnold Engineering Co., Permanent Magnet Division; a member company of Allegheny-Ludlum Industries, Inc.

Arnold Engineering proposed a modularized holding magnet design comprising one or more cylindrical Alnico V permanent magnets 1 in. long by about 2 in. diameter. The magnetic circuit is completed by means of the carbon steel caps or pole pieces, top and bottom, for the Alnico V magnet, and carbon steel structure lateral to the alnico magnet, depending upon the design (see Figures 2 through 5). The magnetic flux originates in the north pole of the Alnico V magnet, continues through the carbon steel hex caps and carbon steel lateral structure of the assembly into the south pole of the alnico magnet, completing the circuit.

This holding magnet assembly design is quite flexible. While the configuration of the Alnico V permanent magnet (the source of the holding flux) remains the same, considerable variation in the design of the carbon steel parts completing the magnetic circuit is possible depending upon geometric requirements of the design.

This approach has the advantage that the carbon steel parts could be manufactured at ANL ready for the insertion of the alnico magnets. The magnet assembly must be completed by the vendor and then properly magnetized. This procedure was actually carried out during FY 1975 in preparing the holding assembly which was used in the Laboratory test program. The details of the testing are covered in Section IV. Photographs of the test assembly manufactured at Argonne (the Alnico V magnets inside were manufactured by Arnold Engineering) are shown in Figures 7 and 8 of Section IV.

While this design is suitable for laboratory testing, it does not fulfill the requirement that there be two full rows of fuel pins in the annulus between the inner and outer ducts. Four more designs satisfying this requirement have been developed. Each one of these proposed designs will be described

and their advantages and drawbacks discussed. The designs are exhibited in Figures 2 through 5. The four concepts have been designated by the following descriptive titles:

(1) Six-Face Horizontal Hold Design

(2) Two-Face Horizontal Hold Design

(3) Snap Ring Vertical Hold Design

(4) Movable Cam Vertical Hold Design

Horizontal hold and vertical hold refer to the direction of the magnetic force which holds the assembly in place. In the horizontal hold designs the magnetic circuit is completed by means of ferromagnetic carbon steel inserts which replace the nonmagnetic stainless steel of the inner duct at the elevation of the assembly. In this way, magnetic material need not be placed in the annulus and two full rows of fuel pins can be accommodated. In the vertical hold designs a carbon steel element is placed inside the inner duct to complete the magnetic circuit and to which the assembly is held by a vertical magnetic force. Again, two full rows of fuel pins can be accommodated in the annulus.

These designs are discussed in more detail below. In all four designs, provision is made for an alternate shunt magnetic flux path. The reason for this additional path and other aspects of the magnetic circuit design are discussed in Section III-D and Appendix I.

1. Six Face Horizontal Hold Design

The six face horizontal hold design is shown in Figure 2. In this design a bolt holds two carbon steel hexagonal caps flush against the ends of a cylindrical Alnico V permanent magnet. The boron carbide absorber pin bundle is held to the magnet by this same bolt.

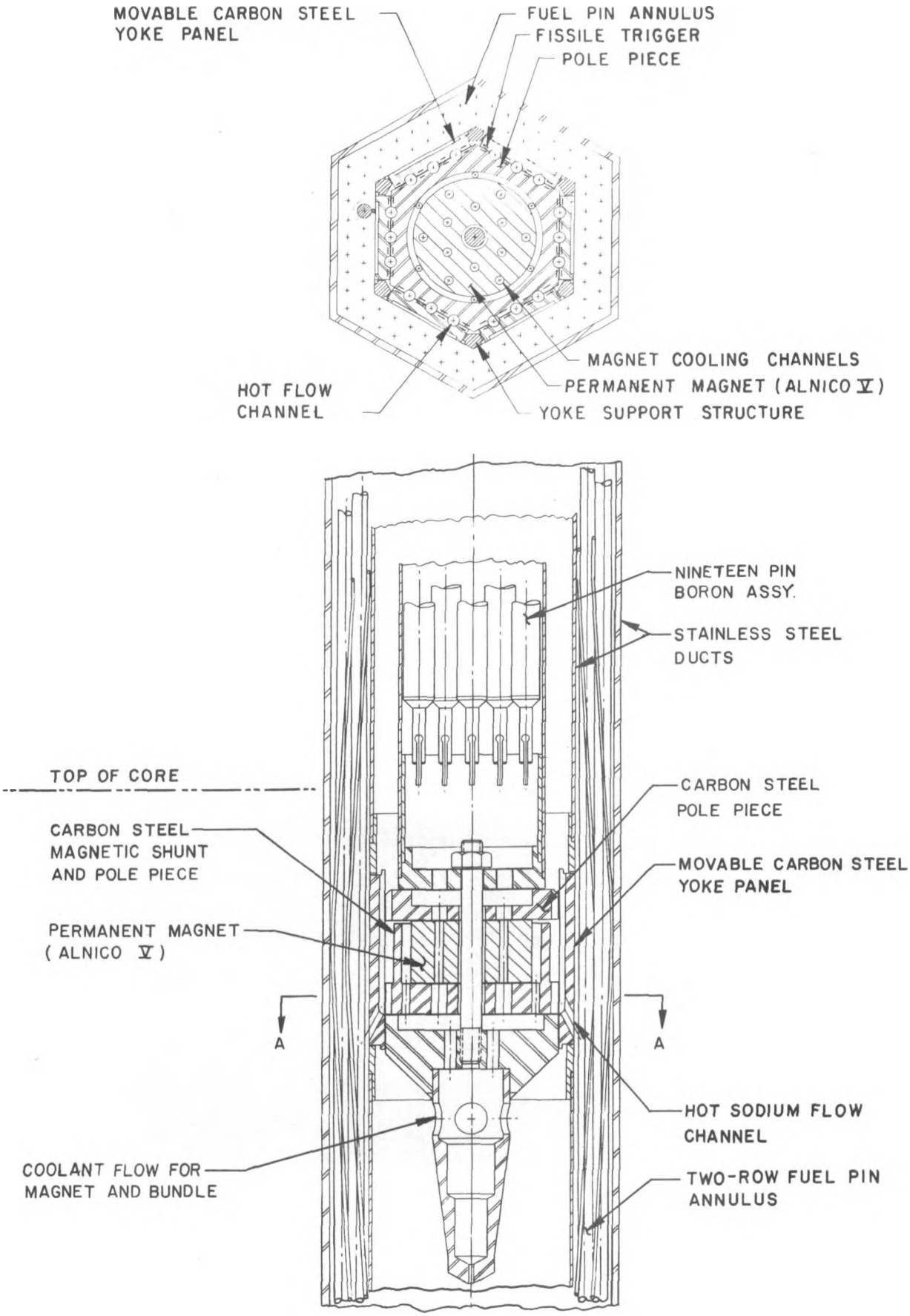

FIGURE 2: Six-Face Horizontal Hold SASS Conceptual Design

There are six movable carbon steel panels inserted into each of the faces of the inner stainless steel duct. These panels are pulled flush with the faces of the upper and lower hexagonal carbon steel caps or pole pieces by the horizontal magnetic force. The interfaces between the movable carbon steel panels and the caps represent the parting planes of the design.

The horizontal force holding the assembly in place is proportional to the total area of contact times the square of the magnetic flux density. The magnetic flux density through the parting plane is determined by the magnetomotive force (MMF) of the magnet and the reluctance of the magnetic circuit external to the magnet. (See Figures I-1 and I-4 of Appendix I for schematics of the magnetic circuit.)

This device detects accident conditions in the core by an increase in temperature of the sodium in the hot stream from the fuel elements, flowing through the assembly. When the material of the magnetic circuit exceeds its Curie temperature it becomes nonmagnetic increasing the magnetic circuit reluctance and thereby decreasing the magnetic flux density through the parting plane. When the total magnetic holding force decreases below the weight of the assembly, it falls under gravity into the core terminating the accident. This mode of operation protects against loss of flow accidents, for example.

In order to detect neutron flux excursions, a fissile UO_2-iron cermet of up to 35% UO_2 by volume is imbedded in the yoke to supply a fission heating source at the parting plane of the device. This mode of operation protects against fast reactivity excursions since a detectable rise in the coolant temperature is delayed until the accident is too well advanced.

The alnico magnet must be cooled both internally and externally since there is considerable heat generation from absorption of radiation in the alnico magnet mass. The temperature of the alnico must be maintained close to 1000°F in order to obtain long term stability of the magnetic holding force. Alnico coolant channels are shown in Figures 2 through 5. Other designs for cooling the magnet are being considered, such as a split magnet. Arnold Engineering is considering the feasibility of casting an Alnico V magnet with coolant channels as shown in Figures 2-5. The details of the magnet thermal-hydraulic design and magnetic circuit design are discussed in Section III-D and Appendices I and II.

A critique of this design produced two possible drawbacks which were overcome in subsequent designs:

(a) Since the inner hex is completely filled by the magnet assembly, there is very little room to accommodate differential swelling between the stainless steel and carbon steel components. Because of large uncertainties in swelling rates of both materials, a design less sensitive to this problem would be preferable.

(b) There is some concern that the horizontal holding force does not fix the assembly positively in place, and that under the inevitable core and blanket vibration, the assembly will shimmy down out of position resulting in variable reactivity effects.

However, item (b) would appear to be a problem only if the assembly moved under equipotential conditions. Clearly as the assembly moves out of the hold position, as shown in Figure 2, field lines are distorted, work is done, and there is a change in potential energy. For the same holding force,

whether horizontal or vertical forces are acting, the same energy is required to remove the assembly completely from its hold position. This was checked in the laboratory, where it was found that the breakaway force was the same for a flat plate held by a magnet, whether the plate was pulled in a direction along, or perpendicular to, the lines of force of the magnet pole. Therefore, it appears that friction effects need not be considered in a horizontal hold device in computing the total holding force.

2. Two Face Horizontal Hold Design

The two-face horizontal hold design shown in Figure 3 will accommodate considerable differential swelling and distortion between the inner duct and the movable part of the ISA, because of the large clearance provided between the movable part and the four inner duct walls to which it is not held. This concept is similar to the six-face horizontal hold design in that identical Alnico V cylinders are stacked, sandwiched between carbon steel caps, and bolted together with the boron pin bundle on the top and the cone on the bottom.

The assembly is held to nonmovable carbon steel inserts in two faces of the inner duct which complete the magnetic circuit. Because the assembly is held now to only two faces, two-thirds of the holding force has been lost. In order to recover some of this holding force, this concept is shown as a two module design, that is with two alnico magnets. This conceptual design is cooled in the same manner as the previous design, works on the same magnetic Curie temperature principle, and also has a fissile heating source, as in the design discussed above.

The same objection could be made of this design concerning whether the assembly can be held in place indefinitely by the horizontal holding force.

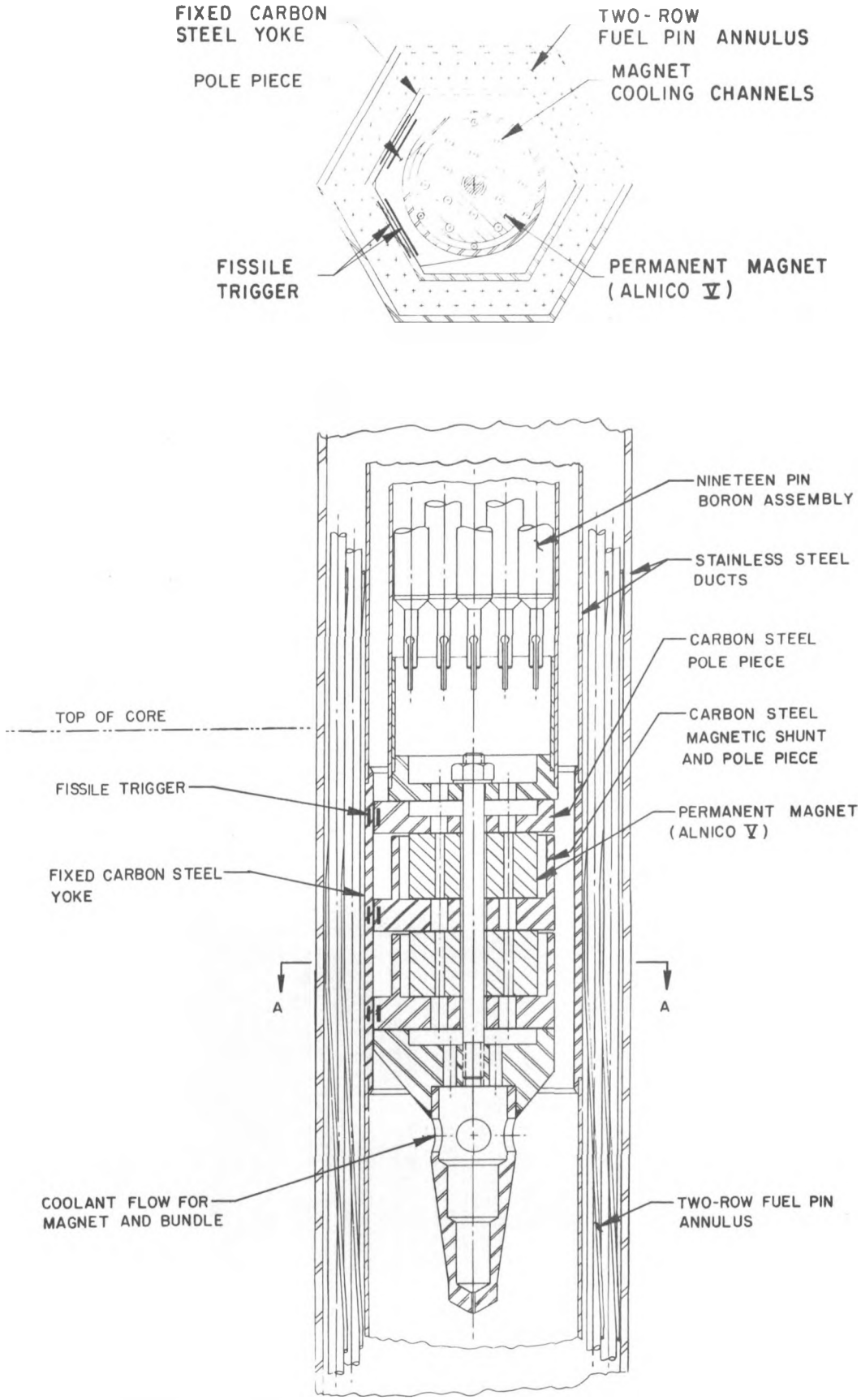

FIGURE 3: Two-Face Horizontal Hold SASS Conceptual Design

The vertical hold devices described below are designed to overcome this objection.

3. Snap Ring Vertical Hold Design

In this design the inside of each one of the six faces of the inner duct is built up by means of a fixed carbon steel insert which protrudes into the inner duct. The bottom of the carbon steel insert provides a contact surface overlapping the top of the bottom carbon steel hexagonal cap or pole piece of the assembly. The magnetomotive force (MMF) is again provided by means of a cylindrical Alnico V magnet. However, to obtain additional MMF the alnico cylinder has been lengthened to 1.5 in. instead of 1 in. as in the previous designs. The magnetic circuit is completed on the top by means of a cylindrical carbon steel cap and a carbon steel segmented snap ring (see Figure 4) which the magnetic force holds to a smaller diameter than in its unstressed state. The hot sodium stream flows through horizontal channels close to the parting plane and up through the snap ring.

The mode of operation of this device is the following: Due to a rise in temperature of the sodium, for example, the carbon steel approaches its Curie temperature. The reluctance of the magnetic circuit is increased, decreasing the magnetic holding flux through the circuit. The vertical magnetic force holding the assembly is reduced at the parting plane as is the force holding the snap ring to the upper cap. When the magnetic holding force is sufficiently diminished, the snap ring opens and the assembly with absorber falls through, terminating the accident. Fissile material is imbedded near the parting plane in the carbon steel of this design also, in order to provide for rapid detection of the fast flux excursion due to a fast reactivity

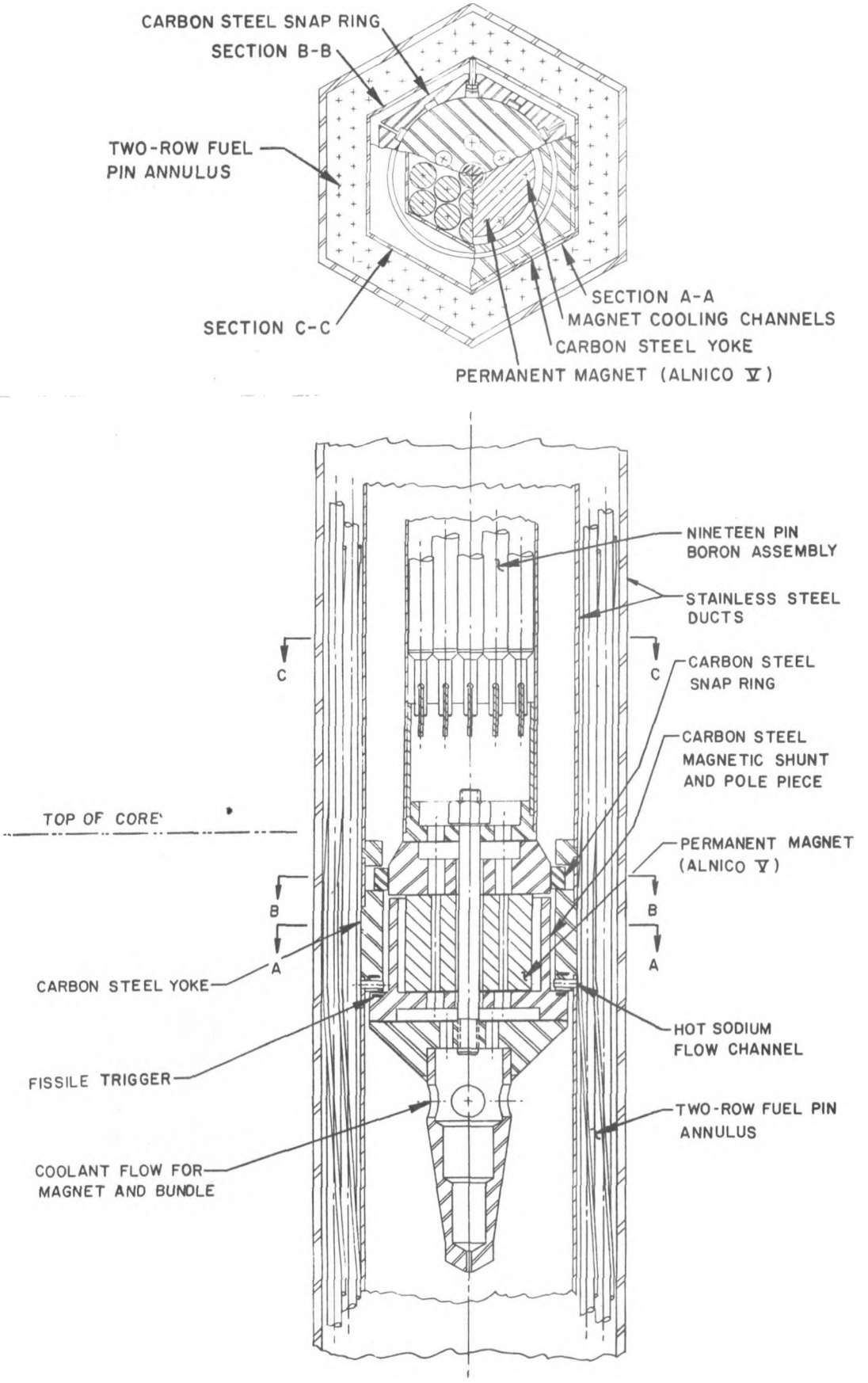

FIGURE 4: Snap Ring Vertical Hold SASS Conceptual Design

insertion accident. The mandatory magnetic shunt circuit is also provided in this design.

This configuration provides a substantial vertical magnetic force holding the assembly in place. There is also a horizontal holding force at the contact between the snap ring and the upper carbon steel pole piece. This design also exhibits some trade-offs:

(a) Because of the carbon steel inserts protruding into the inner annulus, the absorber pin bundle hex is reduced in cross section in order to maintain necessary clearance. This means that less boron can be carried by the assembly, and its worth is reduced for the same B-10 enrichment.

(b) In some places (for example, at the bottom of the assembly) clearances are somewhat reduced. Clearances can be increased at the sacrifice of holding force.

(c) Because of limitations in reducing the cross-section of the inner duct at the assembly elevation, the holding force of this design will be generally smaller than for the horizontal hold design.

(d) Swelling is not as well accommodated in this design as in the two-face horizontal hold design. However, it would appear to be superior to the six-face horizontal hold design in this respect.

(e) The snap ring constitutes an undesirable complication in terms of release and recocking.

4. Movable Cam Vertical Hold Design

A modification of the snap ring vertical hold design has also been developed in order to improve the design with respect to item (e) above.

The bottom configuration of the magnet assembly has been retained, but the snap ring has been replaced by six movable cams. These can pivot inward when the magnetic flux through the circuit is reduced at elevated temperatures. This action, and the loss of vertical magnetic holding force at the bottom of the assembly produces the release of the assembly into the core (see Figure 5).

The first four comments on the snap ring design also apply to the cam design.

The cam vertical hold design has the advantage over the snap ring design in that the action of the cams on release is more direct than for the snap ring design.

5. Comparison of Magnetic Hold Conceptual Design Characteristics

The characteristics of the four conceptual designs are summarized in Table 1. The total weight of each assembly, the mass of boron each assembly can hold, the contact areas and clearance are given all on the same basis for comparison.

It is apparent from the table that the horizontal hold devices would carry the greatest mass and have the potential for highest negative reactivity worth.

The largest holding force for a single module is obtained from the six-face horizontal hold design. A holding force of about 130 lb. would be theoretically available for a holding area of about 4 in.^{2}, the minimum for the designs, at a flux density of about 7500 gauss at 1000°F. All the designs would appear to be feasible on this count since a holding force of at least

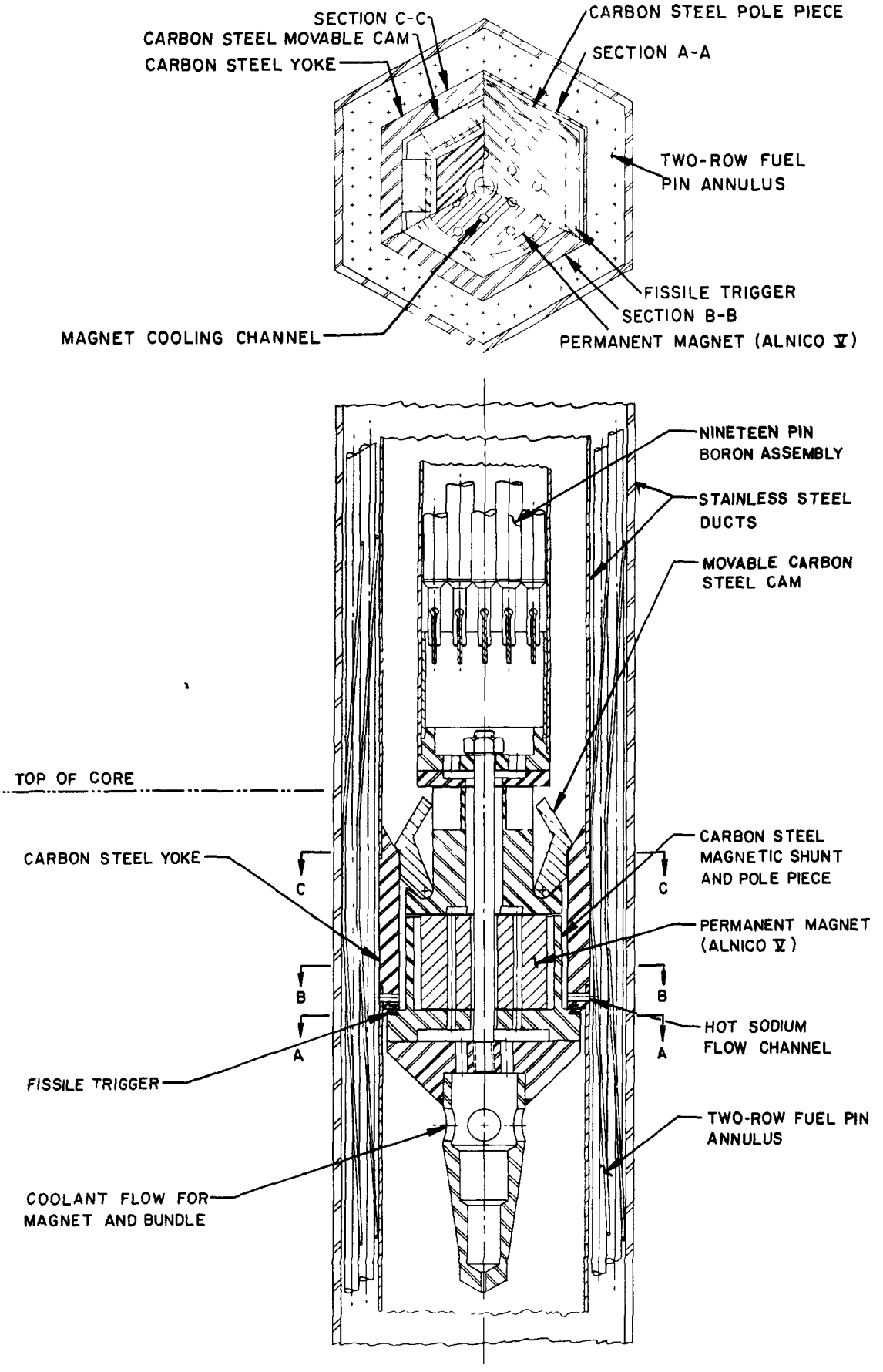

FIGURE 5: Movable Cam Vertical Hold SASS Conceptual Design

TABLE 1. Comparison of Magnetic Hold Conceptual Designs

	SIX FACE HORIZONTAL HOLD	TWO FACE HORIZONTAL HOLD	SNAP RING VERTICAL HOLD	MOVABLE CAM VERTICAL HOLD
ASSEMBLY WEIGHT	34.8 LB. 15.8 KG.	39.8 LB. 18.1 KG.	29.9 LB. 13.5 KG.	30.8 LB. 14.0 KG.
BORON MASS	8.5 LB. 3.8 KG.	10.6 LB. 4.8 KG.	6.4 LB. 2.9 KG.	6.4 LB. 2.9 KG.
MAXIMUM WORTH (75% B-10)	$4.1	$4.4	$3.6	$3.6
VERTICAL HOLDING AREA	- -	- -	1.9 IN.^{2} 12.6 CM.^{2}	2.0 IN.^{2} 12.9 CM.^{2}
HORIZONTAL HOLDING AREA	4.9 IN.^{2} 31.5 CM.^{2}	4.5 IN.^{2} 29.0 CM.^{2}	2.5 IN.^{2} 16.1 CM.^{2}	2.0 IN.^{2} 12.9 CM.^{2}
TOTAL HOLDING AREA	4.9 IN.^{2} 31.5 CM.^{2}	4.5 IN.^{2} 29.0 CM.^{2}	4.4 IN.^{2} 28.7 CM.^{2}	4.0 IN.^{2} 25.8 CM.^{2}
MINIMUM CLEARANCE	0.056 IN 0.142 CM	0.155 IN 0.393 CM	0.052 IN 0.132 CM	0.059 IN 0.150 CM

double the assembly weight is considered desirable. This force level would be needed to offset uncertainties in the design, possible deterioration of holding force, plus a margin of safety to avoid spurious trips.

As expected, the two-face double module design results in the greatest clearance. It should be noted that the clearance of the vertical hold designs at the magnet assembly can be increased with a sacrifice of holding force. Increasing clearance for the boron pin bundle, however, would result generally in a smaller B-10 loading and, therefore, a lesser worth.

Since it is considered that there is an advantage with respect to holding stability in having some substantial vertical hold capability, the movable cam vertical hold configuration has been chosen as the reference design. Its action appears to be more reliable than the snap ring design. The moving cam design should be able to deliver approximately $3.5 worth per assembly if its position and enrichment are properly selected (see Reactor Physics analysis, Section VI). The accident analysis (Section V) indicates that a $3.5 worth would be sufficient for the SASS to protect the plant, as a backup protection system, against loss of flow and reactivity excursion incidents. This would mean that the SASS system would require two assemblies for the core assuming one ISA fails to operate.

D. Results of Analysis of Conceptual Design

1. Magnetic Analysis

It is a well known fact that ferromagnetic materials become nonmagnetic (actually paramagnetic) above a definite temperature, characteristic of the material. This temperature is known as the ferromagnetic Curie point. This effect is the basis for the operation of the proposed self-actuated shutdown system. When the temperature of a part or all of

a magnetic circuit exceeds the Curie point, the magnetic flux in the circuit decreases reducing the magnetic holding force. When this force is reduced below the weight of the assembly it is released, falling into the core and terminating the accident.

For a given magnetomotive force, the flux through a magnetic circuit depends upon its permeability. The relative permeability of soft magnetic materials can be many thousands; that of nonmagnetic materials, or of ferromagnetic materials above the Curie point, is essentially unity.

The relative permeability of a ferromagnetic material, exhibiting its temperature dependence, is given generally by the following formula:

$$\mu_r = \frac{\mu}{\mu_o} = 1 + \chi_o(B) \frac{M_s}{M_o} \left(\frac{T}{T_c}\right) \qquad (1)$$

χ_o is the susceptibility of the material at low temperatures (a function of the magnetic flux density B), M_s/M_o is the ratio of the saturation magnetization of the material at temperature T to its saturation magnetization at absolute zero. M_s/M_o is unity at T = 0, and goes to zero above the Curie temperature, T_c. The relative permeability μ_r at $T > T_c$ is then unity and the material is essentially nonmagnetic. The functional dependence of M_s/M_o which applies to carbon steel and alnico is given in Figure I-2. The nature of the Curie point and Curie temperature is discussed in Appendix 3 of the FY 74 final report[2] and Appendix I of this report.

The magnetic flux producing the holding force in the designs is obtained from a powerful permanent magnet or, as in the two-face holding device, series of magnets (see Figures 2-5). The magnets are in the form of circular cylinders of Alnico V. This material exhibits the very high coercive force and moderately high magnetic flux density characteristics of permanent magnet materials. In addition, Alnico V was selected based upon the extensive temperature testing carried out in the development of LMFBR flowmeters.[12] These tests demonstrated the stability of Alnico V in temperature and radiation environments similar to those expected for the ISA. It is one of the most stable high temperature magnetic materials available.

The coercive force times the length of the permanent magnet gives the magnetomotive force (MMF) which drives the flux through the external magnetic circuit composed of a soft magnetic material, in this case low carbon steel. An equivalent magnetic circuit for the conceptual designs is shown in Figure I-1 of Appendix I.

Soft ferromagnetic materials, because of their high permeability, exhibit a low resistance to penetration of magnetic flux. This resistance to the penetration of magnetic flux is called reluctance. The reluctance of a part of a magnetic circuit is proportional to the length of the material and inversely proportional to its cross-sectional area and permeability as follows:

$$R = \frac{\ell}{\mu A} = \frac{\ell}{\mu_o \mu_r A} \tag{2}$$

where μ is the permeability of the material, μ_r the relative permeability of the material, and μ_o the permeability of free space. (See Appendix I for a discussion of these magnetic parameters.)

Using the magnetic circuit analog of Ohm's law, the flux through a magnetic circuit is given by the magnetomotive force (MMF) divided by the total reluctance.

$$\phi = \frac{MMF}{R} \tag{3}$$

The assembly is arranged so that the hot stream of sodium from the fueled annulus flows through channels at the parting plane of the device. When the temperature of the sodium, due to accident conditions in the core, increases toward or above the Curie temperature for carbon steel (1418°F), that portion of the magnetic circuit at the parting plane becomes demagnetized, causing a large increase in the reluctance of that part of the magnetic circuit. This insures a decrease in the magnetic flux through the parting plane. Since the reluctance of the carbon steel is very low below the Curie temperature, most of the reluctance of the circuit is contributed even by a demagnetized zone of limited extent in the carbon steel. A detailed calculation of this effect is given in Appendix I.

Demagnetization at the parting plane is also produced due to a rise in neutron flux. This causes an increase in heat generation in the UO_2-cermet fissile sources imbedded in the carbon steel and therefore a rise in the temperature of the carbon steel. In this way the device can protect against rapid insertions of reactivity.

The reduction in the magnetic flux through the circuit is actually a reduction in the magnetic flux density B at the parting plane which results in a reduction in the magnetic holding force at the parting plane. This force per unit area is given by:

$$P = \frac{F}{A} = \frac{B^2}{2\mu_o} \tag{4}$$

where F is the holding force, A the holding area of contact, B the magnetic flux density and μ_o the permeability of free space. This equation and units are discussed in Appendix I.

For a nominal magnetic flux density of 10,000 gauss (1.0 weber/m^2), the approximate flux density at room temperature for the assemblies, the holding force per unit area is given by Equation (4):

$$P = \frac{B^2}{2\mu_o} = \frac{1}{2 \times 4\pi \times 10^{-7}} = 3.98 \times 10^5 \ \frac{\text{newton}}{\text{meter}^2}$$

$$P = 4.06 \ \frac{\text{kg}}{\text{cm}^2} = 57.6 \ \frac{\text{lb}}{\text{in}^2}$$

All of the designs discussed above utilize a magnetic shunt in the magnetic circuit design. The shunt has been included for two reasons. First, it is a usual magnetic circuit design practice to provide an alternate low reluctance flux path in addition to the main flux path. This acts as an effective keeper for the magnet of the assembly when it is not in place and the main holding flux path is not completed. The alternate shunt path arrangement is necessary to preserve the remanance flux level of the magnet, which would otherwise tend to deteriorate when removed from its holding position or while on the shelf. Second, the presence of the shunt provides an alternate path when the flux in the main holding path is being reduced, because of an increase in its reluctance, as the Curie point is approached. The resulting proportionately greater magnetic flux in the shunt path makes for improved operation of the release mechanism of the device since there is therefore a sharper reduction in the holding flux.

2. Thermal-Hydraulic Analysis

A thermal and hydraulic analysis has been performed for one of the designs of the ISA, specifically the six-face horizontal hold design.

The hydraulic analysis shows that, for the six-face horizontal hold configuration, part of the hot flow from the fuel pins will be diverted through the assembly hot channels with a pressure drop of about 2 psi. This pressure drop occurs from the entrance port "a" of the assembly to the exit port "f" downstream of the assembly as shown in Figure II-1 of Appendix II.

The total flow in the ninety element ISA annulus is assumed to be about 69,750 lb/hr, based upon that for an average element in the CRBR core (see Appendix II).

With an equalizing pressure drop in the fuel annulus of about 2 psi, approximately 9.2% of the total annulus flow, or 6444 lb/hr, will be diverted through the assembly channels of the parting plane. Most of the pressure drop is contributed by the exit and entrance losses.

It has also been shown that sufficient heat transfer can occur so that the temperature at the parting plane can be elevated above the Curie point in about one second or less, as required by the accident analyses. A simple lumped parameter analysis indicates a time constant of about 0.25 sec. A more detailed analysis based upon a three node thermal-hydraulic model also indicates a dominant time constant of this magnitude as does a thermal diffusion calculation (see Appendices I and II). It was not possible to check this time constant in the present SASS experimental program as explained in Section IV.

The magnet assembly will be placed in the reactor just below the interface between the core and upper axial blanket. There will be internal heat generation in the materials of the assembly due to the absorption of high energy gamma and neutron radiation produced directly or indirectly by the fission process. This results in a temperature rise in the materials. It is necessary to cool the Alnico V magnets so that they do not operate at an internal temperature too much above the sodium ambient. This has been accomplished by providing cooling channels through the alnico in the form of holes as shown in the several designs (Figures 2-5). These cooling channels are in addition to the sodium cooling at the outside surface, and that obtained from the sodium flow through the central hole which also contains the bolt holding the assembly together. Another method of cooling the alnico is to split the magnet into two or more segments (see Figure II-5 in Appendix II). Calculations indicate that it is feasible to maintain a temperature peak above the sodium ambient of not more than 25°F.

The sodium to cool the magnet is obtained from the sodium in the inner channel below the assembly. A hydraulic analysis of this colder sodium flow has been carried out in Appendix II, where it is shown that sufficient sodium flow is maintained to provide effective cooling to the magnet. This sodium also flows through the boron carbide absorber pin assembly above the magnet. A thermal-hydraulic analysis of the cooling of the absorber assembly was carried out in the FY 1974 final report[2] and has been amplified in Appendix II.

It should be noted that, in addition to making the magnet design more complicated, the presence of cooling channels in the magnet reduces its mass and therefore has the effect of reducing the available holding force. However, even with a single magnet module, it appears that there is sufficient excess holding force so that the required amount of cooling is feasible.

IV. SASS TEST RIG AND EXPERIMENTAL PROGRAM

A. Purpose of Tests

In order to demonstrate the principle of operation of the SASS, an experimental program was designed for step-by-step measurement and testing of significant parameters of the device. Initially, the components were assembled at the bench to see that proper mechanical mating and interaction of the components was achieved. This was followed by assembling the mechanism in the vertical test position. Initial room temperature tests established the force necessary to break the yoke away from the magnets, and the statistical variation in the required force. In addition to establishing this base level, the measurements indicate whether variability is to be anticipated during operation. Subsequently, the assembly was heated to the reactor ambient temperature of 520°C. It was held at this temperature for eleven days. During this period, breakaway force measurements were performed regularly to see if any progressive deviation in operation is experienced or if spurious drops occur.

When these tests were completed satisfactorily, Curie point operation was tested by immersing the yokes in high-temperature sodium.

B. Basis for Experimental Procedure and Design of Test Assembly

1. Radial Vane Design

A simplified design was chosen for the test assembly to facilitate construction and testing in the laboratory. A modular configuration was chosen so that modifications could be readily made.

The cross section of the magnet and yoke section is shown in Figure 6. Four magnets are stacked in tandem within their individual carbon steel hexagonal box enclosures with like poles opposing. When the yokes are not in position, the magnetic flux links through the box wall, which acts as a magnetic shunt and across the small gap between the top and bottom sections of each box. Contact of the high permeability yoke vanes with the radial protrusions located along the hexagonal faces of the boxes allows the magnetic flux to link through the yoke. This occurs because the steel yoke represents the path of lowest reluctance. The yokes, when held in position, form an extension of the radial vanes, which protrude normally from the hexagonal faces of the boxes. Between the radial vanes are channels through which heated sodium can pass. These were designed for maximum heat transfer surface to minimize the time constant for heating the interfaces between the assembly and yoke. These yokes are fastened to the upper support structure permitting suspension of the rod within the yoke tube. Figure 7 is a photograph of the magnet assembly detached from the yokes. The photograph of Figure 8 also shows the disassembled magnet assembly.

2. Basic Requirements for Tests

To achieve the objectives of the testing program, the structure and apparatus were constructed in a manner to facilitate collection of data. The structure incorporated a technique for raising and positioning the rod which protruded from the interior of the container holding the yoke tube. The container was fitted with heaters to supply the ambient temperature conditions needed under an inert gas environment. A jack located at the top of the rod was used to exert the force needed to break the rod away from the magnet. The jack was also fitted with a Dillon force gauge

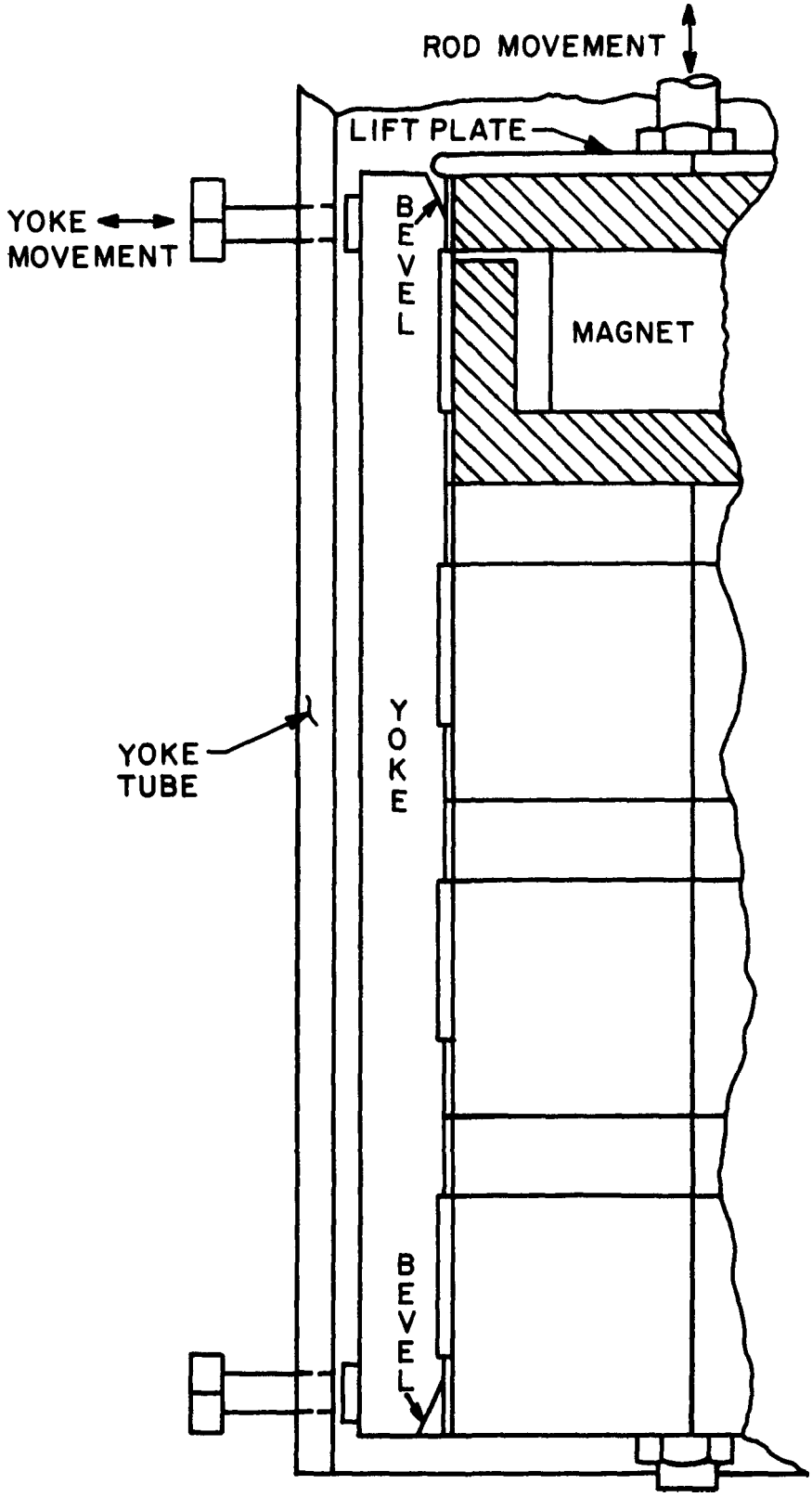

FIGURE 6: Cross-Section of Magnet and Yoke Used in Experimental Rig

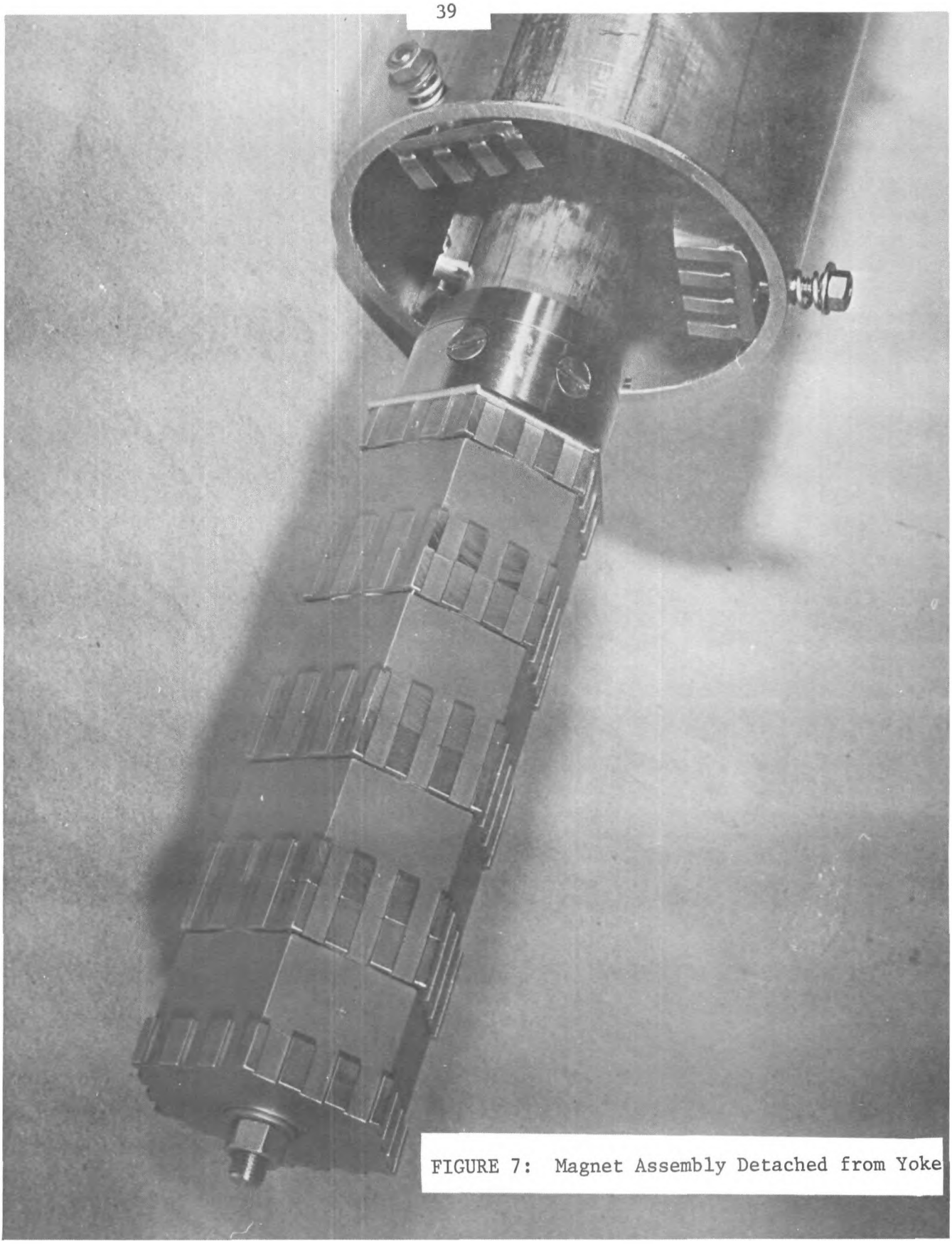

FIGURE 7: Magnet Assembly Detached from Yoke

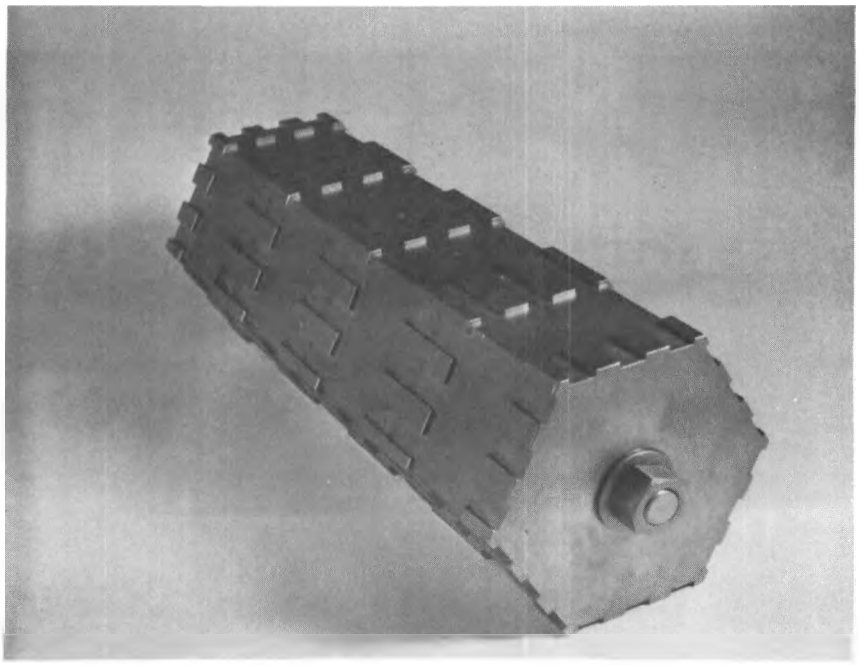

(a) ASSEMBLED

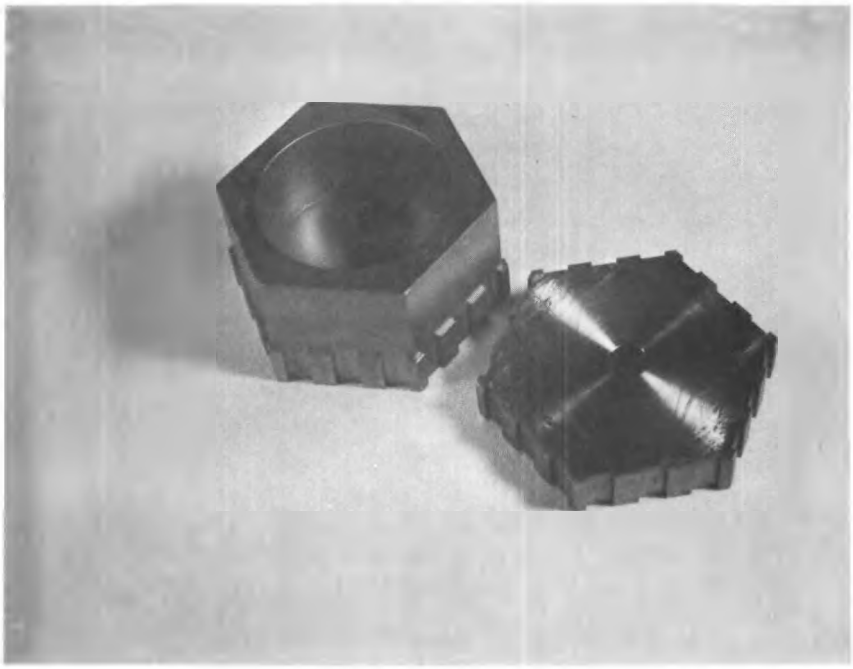

(b) DISASSEMBLED
HEXAGONAL BOX AND POLE PIECE

FIGURE 8: Magnet Assembly

which gave a reading of the required breakaway force.

3. Analysis of Heating Time for the Radial Vane Design

A 2-D computer calculation of the test assembly shows that the Curie point would be reached in less than 2.0 sec with the temperature rising parabolically from 520°C. The basic model for the operation of the SASS test device was taken to be a single unit with the yokes heated by sodium flowing upward at 26 ft/sec. However, since the controlling factor is the thermal diffusivity of the carbon steel, the sodium can be stagnant and still attain high heat transfer. Figure 9 consists of a series of curves calculated for stagnant sodium at 770°C using a standard numerical method. The curves show the temperature profile from one face to the interior of the yoke for various time intervals after immersion starting at 520°C. They also indicate that the Curie point is rapidly approached in less than 0.5 seconds. Thus it was decided that the immersion method should be satisfactory for the proof of principle test. This method was consequently adopted for the program.

C. Description of Test Apparatus and Operation

A schematic of the apparatus is shown in Fig. 10. In this figure, the central, cylindrical, rod is securely fastened to the top of the magnet stack. The magnets contact the yoke along three alternate faces, four yokes per face. The yokes are fastened to the inner surface of the yoke tube. The rod rides in bearing guides mounted in the yoke tube moving in a vertical direction. The yoke tube also moves vertically in bearing guides in the furnace tube and is limited in its travel by the trunion supports. The entire structure is supported above the sodium container. Upper concentric electric heaters, thermally insulated, are located at the yoke suspension zone. These heaters serve to keep the yokes and magnets at an ambient temperature of 520°C.

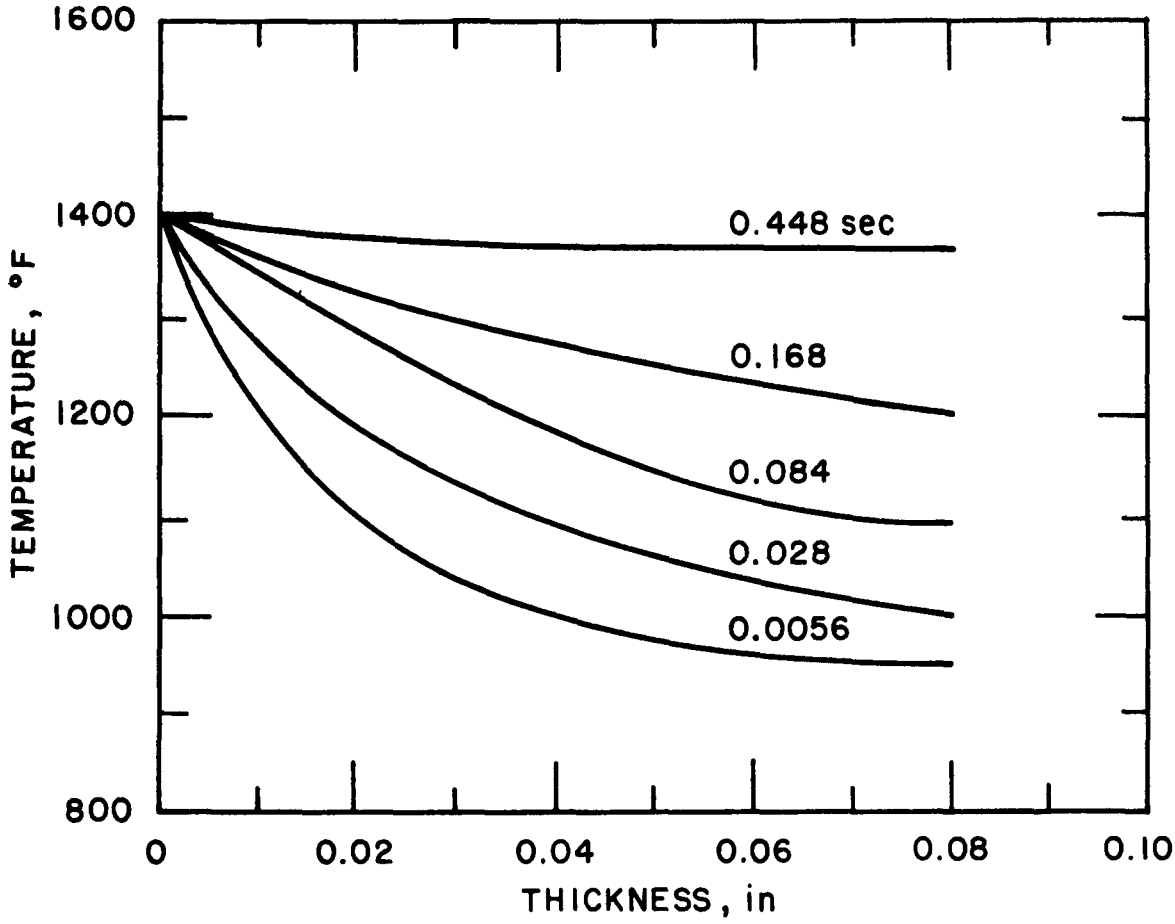

FIGURE 9: Calculated Temperature of Yoke After Sodium Immersion (Sodium Temperature Constant)

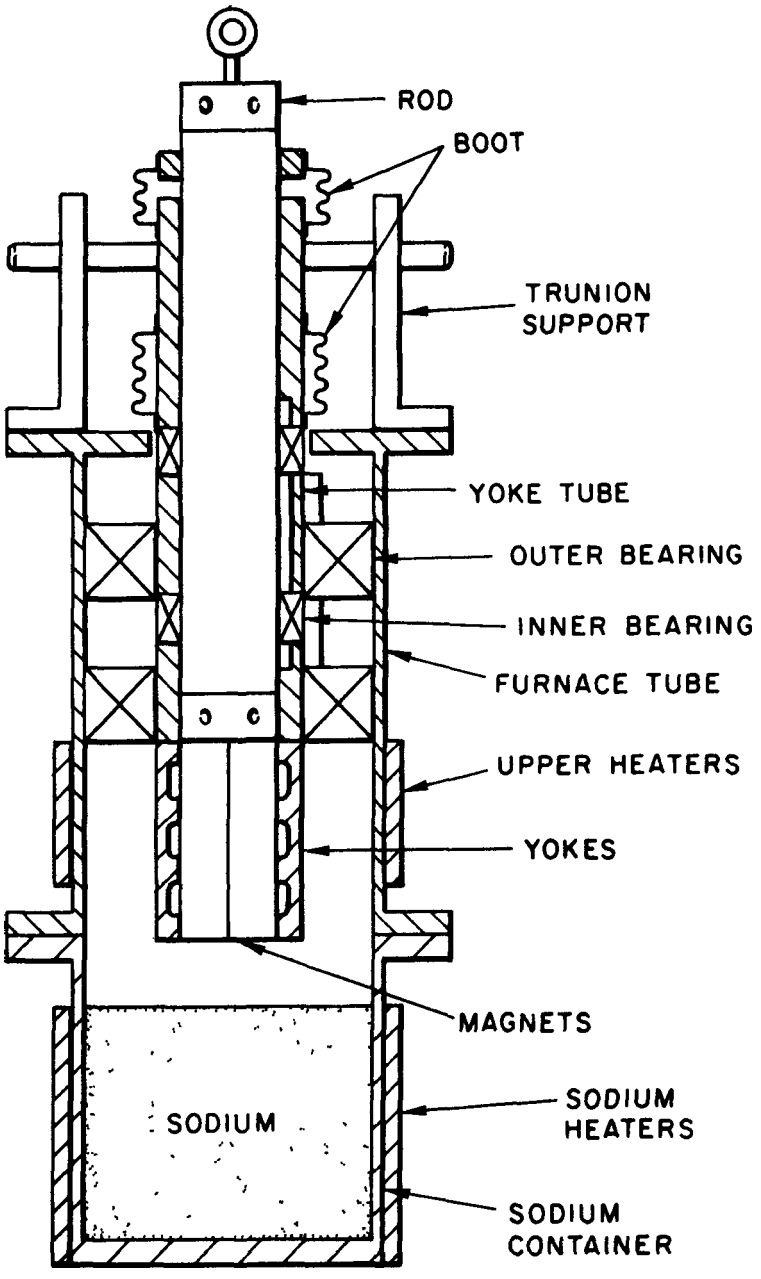

FIGURE 10: Sketch of SASS Test Fixture

Lower heaters around the sodium container are used to raise the sodium above the yoke Curie temperature prior to immersion of the yoke tube. The entire structure is supported by means of a unistrut tower located above a pit in the laboratory. An automobile-type jack connected to the Dillon compression gauge is mounted above the top of the rod. This jack is used to apply a downward force on the upper end of the rod for breakaway tests. The magnitude of the force is recorded on the Dillon gauge.

The interior of the apparatus is pressurized with argon gas. The interior is also isolated from exposure to the atmosphere by means of a bellows at the top. The bellows allows free movement of the rod and yoke tube. After release the rod is brought to rest by means of shock absorbers.

D. Instrumentation

The temperatures in the upper and lower zones are measured with chromel-alumel thermocouples connected to strip chart recorders. The temperatures are controlled by means of variacs which supply power to the resistance heaters.

A Dillon compression gauge with a maximum step pointer is used to read the maximum force at breakaway. The range of the Dillon gauge is 0-1000 kilograms.

The rod is connected to a microswitch in series with an electric clock. During the test a spurious drop of the rod would interrupt the power to the clock if this should occur during off-hours.

The time for the rod to drop after immersion was measured with a counter connected to two microswitches. The counter is turned on at the time of the immersion of the yoke tube in the sodium. The couter continues to record counts until the rod releases and falls. Dropping of the rod triggers a second microswitch which turns off the counter.

E. Experimental Plan

The experimental plan was based upon the following sequence:

(a) Initial delivery of the components was followed by examination and checking to see that proper fits and clearances were obtained. At this time, the superstructure was constructed and the apparatus was erected.

(b) The first measurements consisted of a series of room-temperature breakaway tests to establish base data along with a determination of statistical variability.

(c) After these measurements were completed, the upper heaters were energized and the yokes and magnet assembly raised to an ambient temperature of 520°C. When this temperature was reached and thermal equilibrium attained, another series of breakaway tests were made at the elevated temperature for comparison.

(d) The system was held at this temperature for more than a week to see if spurious drops would result. During this period, breakaway measurements were taken from time to time to determine the variation in holding capability and to investigate whether any lasting offset was caused by the high temperature.

(e) Upon completion of these tests, the lower container was filled with sodium and heated to 770°C. At the same time the yokes and magnets were held at 520°C. With this thermal differential established, the low temperature yokes and magnet assembly were immersed in the higher temperature sodium. The time for the release was recorded. The yoke temperature was also recorded at the time at which the drop took place. Subsequently, the yoke tube was retracted to remove it from the sodium and to allow it to cool to the 520°C ambient. After relatching, the breakaway force measurement was repeated.

F. Discussion of Test Results

1. Bench Test Breakaway Force Measurement

Before the breakaway test was performed upon the test rig, the force required to separate the yoke from the magnet assembly was measured at the bench. The measured force was 339 kg for three yokes as shown in the photograph of Figure 7. The magnet and yoke contact area for the three yokes is 77.4 cm^2. This corresponds to a magnetic flux density level at the contact area of about 10,390 gauss as expected.

This measurement was repeated after heating the assembly for 24 hours at 520°C. A holding force of 237 kg was then measured at room temperature, equivalent to a magnetic flux density level of about 8690 gauss. This represents a 30% reduction in the holding force due to the heat treatment. However, the holding force is still more than enough to hold the magnet test assembly in place.

2. Modification of Test Assembly

The yokes are fastened to the bottom of the yoke tube but are spring loaded and free to move horizontally approximately one-half inch. As the rod is lifted into position, the magnet assembly enters between the yokes. The magnetic induction draws the yokes toward the magnet faces. In order to prevent the yokes from contacting the faces before the rod is drawn up fully, a hexagonal nonmagnetic lift plate was installed above the magnets (see Figure 6). The lift plate prevents the yokes from seating since it protrudes beyond the magnet contact faces. When the magnets are drawn up fully, the lift plate is situated above the yokes and, consequently, seating of the yokes takes place. This provides positive latching action.

Conversely, as the rod is pushed downward, the rounded end of the lift plate contacts the bevelled upper portion of the yokes (see Fig. 6). This contact of the inclined plane surface converts the downward force into a horizontal component which acts to lift the yokes from the magnet faces. When the yokes are lifted off, the magnetic circuit is abruptly broken and a positive release is obtained. The mechanical advantage of the inclined plane results in a lesser force being required to drive the rod downward than would be needed for direct detachment of the yokes by means of a force normal to the magnet contact faces. Because of this, the breakaway force measured in the assembly is less than that obtained in the bench testing by about one-half; this is due to the presence of the inclined plane of about 30° to the vertical.

It should be noted that the lift plate is a convenience for latching and for laboratory testing. It does not perform any function during the Curie temperature sodium immersion test of the rod.

3. Measurement of Breakaway Force in Test Rig

The breakaway force was measured in the test rig with the test assembly modification. At room temperature the breakaway force was 159.9 kg. This represents the sum of the applied force of 142 kg, plus the weight of the rod and magnets of 17.9 kg. The assembly was then heated to 520°C (968°F) and permitted to attain thermal equilibrium. The breakaway force at the elevated temperature was measured to be 143.9 kg, which is 90% of that observed at room temperature. This value was observed during ninety breakaway tests performed periodically over an eleven day heating period at 520°C with a variability of ± 10%. No deterioration of the breakaway force over the eleven day time period at the elevated temperature of 520°C (968°F) was detected. This is approximately the

temperature environment in the CRBR at the core outlet.

After each of the high temperature breakaway tests, the assembly was relatched. No spurious drops occurred at any time during the eleven day period.

4. Immersion Tests in High Temperature Sodium

Two immersion tests were carried out in high temperature static sodium. When the first test was performed, the upper heater was not operating. The magnet and yoke temperatures were therefore originally at 105°C. The yoke tube carrying the yoke and magnetically latched assembly was immersed in the sodium which was maintained at 793°C by the bottom heater. After immersion, the yoke temperature rose to 767°C, just below the Curie point of low carbon steel. At this time the assembly was released and dropped out of the yoke tube.

When the yoke was removed from the sodium, its temperature decreased to 587°C. The magnet assembly and rod were then pulled up into the yoke tube where it was relatched and held firmly to the yoke. The immersion test could not be repeated at this time since heater arcing required the sodium heater to be shut down.

Subsequently, a second immersion test was carried out with the magnet initially at 528°C, since the upper heater was now operating. The sodium in the container was maintained at 800°C. After immersion of the yoke tube, the yoke temperature rose eventually to 758°C when the drop occurred.

It was not possible to measure the time constant of the device in this test set-up. After immersion the sodium temperature decreased at first to 720°C. This temperature is far enough below the Curie point of

770°C so that the rod was not released. The temperature decrease in the sodium was caused by the absorption of heat by the yokes, magnets, and yoke tube. Continued heating eventually raised the temperature of the yokes so that the release occurred at 758°C. It took approximately ten minutes to heat the system from 720°C to 758°C. This heat-up time is dependent upon the heating capacity of the heaters and the heat losses from the test fixture. The situation would, of course, be much different in a reactor which would act like an infinite heat source.

It was not considered desirable to perform the test with the sodium initially at a higher temperature since the sodium boiling point is 883°C. Another possibility for measuring the time constant of the device is to use a liquid metal with a higher boiling point than sodium.

After the second immersion test, it was found that, upon cooling down to room temperature, the magnet could not then be relatched. Heating the magnet over a relatively long period of time at about 1350°F (730°C) had undoubtedly contributed to the degradation of the magnetic properties of the Alnico V. This is to be expected since Alnico V begins to loose its stability somewhat above 1000°F (538°C) if exposed for extended periods of time.

5. Conclusions and Recommendations

The following have been demonstrated:

(1) The holding force is about that expected from the magnetic holding force formula. This has been proved by the breakaway tests.

(2) The assembly will be held positively in place at elevated temperatures below the Curie point over extended periods of time without spurious trips.

(3) Over the period tested, the holding force stabilized within a variability of $\pm$ 10%.

(4) When the yoke and assembly approach the carbon steel Curie point of 770°C, the magnetic force is diminished and the assembly drops.

(5) After cooldown of the assembly and yokes to a temperature substantially below the Curie point the magnetic force was restored and the assembly relatched. This proves the recockability of the device. However, if the device were exposed to high temperatures (well above 1000°F) for an extended time period, it might loose its magnetism and not be recockable. This could occur only if there were a severe accident condition, in which case the ISA would have already performed its function and would be replaced before returning to power.

These tests demonstrated the proof of principle that a ferromagnetic Curie point ISA magnet could be depended upon to hold an absorber assembly at reactor ambient and release it into the core when the yoke approaches the Curie point.

Recommendations for the future would include fabricating an assembly in which the yokes can be heated electrically so that tests can be readily repeated. Also installation of a simulated unit in an operating reactor for a long period of time should be considered in order to test whether spurious trips occur in situ under reactor temperature, radiation, and flow environments.

Neutron excursion trip tests in a reactor such as TREAT would also be desirable.

V. ACCIDENT ANALYSIS IN SUPPORT OF SASS DESIGN

A. Description of Accident Analysis

Accident analyses were carried out (based on an LMFBR very similar to the current design of the CRBR) to evaluate the performance of a self-actuated, self-contained shutdown system (SASS), particularly its capability to avoid core damage for various types of accident initiators. These accident analyses were performed using ANL's SAS computer code.

Table 2 summarizes the various computer runs. For all runs, the insertion of negative reactivity was initiated 0.5 sec after reaching the trip point, and was assumed to be approximately linear, at a rate of -8 $/sec up to a value of -4.0$.

Figures 11 to 21 show some of the information obtained for the eleven computer runs. They are placed at the end of this section. For each computer run, five graphs are given except for Run No. 10 where one additional graph is included to show initiation of boiling in the hottest channel. Coolant and fuel temperatures, respectively, at the core outlet and at the core midplane, are given as a function of time for the hottest channels (denoted in the graphs by channel type 2), which in CRBR are slightly off-center in the core. Also, some of the reactivity components (Doppler, coolant, etc.) are presented.

B. Results and Conclusions

From the analyses performed, the following conclusions can be drawn:

TABLE 2. List of Accident Analyses Performed

Run No.	Fig.No.	Accident Initiator	Run Description
(1)	11	TOP	10¢/sec up to $3.00 with scram (SASS)†
(2)	12	TOP	10¢/sec up to $3.00 without scram
(3)	13	TOP	30¢/sec up to $3.00 with scram (SASS)
(4)	14	TOP	30¢/sec up to $3.00 without scram
(5)	15	TOP	50¢/sec up to $3.00 with scram (SASS)
(6)	16	TOP	50¢/sec up to $3.00 without scram
(7)	17	TOP	step of 50¢, at power, with scram (SASS)
(8)	18	TOP	step of 50¢, at power, without scram
(9)	19	LOFA	all pumps, with scram (SASS)*
(10)	20	LOFA	all pumps, without scram
(11)	21	LOFA	all pumps, with scram (SASS)*

†For all TOP analyses with scram, the trip point was assumed to be 150% of nominal power.

*For the LOFA analyses with scram, pertaining to runs 9 and 11, the trip points were assumed to be, respectively, 750°C (1382°F) and 800°C (1472°F) for the coolant outlet temperature.

(a) For all of the above postulated transients, core damage can be averted by means of SASS for the assumed combination of values for trip level, delay time, and rate of reactivity insertion. The maximum values reached for the fuel centerline and coolant temperatures for runs (1), (3), (5), (7), (9), and (11) are given in Table 3.

TABLE 3. Results of Accident Analyses - Maximum Fuel Centerline and Coolant Temperatures

Run No.	Run Description	Max Centerline Fuel Temp. (°C)	Max Coolant Temp. (°C)
(1)	Ramp 10¢/sec	∿2450	∿640
(3)	Ramp 30¢/sec	∿2260	∿620
(5)	Ramp 50¢/sec	∿2240	∿610
(7)	Step 50¢ (at power)	∿2220	∿600
(9)	Coastdown (trip at 750°C)	∿2010	∿760
(11)	Coastdown (trip at 800°C)	∿2020	∿810

(b) If one imposes as a limit that no fuel melting may occur in the centerline of the hottest fuel pins, then one finds for the allowable combinations of delay time and trip level the values listed in Table 4.

TABLE 4. Results of Accident Analyses - Limits to Avoid Fuel Centerline Melting

Run No.	Run Description	Delay Time (sec)	Trip Level (% of nominal power)
(1), (2)	Ramp 10¢/sec	0.5	∿180
		1.0	∿175
		2.0	∿160
(3), (4)	Ramp 30¢/sec	0.5	∿220
		1.0	∿190
		2.0	∿150
(5), (6)	Ramp 50¢/sec	0.5	∿250
		1.0	∿200
		2.0	∿120

(c) Table 5 gives the combinations of values for the delay time and the trip level which are permissible for the assumed pump coastdown characteristics, if one imposes the limit that no coolant boiling may occur in the hottest channels.

TABLE 5. Results of Accident Analyses - Limits to Avoid Coolant Boiling

Run No.	Run Description	Delay Time (sec)	Trip Level (°C at Core Outlet)
(9), (10), (11)	Pump Coastdown (all pumps)	0.5	∿925
		1.0	∿915
		2.0	∿900
		3.0	∿880

(d) If one imposes the limit that the coolant temperature may not exceed 750°C in the hottest channel, then one finds for the allowable combinations of the delay time and the trip level the values listed in Table 6.

TABLE 6. Results of Accident Analyses - Limits to Avoid Coolant Temperature > 750°C

Run No.	Run Description	Delay Time (sec)	Trip Level (°C at Core Outlet)
(9), (10), (11)	Pump Coastdown (all pumps)	0.5	∿730
		1.0	∿715
		2.0	∿685
		3.0	∿655

(e) Similarly, if one imposes the limit that the coolant temperature may not exceed 800°C in the hottest channel, then one finds for the allowable combinations of the delay time and the trip level the values listed in Table 7.

TABLE 7. Results of Accident Analyses - Limits to Avoid Coolant Temperature > 800°C

Run No.	Run Description	Delay Time (sec)	Trip Level (°C at Core Outlet)
(9), (10), (11)	Pump Coastdown (all pumps)	0.5	∿780
		1.0	∿765
		2.0	∿735
		3.0	∿705

(f) The combinations of values for delay times and trip levels, presented in Tables 3 through 7 also give an indication of the sensitivity to changes in the insertion time of the SASS, since an increase of the insertion time by a certain amount can conservatively be traded against a decrease in the delay time by the same amount.

In summary, it can be concluded from the above that core integrity for the present CRBR design can be maintained (for the type of accident initiators considered) by means of self-actuated shutdown systems, without the need for either very short response times or very large insertion rates. It would appear that the range of response times and insertion rates required for protecting against core damage, or for keeping core damage within predetermined limits, are achievable without too much difficulty for an actual SASS design.

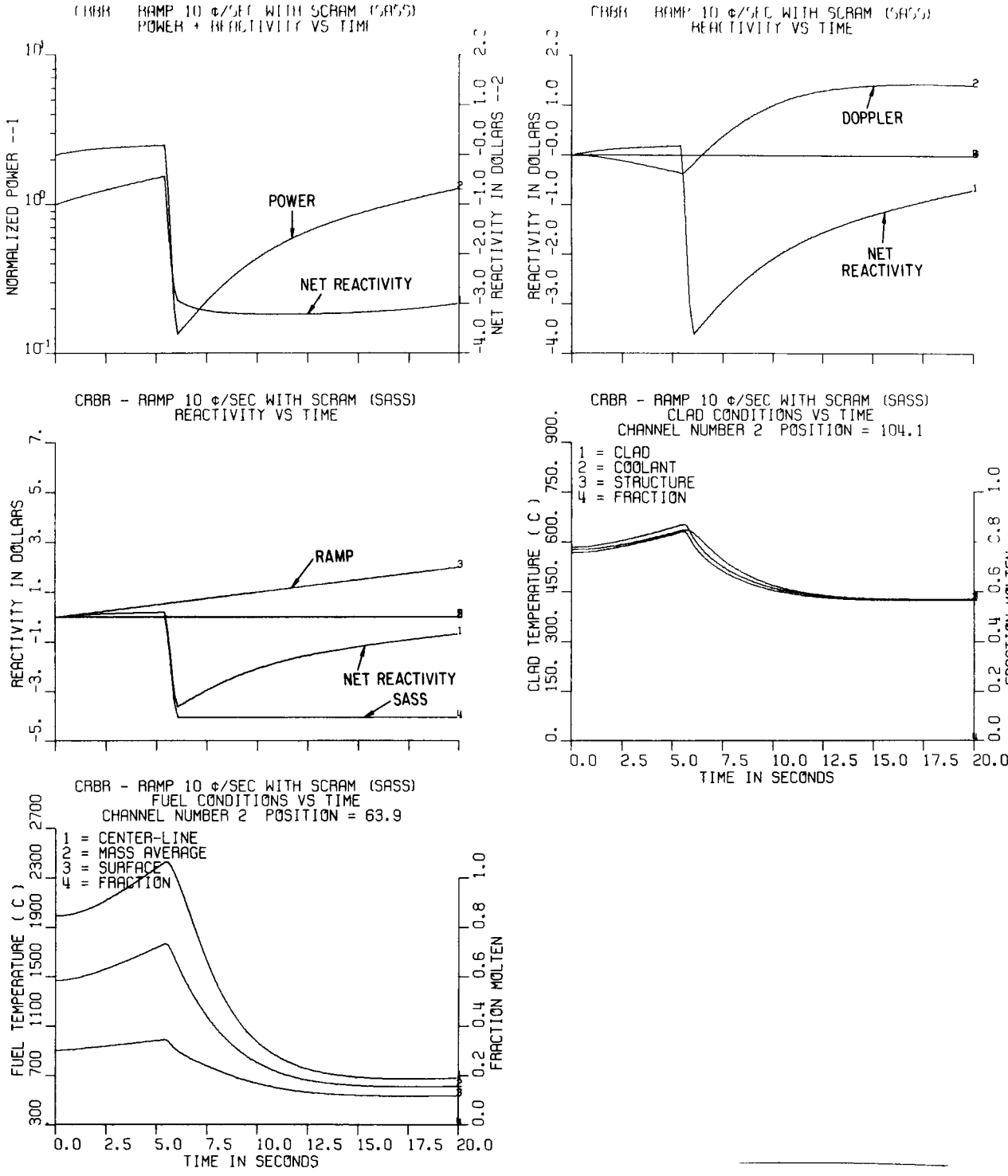

Run (1)

FIGURE 11: Ramp-type reactivity insertion of 10 ¢/sec, with reactor shutdown by means of SASS having trip-setpoint at 150% of nominal power.

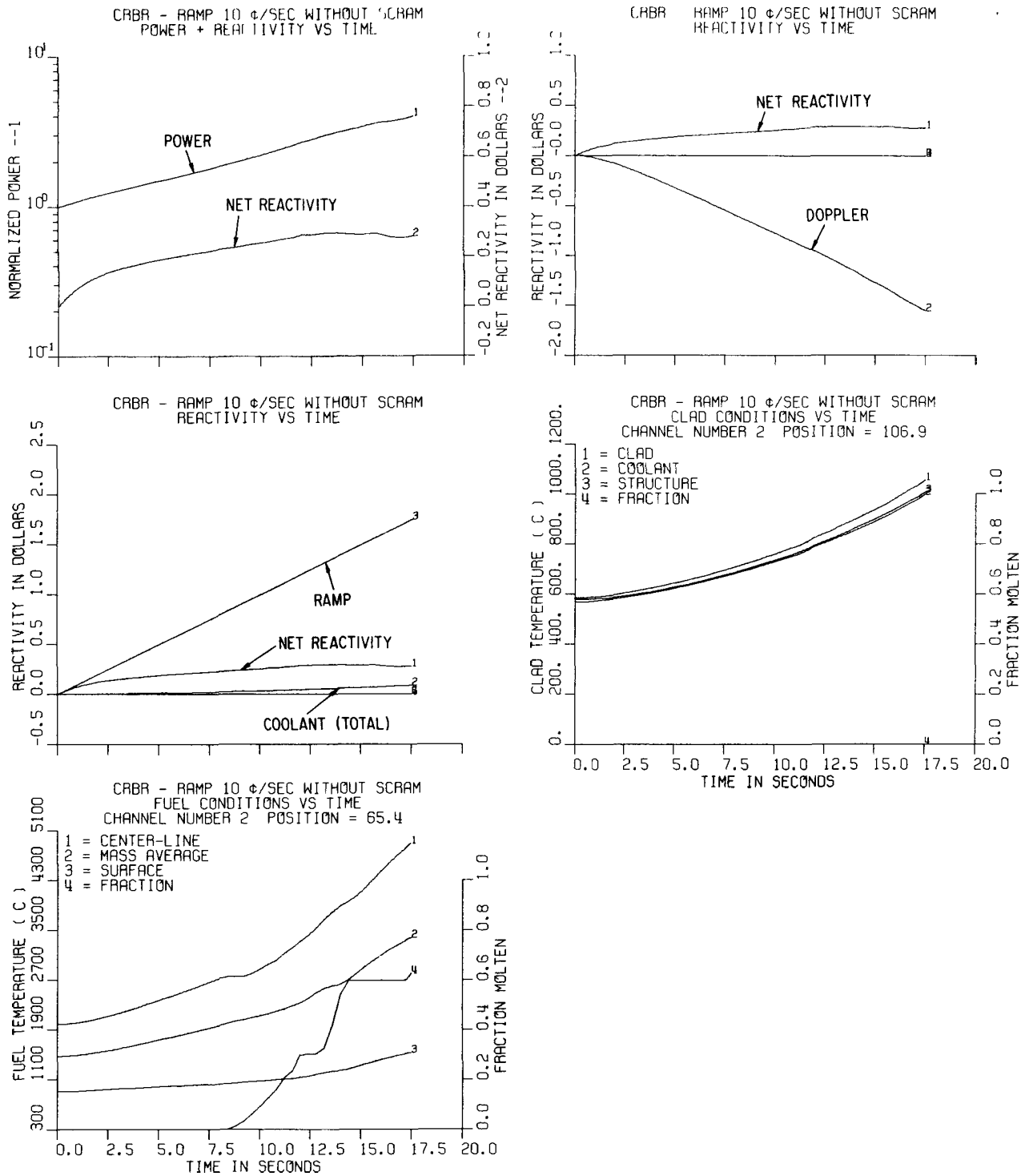

Run (2)

FIGURE 12: Ramp-type reactivity insertion of 10 ¢/sec, without reactor shutdown.

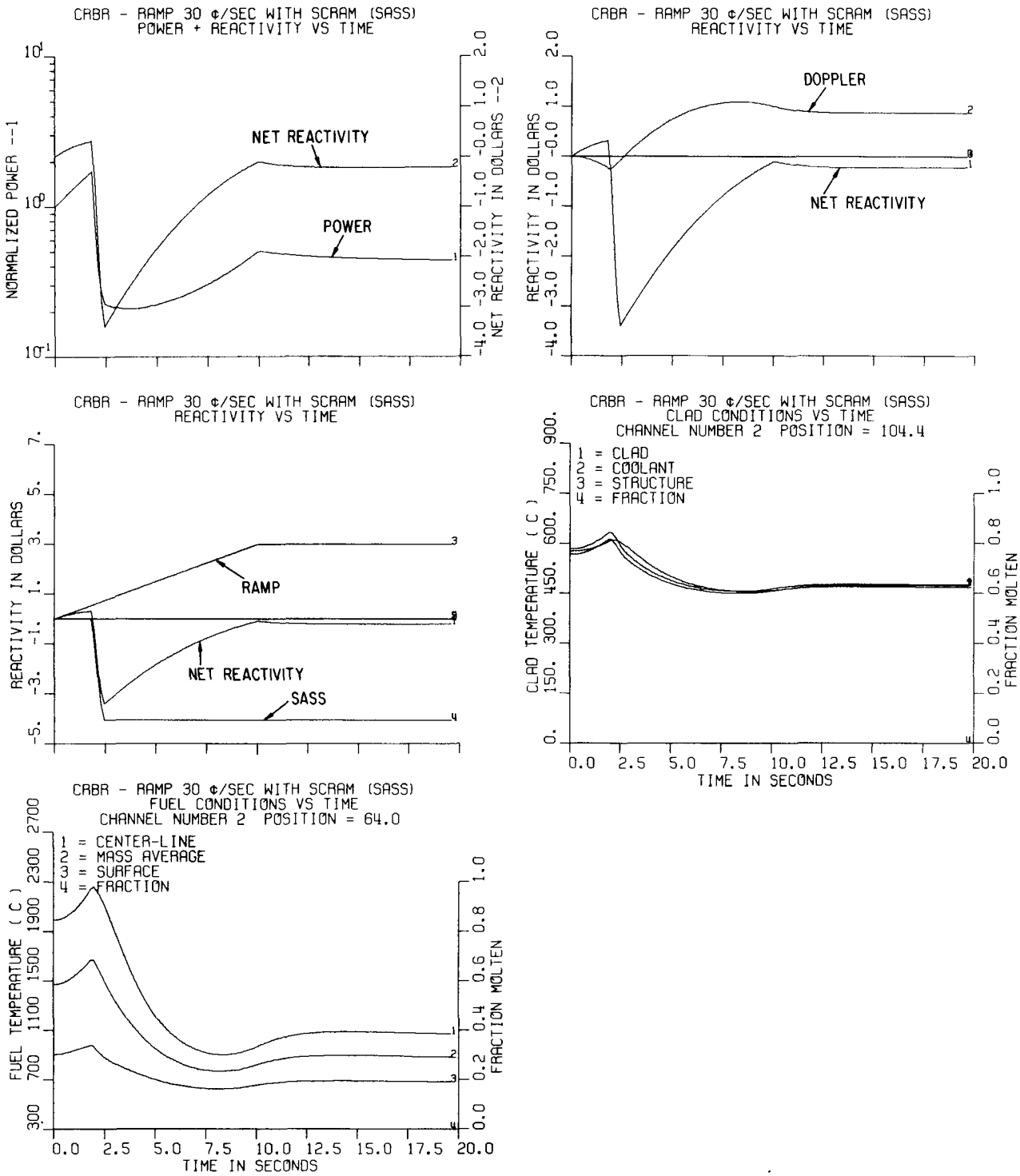

Run (3)

FIGURE 13: Ramp-type reactivity insertion of 30 ¢/sec, with reactor shutdown by means of SASS having trip-setpoint at 150% of nominal power.

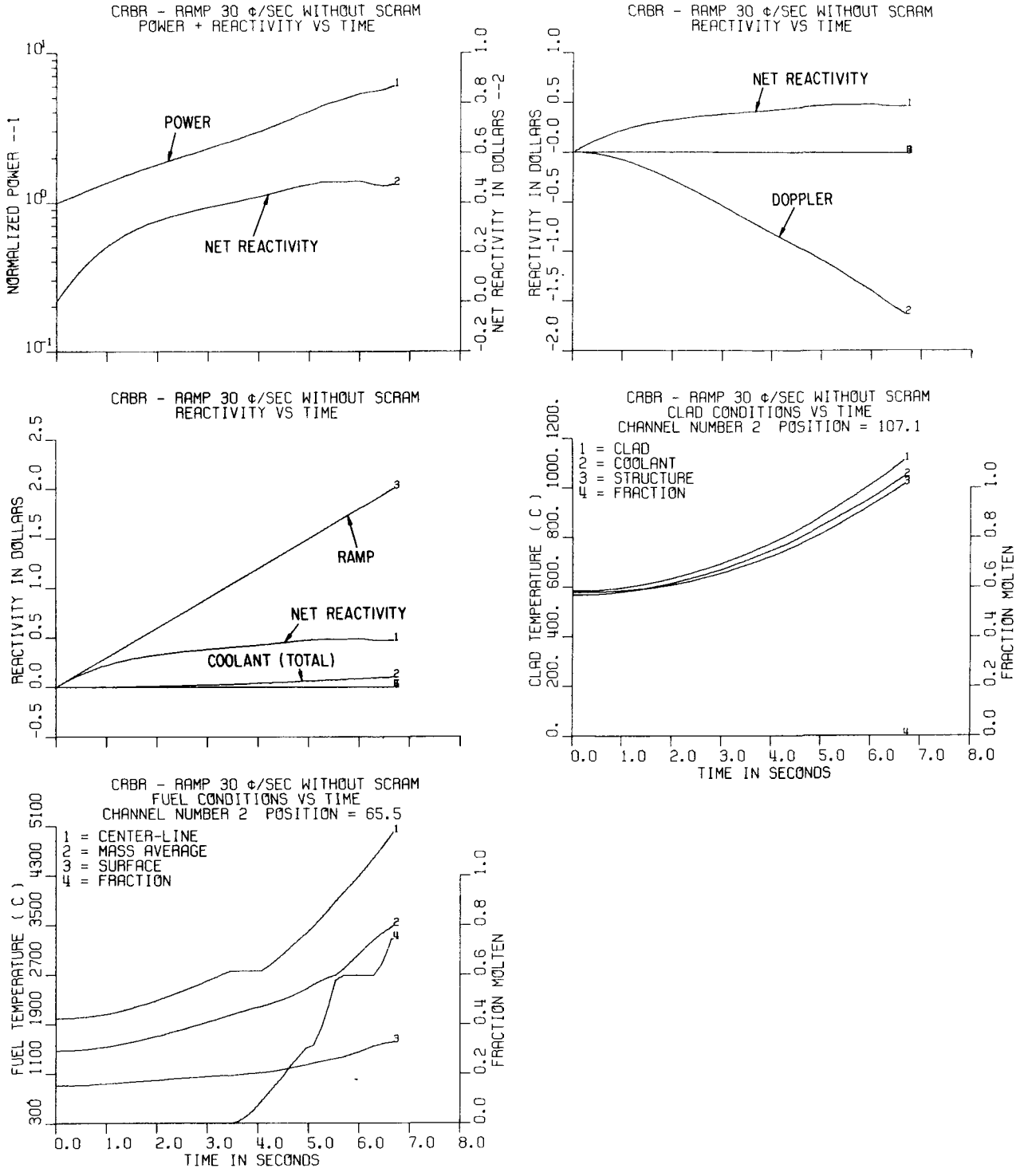

Run (4)

FIGURE 14: Ramp-type reactivity insertion of 30 ¢/sec, without reactor shutdown.

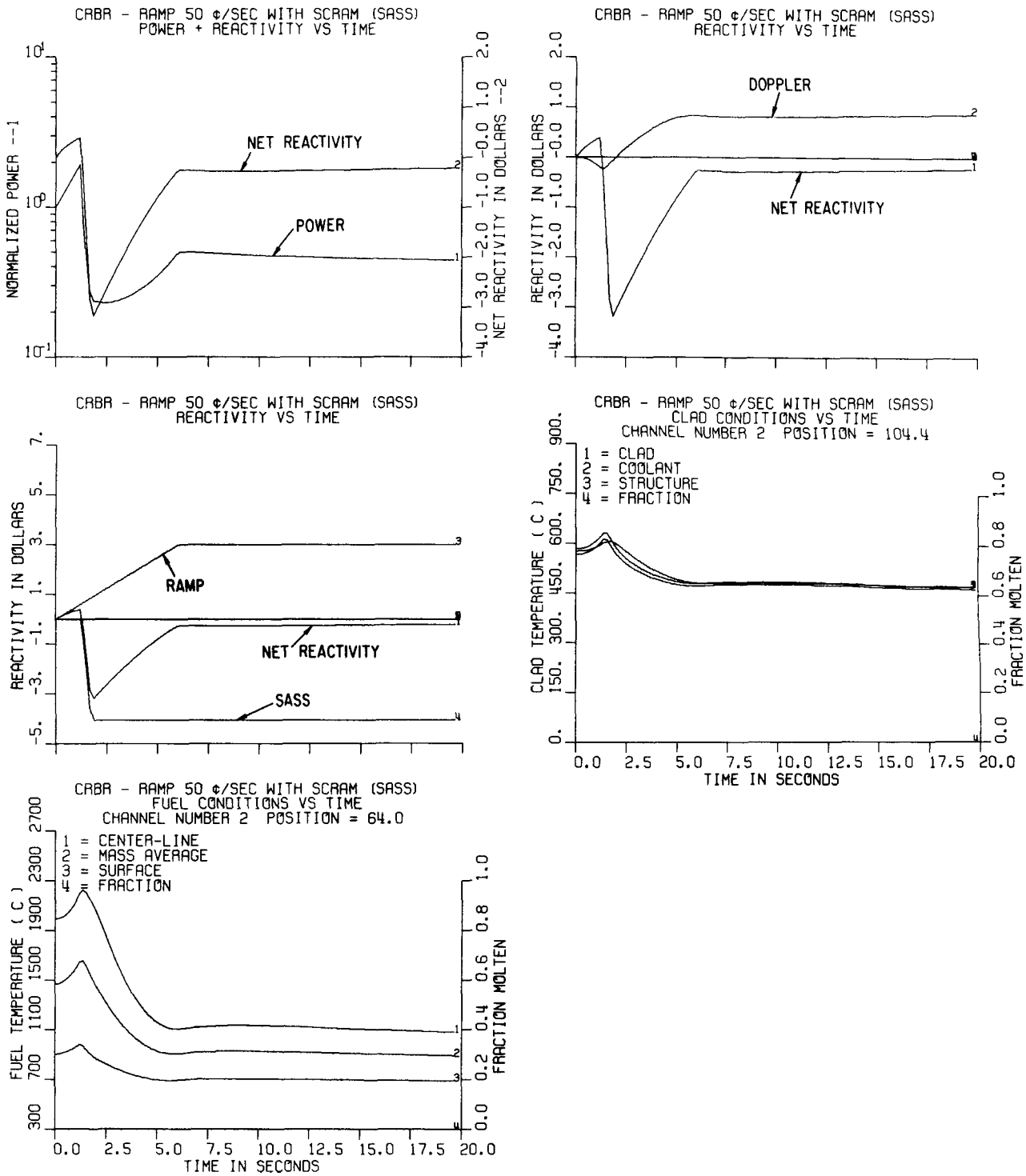

Run (5)

FIGURE 15: Ramp-type reactivity insertion of 50 ¢/sec, with reactor shutdown by means of SASS having trip-setpoint at 150% of nominal power.

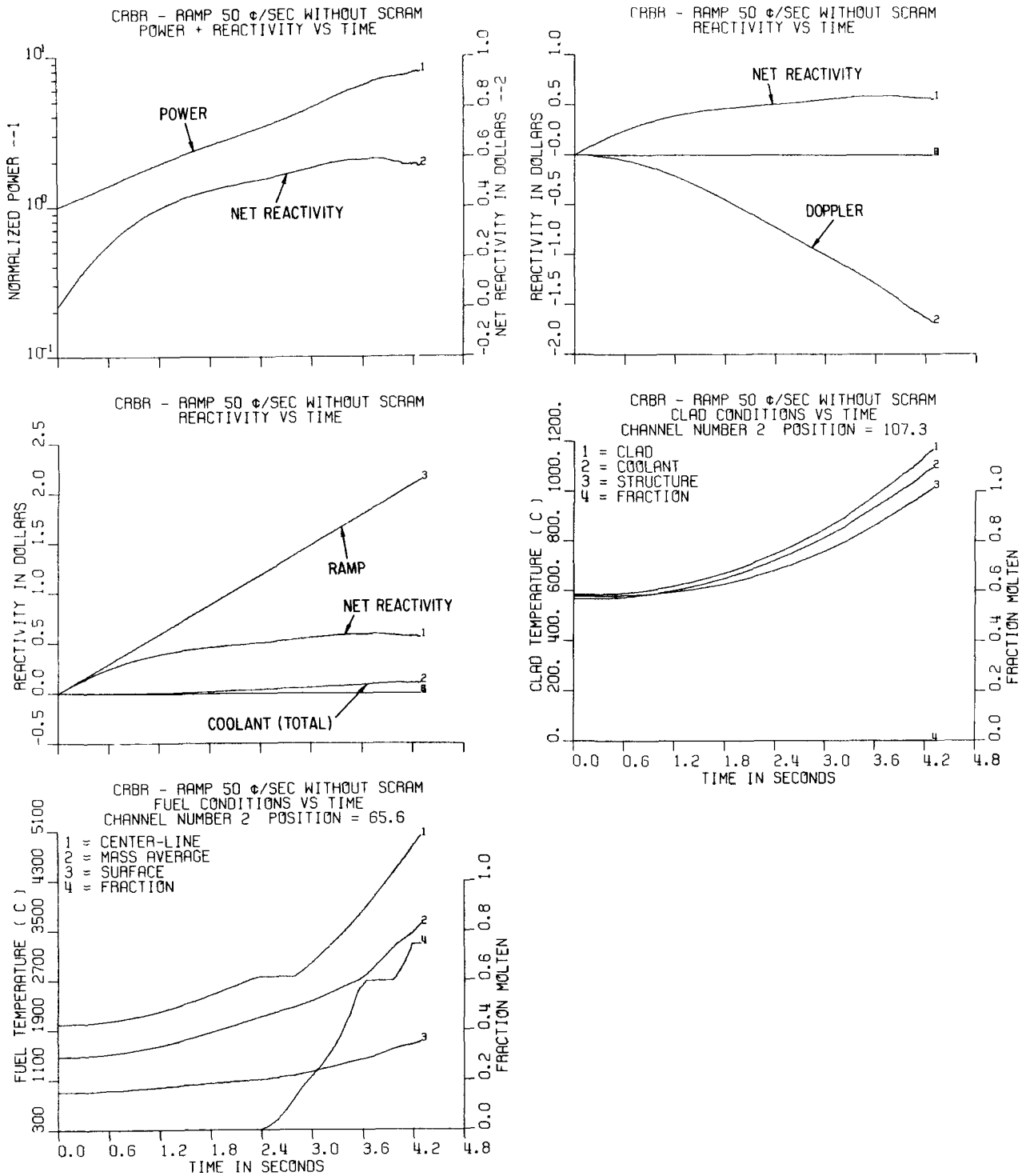

Run (6)

FIGURE 16: Ramp-type reactivity insertion of 50 ¢/sec, without reactor shutdown.

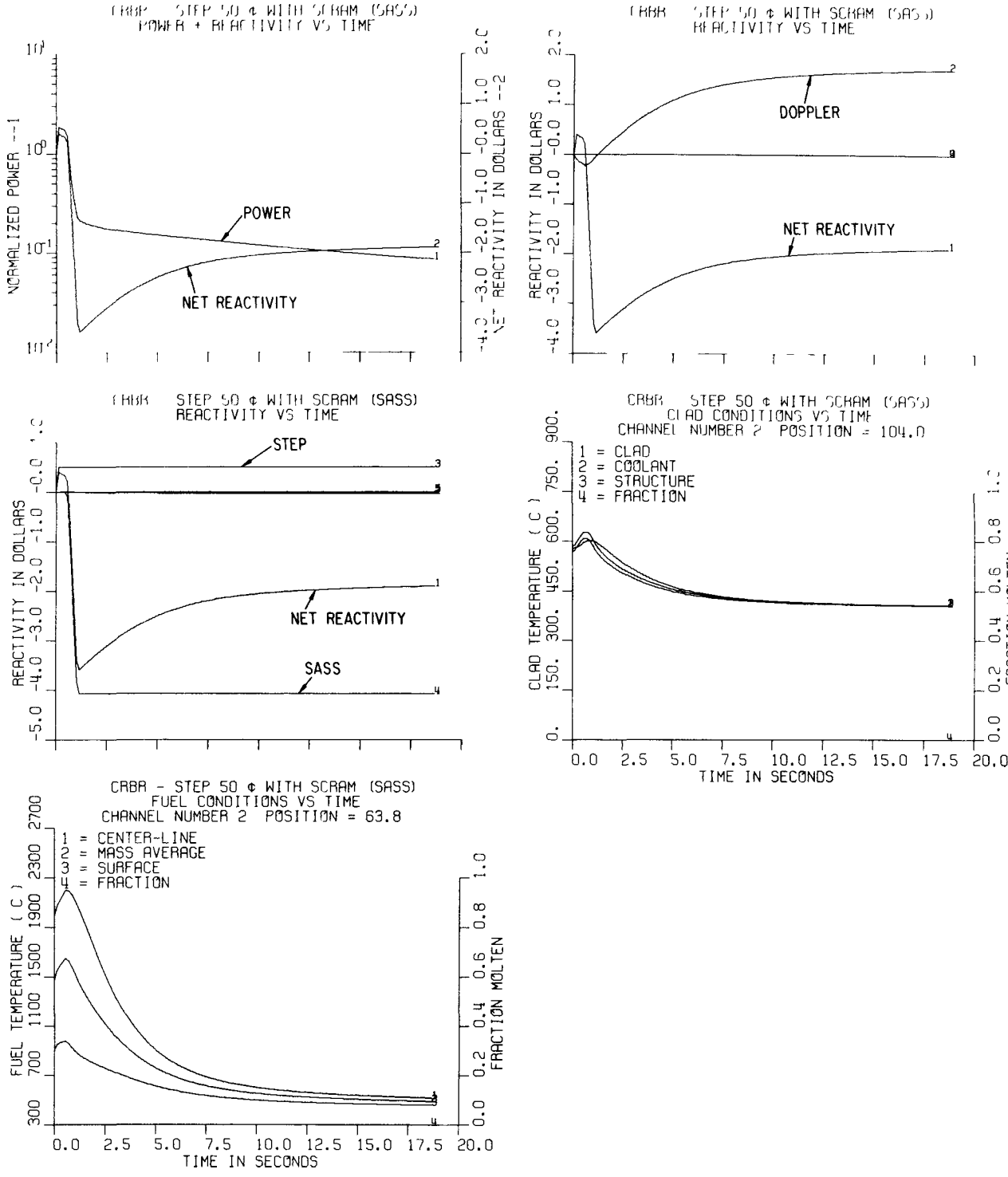

Run (7)

FIGURE 17: Step-type reactivity insertion of 50 ¢, with reactor shutdown by means of SASS having trip-setpoint at 150% of nominal power.

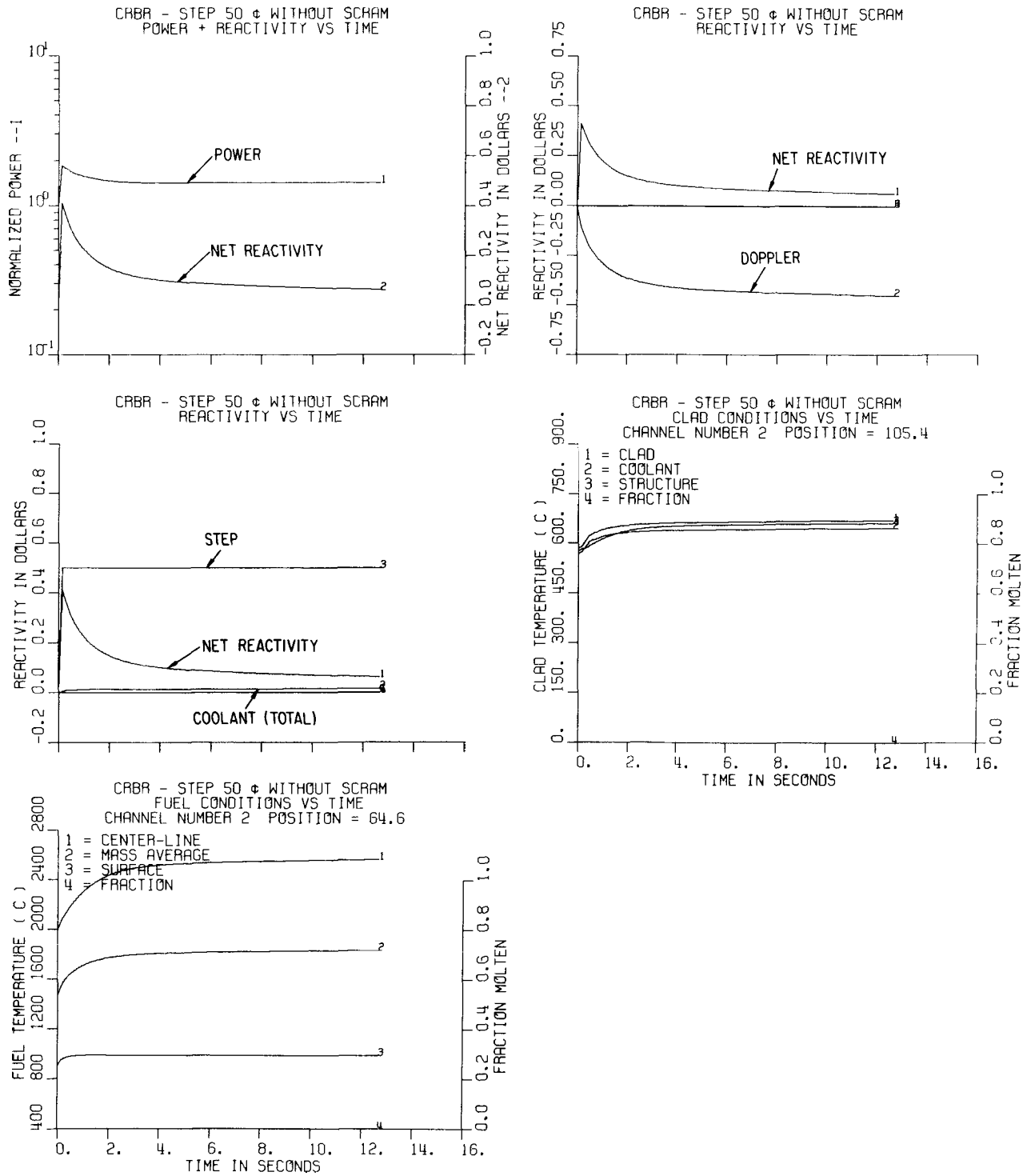

Run (8)

FIGURE 18: Step-type reactivity insertion of 50 ¢ without reactor shutdown.

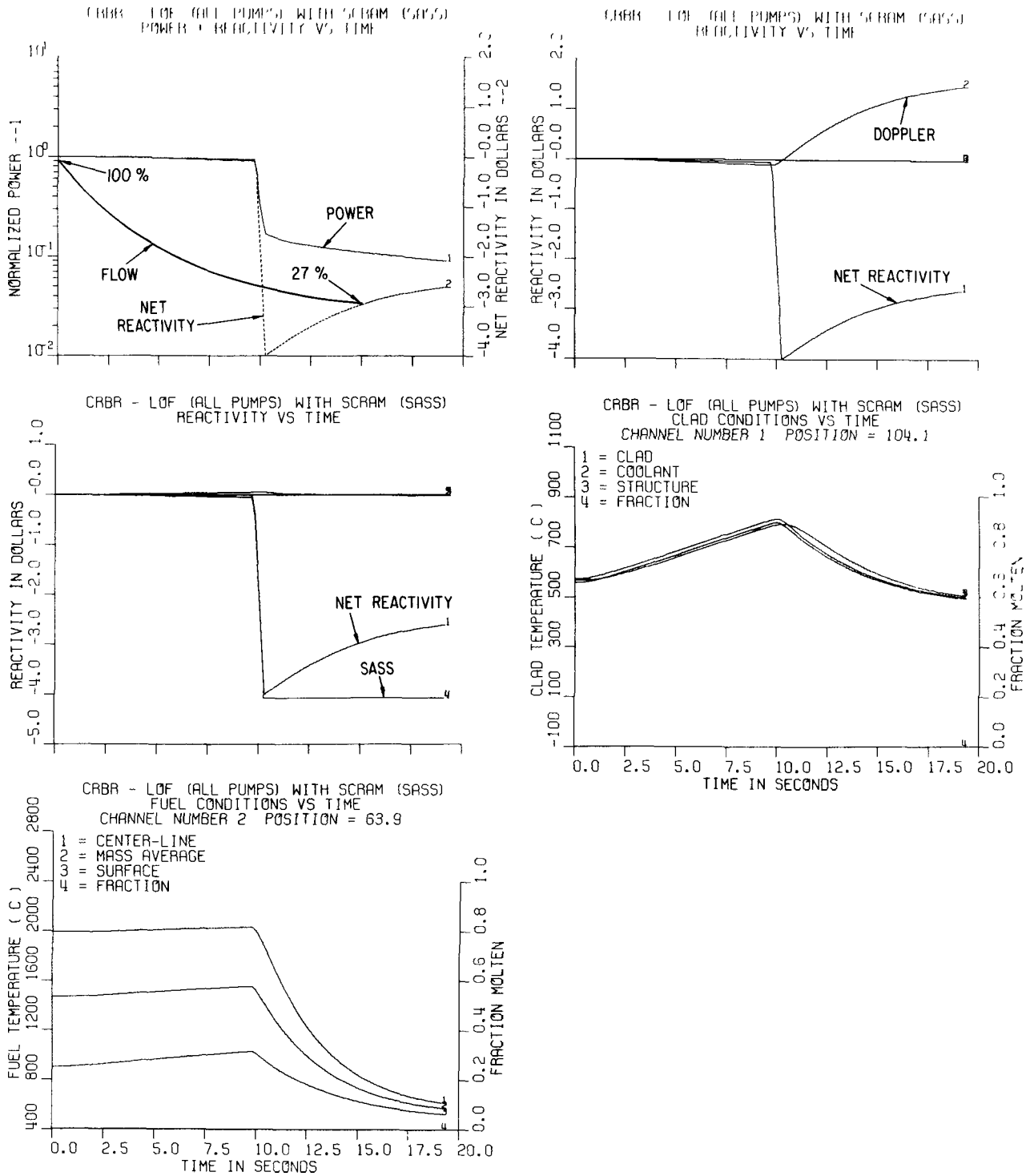

Run (9)

FIGURE 19: Coastdown of all pumps with reactor shutdown by means of SASS with trip on coolant outlet temperature at 750°C.

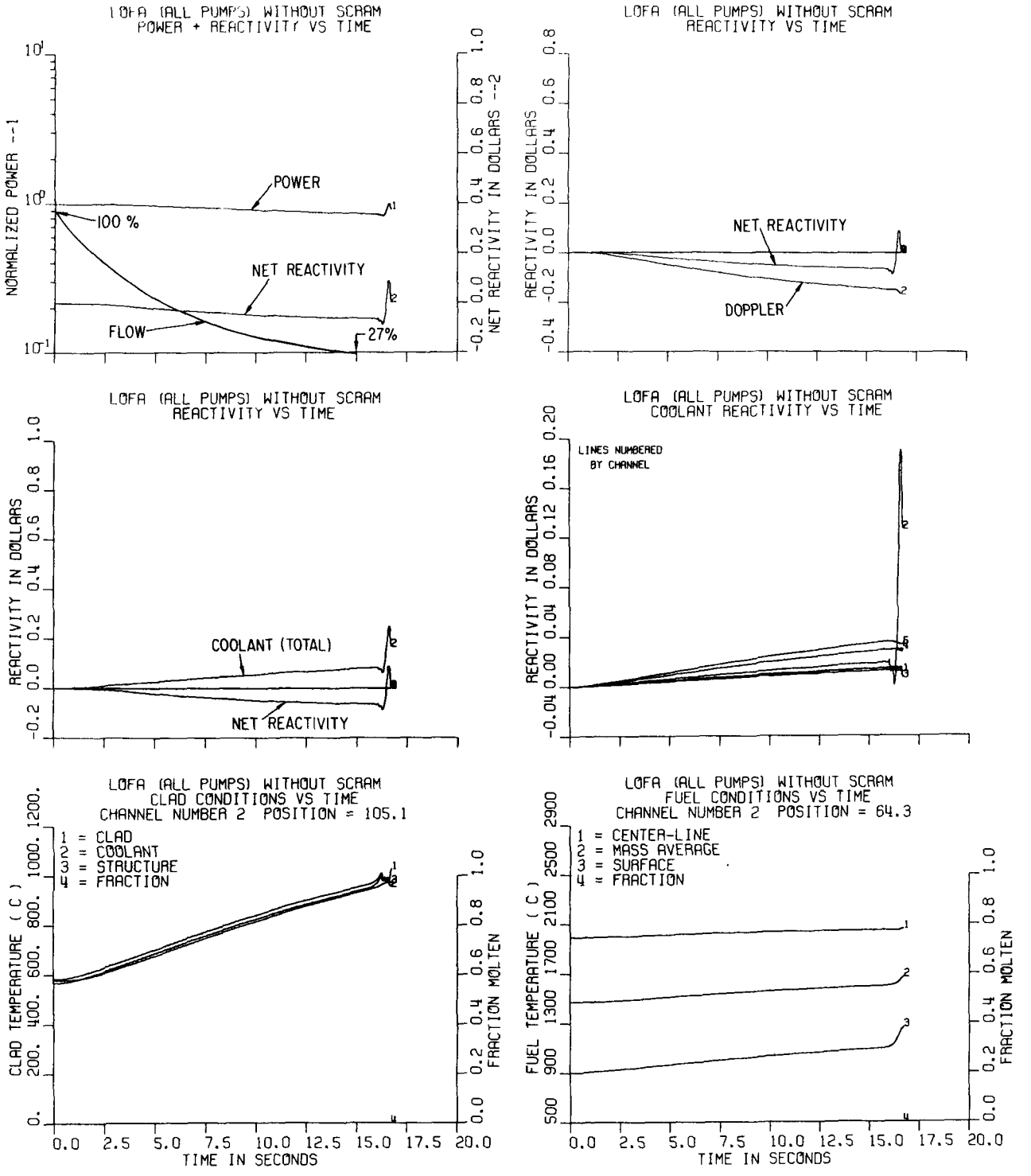

Run (10)

FIGURE 20: Coastdown of all pumps without reactor shutdown.

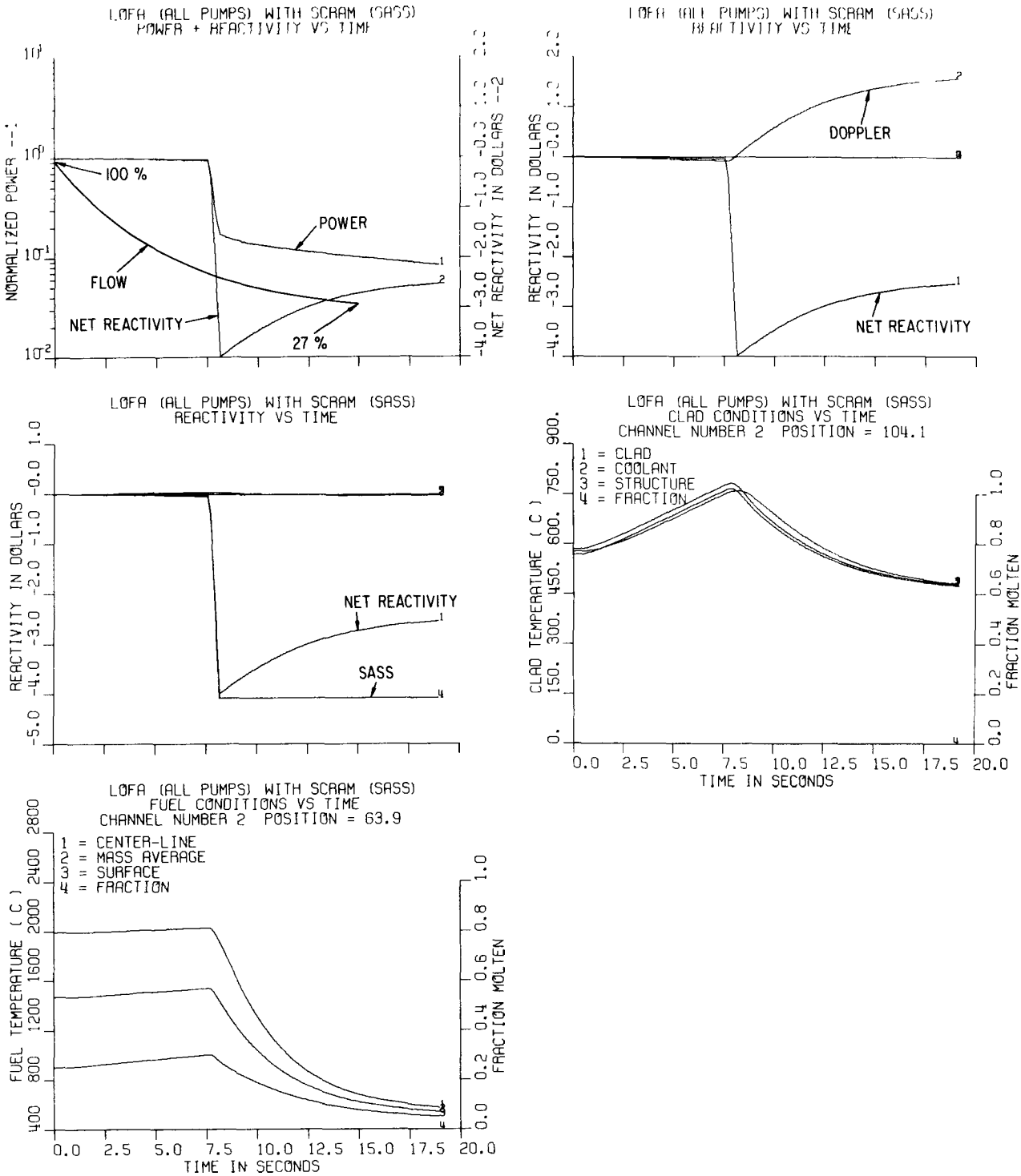

Run (11)

FIGURE 21: Coastdown of all pumps with reactor shutdown by means of SASS with trip on coolant outlet temperature at 800°C.

VI. REACTOR PHYSICS ANALYSIS OF SASS

The physics evaluation of the SASS in a CRBR environment included the determination of the optimum ISA absorber enrichment and position, and an assessment of the ISA impact on core parameters. In order to perform these calculations, a mockup of the CRBR first and equilibrium cores was synthesized. A general description of these models is given in Appendix III-A.

In addition, heating rates due to radiation deposition in the Alnico V magnet placed in the CRBR environment were also computed. The power generation to be expected from the fissile heat sources used in conjunction with the ISA for the detection of fast flux transients was also estimated.

A. ISA and CRBR Control Assembly Absorber Worths

It has been found that the overall ISA worth increases with increasing boron enrichment, but the relative gain in worth for an increase in enrichment becomes marginal at about a 75% B-10 enrichment as shown in Figures 22 and 23. This corresponds to approximately 3 kg of B-10 per ISA.

Using a B-10 enrichment of 75%, ISA worths were obtained for all CRBR inner core assembly positions. Table 8 gives ISA worths in dollars for both a first core and an equilibrium core. The corresponding assembly locations are shown in Fig. 24. The highest worth ISA positions are in the 5th fuel ring at (5,1) and (5,3) with respective worths of 3.38 and 3.37 dollars. The (5,1) position is undesirable because of the strong coupling with row 4 safety rods at position (4,1). From a maximum worth standpoint the (5,3) position is most desirable since it has a high relative worth and a minimum interaction with existing control

Table 8. ISA Worths versus Position in Core for 75% B-10 Enrichment

SASS Assembly Position	ISA Worth ($) First Core	ISA Worth ($) Equilibrium Core
(2,1)	1.682	1.467
(3,1)	2.584	2.328
(3,2) & (3,12)	2.348	2.096
(4,2)	2.694	2.455
(5,1)	3.380	3.201
(5,2)	3.163	2.956
(5,3) & (5,23)	3.372	3.150
(6,1)	2.843	2.746
(6,2)	2.974	2.841
(6,3)	2.451	2.306
(7,2)	2.329	2.261
(7,3)	2.211	2.118

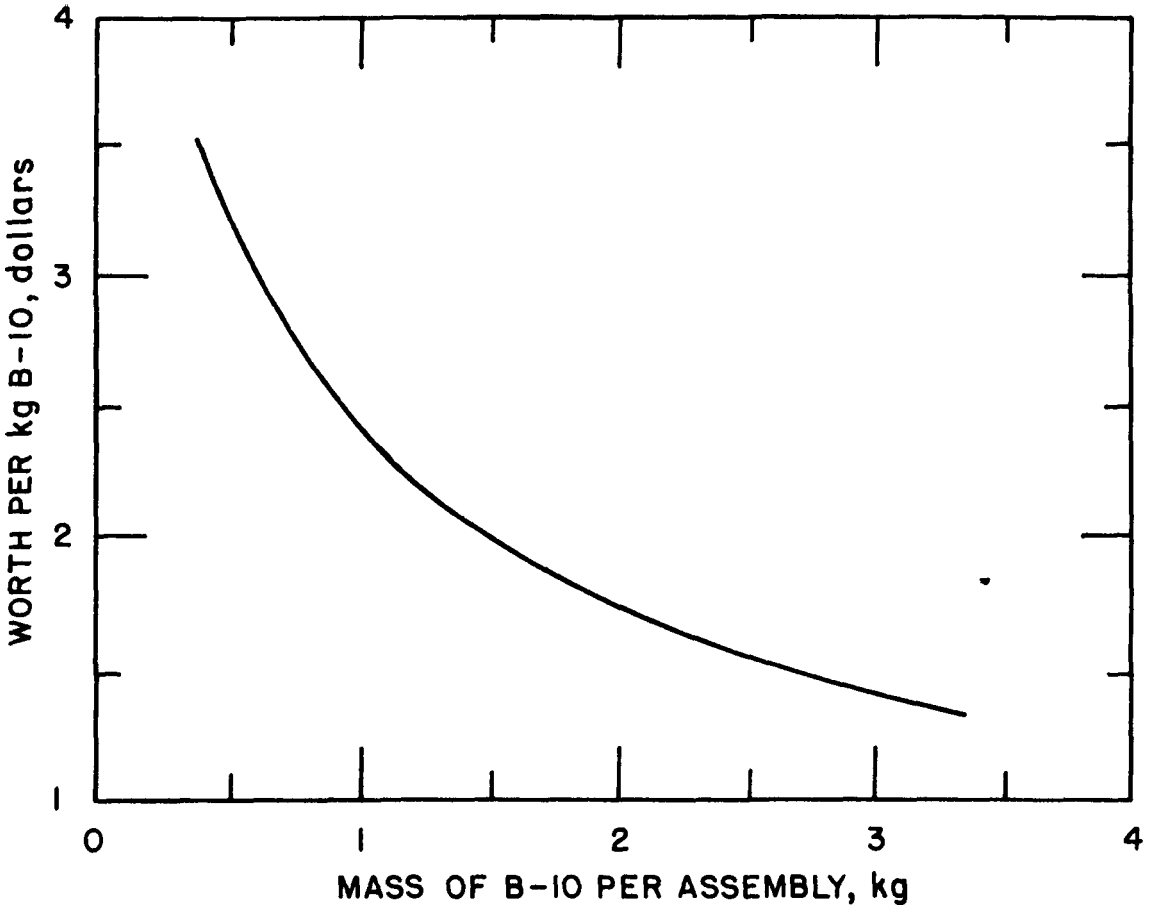

FIGURE 22: Specific ISA Worth vs. B-10 Mass per Assembly

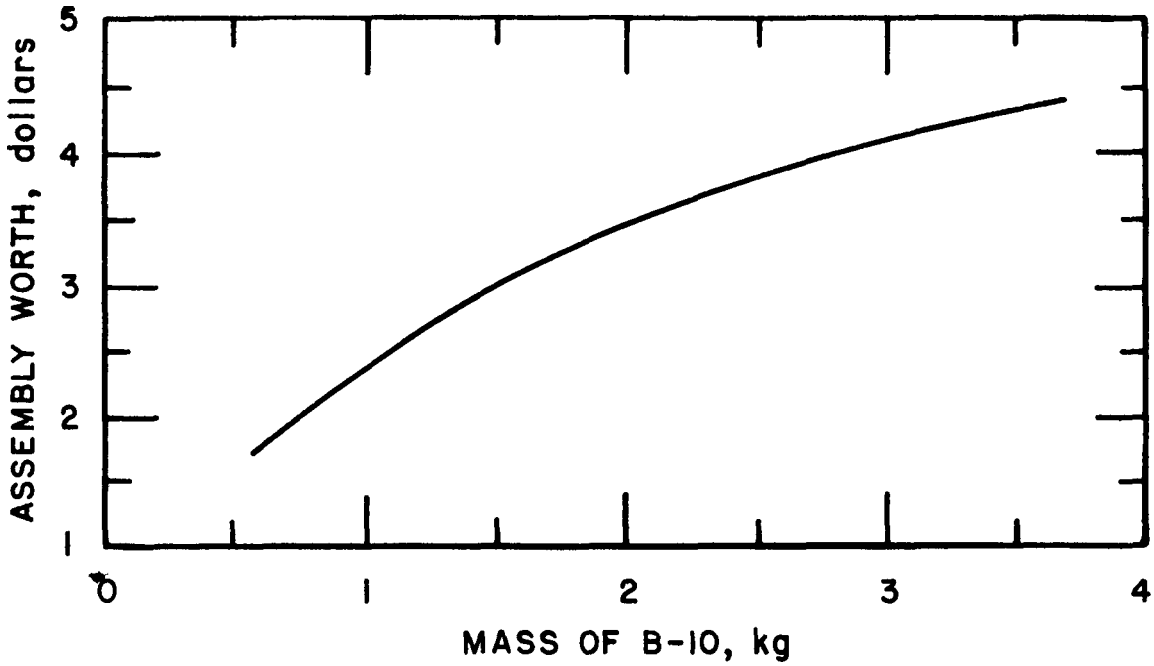

FIGURE 23: ISA Worth vs. B-10 Mass per Assembly

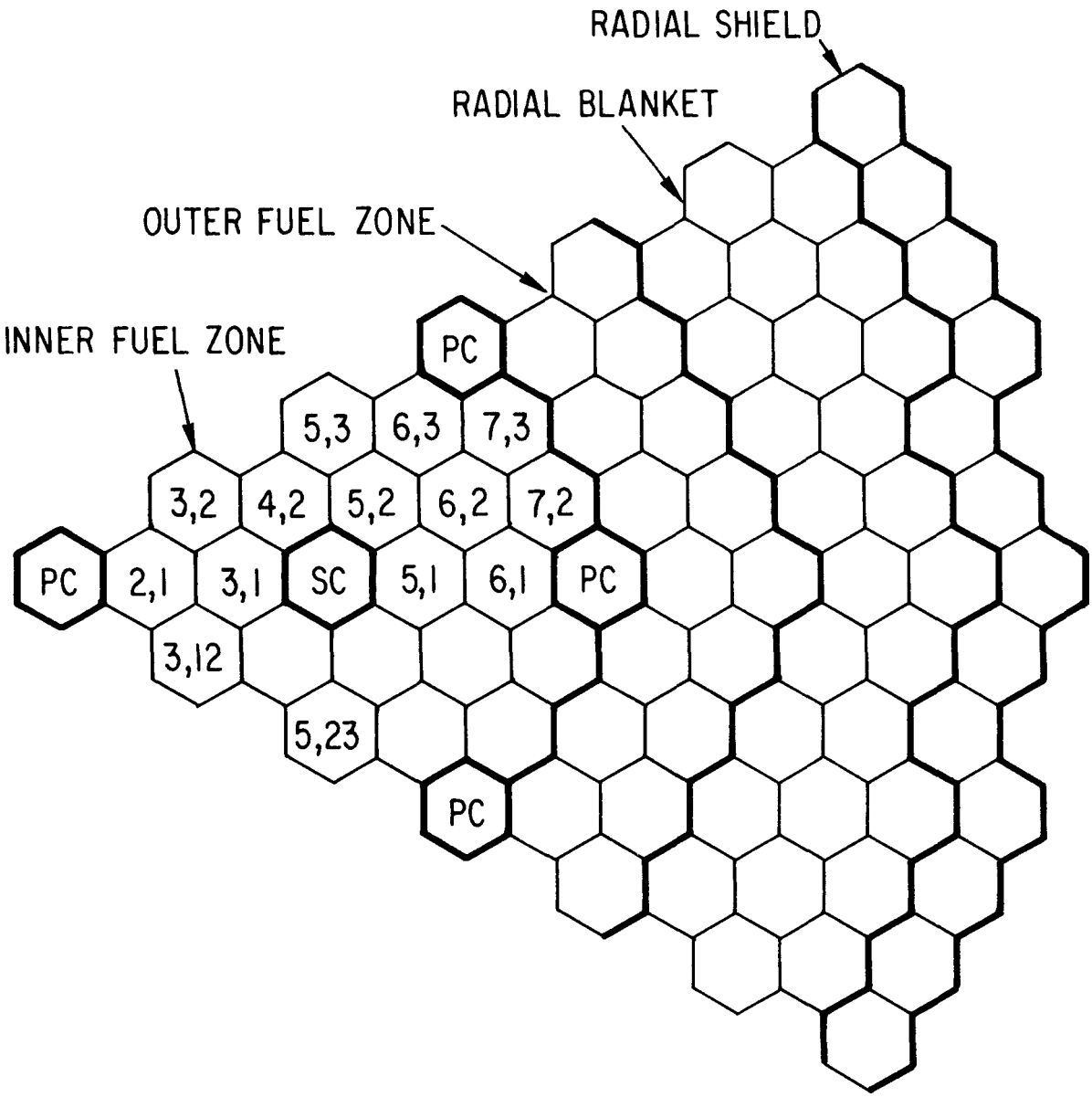

PC PRIMARY SYSTEM CONTROL ASSEMBLY

SC SECONDARY SYSTEM CONTROL ASSEMBLY

x,y ISA ASSEMBLY POSITION (RING NUMBER, POSITION)

FIGURE 24: Possible ISA Position in Core

assemblies. It also lends itself quite well to placing 2, 3, or 6 ISAs in the inner core. Outer core and radial blanket ISA positions were not considered because of their low relative worths.

A highly enriched ISA has approximately the same or slightly more than the maximum worth CRBR safety rod. Thus a single ISA at a (5,3) type location is adequate to compensate for the ejection of a single CRBR safety rod.

B. Impact of SASS on Core Performance

The replacement of two CRBR inner core fuel assemblies by ISAs results in two basic parameter changes. The first is the removal of a small amount of fuel from a high worth region ; the second is the placement of a substantial amount of absorber material in the upper axial blanket. Removing a small amount of high worth fuel reduces the excess reactivity which in turn lessens the operating cycle length. An ISA positioned at (5,3) reduces the excess reactivity by a factor of 3.8%. The two ISAs reduce the normal cycle length by 20 days. This can be compensated by substantially increasing the enrichment of the two rows of fuel in the ISA assembly or by a small increase in the core enrichment. The former would result in undesirable localized power peaks. The latter would require the overall core enrichment to be increased by a factor of 1.5% in order to keep the initial cycle length the same. Increasing core enrichment would lower the reactor breeding ratio by a factor of 2.8%. Replacing the inner core assemblies without compensating for the reduction in excess reactivity would have essentially no impact on the breeding ratio, power peaking, or peak flux.

The addition of ISA control poison in the axial blanket degrades neutron economy and depresses the flux as shown in Fig. 25. The ISAs are assumed at the (5,3) position. This results in a 5.5% reduction in axial blanket breeding and a 0.6% reduction in overall reactor breeding. The additional control hardens the blanket spectrum, lessening the Doppler broadening which reduces the negative Doppler contributions slightly.

C. Alnico Magnet Heating Rate

The energy deposition rate for the alnico magnet was calculated at three different axial positions within the central rod. These were at the core centerline, and just above and below the core-axial blanket interface. The alnico composition is given below (see Table I-1 of Appendix I).

ALNICO V COMPOSITIONS IN W/O

Fe	51.0
Ni	14.0
Co	24.0
Cu	3.0
Al	8.0

Heating rates were calculated using a full core r-z model with the reactor operating at full power. The energy deposition rate includes contributions from neutron capture, scattering, prompt fission gammas, and delayed fission product gammas. The computed heating rates per gram of Alnico V are:

Core centerline	6.00-6.40 $\frac{\text{watts}}{\text{gm}}$
Below core-blanket interface	3.58-3.80 $\frac{\text{watts}}{\text{gm}}$
Above core-blanket interface	1.73-1.92 $\frac{\text{watts}}{\text{gm}}$

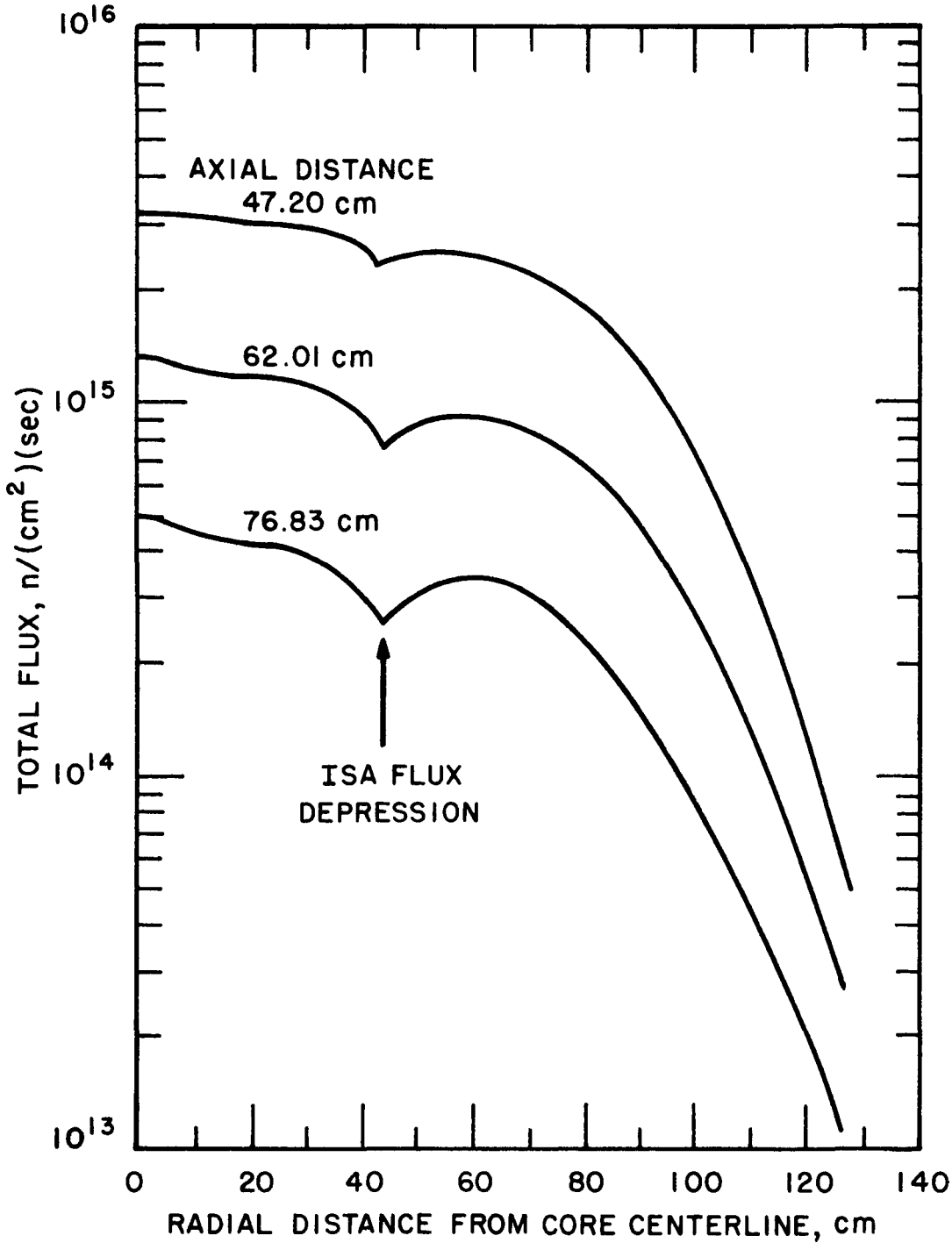

FIGURE 25: Axial Blanket Flux Depressions due to ISA

D. Fissile Source Heating Rate

In order to obtain a direct response to a neutron flux excursion by the ISA release mechanism, a fissile UO_2-iron cermet is imbedded in the magnetic yoke. The cermet can contain up to 35% UO_2 by volume. The heating rate is roughly proportional to the fission rate of UO_2 , hence the cermet acts as an intense heating source at the parting plane of the device. This decreases the time of response of the magnetic release mechanism to a power excursion.

The fissile source heating rate in watts/gm of UO_2 is shown in Fig. 26 as a function of uranium enrichment and axial position. Heating rates were calculated at axial positions that ranged from 37 cm to 55 cm above the core centerline. A radial adjustment factor is also included so that heating rates as a function of radial distance from the core center can be determined as shown in Figure 27. These rates range from about 10 watts/gm for natural uranium to about 700 watts/gm for 100% U-235.

E. Results and Conclusions

It has been shown that the ISA can insert a substantial amount of negative reactivity into the core with a minimal impact on reactor performance. The placement of two ISAs in row 5 CRBR positions, with at least 3 kg of B-10 (approximately a 75% B-10 enrichment) in each, will provide more than enough negative worth to compensate for the ejection of the maximum worth CRBR safety rod even if one of the ISAs fails to function. Figure 28 shows the optimum placement of two ISAs in the inner core which have a combined worth of 6.7 and 6.3 dollars for the first core and equilibrium cores respectively. The major impacts on

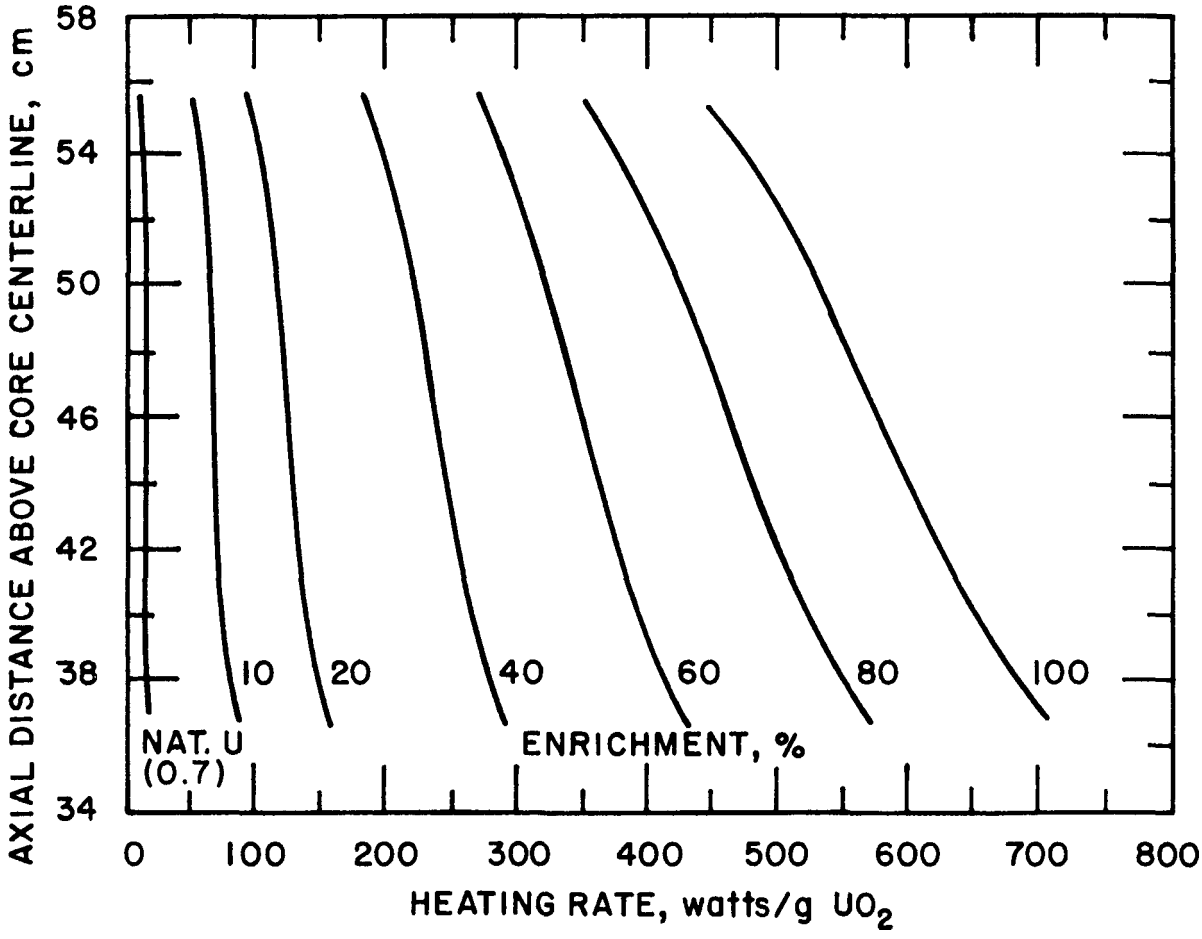

FIGURE 26: Fissile Source (UO_2) Heating Rate vs. Axial Position in Core and Enrichment (CRBR Full Power Flux Level)

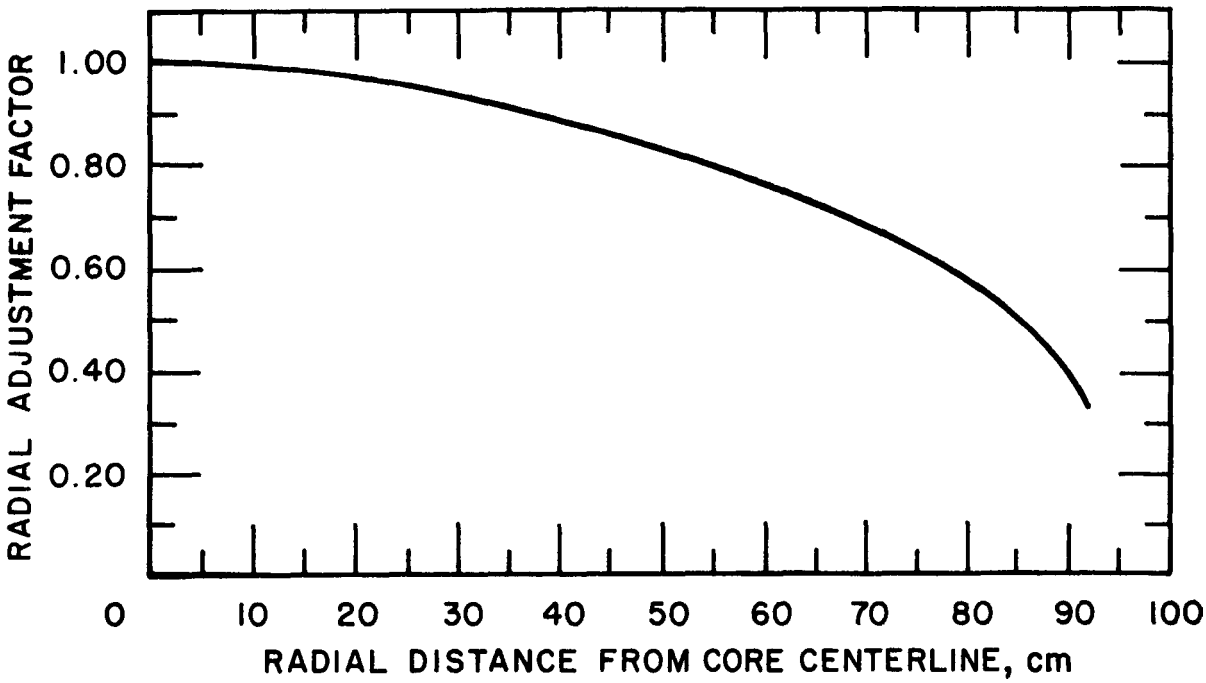

FIGURE 27: Fissile Source Radial Adjustment Factor

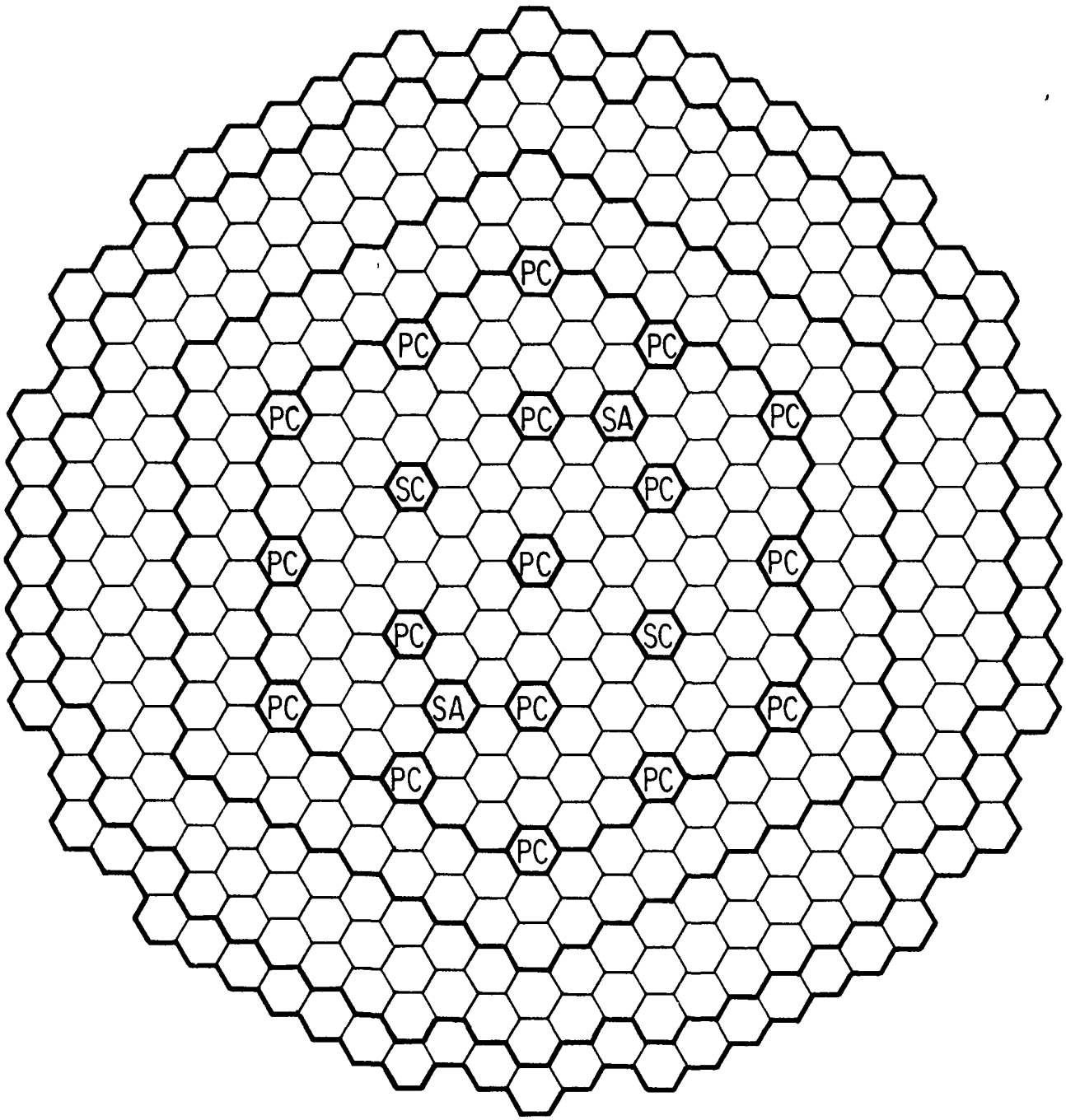

		QUANTITY
PC	PRIMARY SYSTEM CONTROL ASSEMBLY	15
SC	SECONDARY SYSTEM CONTROL ASSEMBLY	4
SA	SASS SYSTEM CONTROL ASSEMBLY	2

FIGURE 28: Optimum Placement of ISAs in CRBR

performance are slight reductions in excess reactivity and axial blanket breeding. Both of these effects can be accommodated by adjusting enrichments or blanket fuel volume fractions.

VII. MATERIALS ASPECTS OF SASS DESIGN

Several of the materials associated with the SASS design are not normally used in high temperature sodium systems and in reactor environments of high neutron and gamma fields. These special environments may adversely affect the properties and usefulness of the preferred materials. This section will present briefly some of the properties and the known effects of these environments on those properties for Alnico V, low-carbon steel, nickel-iron alloys, and stainless steel.

A. Radiation and Temperature

Radiation will not affect the magnetic properties of these materials since magnetic properties are electronic in nature. The only associated effect would be due to internal heat generation which may enhance the "aging" (loss of field strength) in the Alnico V.[7] The strength and swelling characteristics as a function of radiation will not be a problem in low carbon steel at the operating conditions (higher than 850°F)[8] of the device. The effects of radiation on Alnico V are not expected to be of significance with respect to strength properties. The neutron irradiation swelling characteristics are not known. However, since the ISA is located at the core edge, the total fluence during the life of the device should be low enough to preclude serious swelling in the Alnico V or nickel/iron steels.

The high energy neutron fluence at the device is about 10^{23} n/cm^2 during a three year operating period (819 full power days). This, at a temperature of 995°F, will give a volumetric expansion in 316 stainless steel of about 4% (linear expansion of .013). This expansion over a 2.5 in. dimension will be about 30 mils. High nickel-iron alloys which might be

preferred for the yokes and pole pieces could suffer equivalent swelling damage. Clearances of 55 mils on a side (110 mils across the diameter) will be adequate for the service expected including thermal expansions.

The temperature (995°F) in the device is significantly below any phase changes in the materials being considered. The effects of temperature will only be of significance with respect to changes in structural properties (see F below); solution rates in sodium and corrosion are of concern.

B. Corrosion and Erosion

The solubilities of iron, nickel, cobalt, aluminum and copper are of the order of 2 wt. ppm Fe in Na, 2.5 wt. ppm Ni in Na, 1 wt. ppm Co in Na, 30 wt. ppm Al in Na and 40 wt. ppm Cu in Na, respectively. These are the individual solubilities of pure materials. The complexities of alloys change the solubility. For example, aluminum in bronze reduces the solubility of both the copper and aluminum. A small addition of aluminum in steel can reduce the propensity of self-welding in some steels. [Self-welding is enhanced in high temperature sodium, presumably due to the cleaning (deoxidation, etc.) action of the surfaces.] At the temperatures of interest in these devices, it is recommended that hollow molybdenum o-rings be used in preference to aluminum or copper where a metal seal may be desired, for example, the gap between the magnet shunt and pole piece.

There is evidence of carbon mass transfer in systems containing both stainless steel and ferritic steels.[9] At temperatures of about 800°F, decarburization occurs in ferritic (Cr-Mo) steels and carburization of stainless steels occurs above 900°F to 1000°F. The choice of steel for

the yokes and pole pieces should be made on the basis of low carbon content. Armco (TM) iron with 0.03% carbon should be acceptable where strength is not important.

Erosion is no more serious for the materials considered than for the normal reactor materials. An exception may occur near exits to flow channels of small diameter, for example, diversion channels into the magnet yokes, where large velocities and velocity changes occur. Cavitation and stagnant volumes could lead to erosion. Based on calculations made in the thermal hydraulic sections of this report, the only area of concern might be in orifice exits. These are not critical from a dimensional standpoint and are only of interest in relation to the amount of debris which might be added to the system.

C. Self-welding and Pickup of Debris on Magnet

Self-welding is known to occur between mating metal surfaces exposed to the cleaning action of high temperature sodium. It normally is of concern where high unit loads (several thousand psi) occur at high temperatures (greater than 1000°F). Self-welding can be enhanced in a neutron radiation field. The area of concern in the current design is the surfaces between the magnet pole faces and the yoke pole faces. The unit loads are less than 200 psi and the temperature is normally about 1000°F. There appears to be no reason to expect a self-welding problem in this area.

If impurities or debris in the circulating sodium were preferentially deposited in the magnet region, it could lead to difficulty during the release or resetting of the ISA. It is not expected that there will be any more propensity for plate out of dissolved elements in the magnet than in other parts of the fuel system. Dissolved elements are elemental and have no

preferred magnetic properties.

There is the potential for particulate materials, which have a magnetic character (weld debris or eroded bits), to be gettered preferentially in the magnet. The size of these particles would necessarily be small, since they would have had to survive passage through the close clearances in fuel bundles. No particulate materials found in sodium systems have been identified as preferentially magnetic.

D. Cladding of Magnetic Materials

Because of possible concern for mass transfer of aluminum and carbon from the magnet materials, consideration has been given to canning parts of the assembly. Surfaces of the magnet could be plated with nickel and/or chromium to reduce carbon, aluminum, or copper solubility. Canning of magnet parts is possible but will of course introduce low permeability gaps in the magnetic circuit. Such measures should not be required. However, prototype systems should be tested in appropriate in-pile and out-of-pile environments for periods comparable to expected lifetimes.

E. Fissile Source Materials[10,13]

Uranium oxide (fully or partially enriched) can be fabricated as a cermet to provide a power (flux) sensitive heat source to actuate the ISA. Uranium oxide as spherical particles (in the size range of 150-300 μ) are homogeneously mixed with iron, nickel, or stainless steel powder as a matrix. Isostatic pressing at an elevated temperature produces a high density (low porosity) body. The cermet can be produced as wires, pellets, or flat plates. It is suggested that the iron yoke pieces be machined to shape and holes milled where the fissile heater is to be

located. A mixture of UO_2 particles and iron powder would then be pressed into the milled holes. A sealing cover would then be formed by pressing pure iron powder into the top of the hole. A fusing process could be used to complete the seal. This technique would be preferred to embedding encapsulated cermet pellets into the yokes since the thermal contact between the UO_2 and the yoke would be better. The use of iron as the matrix material improves the magnetic properties and enhances the sensitivity to the Curie point release characteristics.

F. Structural Properties of Materials

1. Alnico

Alnico V and VIII are, respectively, made up of (8 Al, 14 Ni, 24 Co, 3 Cu, bal Fe) and (7 Al, 15 Ni, 35 Co, 4 Cu, 5 Ti, Bal Fe). It is normally sand cast and machined to tolerances of $\pm$ 0.004 in. or better.

2. Low Carbon Steel

Low carbon steel is available with carbon content of 0.03% to 0.06%. The carbon content is sufficiently low to reduce concern for carbon transfer. After machining or forging, the steel should be annealed to a temperature of 1500-2100°F for about two hours, then cooled slowly to remove stresses and to stabilize the magnetic properties. At room temperature it has a tensile strength of 40,000 psi, yield strength of 24,000 psi, and an elongation of 40%. It has a Rockwell B hardness of 40 and a magnetic permeability of about 2500 maximum (1000 at 200 gauss). The strength is lower by a factor of two at 1000°F.

3. High Nickel Alloys

High nickel alloys are of interest because their Curie points are lower than that of iron. Typically, several alloys have Curie points from 790° to 1080°F (Fe ∿ 1400°F).[11] These should all be annealed after machining operations to improve and stabilize their magnetic properties. Their structural strength is low and they are relatively soft. (TS = 65,000 psi, YS = 21,000 psi, Rockwell B 60). The permeability is about 50,000 maximum (4000 at 20 gauss). See Tables 7, 11, 12 of the Metals Handbook.[11]

G. Stability of Materials

1. Alnico

Forster[12] describes experiments performed at ANL on Alnico V and VIII magnets. He observed that they lose field strength with time above 700°F. The rate of loss increases with operating temperature. He concludes that the stabilization process helps to balance the loss and recovery processes of elevated temperature aging. Raptis[7] has assessed the properties of Alnico up to 1200°F.

2. Low Carbon Steel and Nickel-Iron Alloys

These materials are temperature and age stable both magnetically and structurally if they are used in the annealed condition. Machining and process working should be relieved to optimize the magnetic properties and the structural stability. Radiation damage (resulting in increased strength and hardness), normally present in structural materials, are not present in low carbon steel above 850°F. Some irradiation effects are expected in Ni-Fe alloys.

H. Recommendations

Prototypical tests of the assembly should be made. Conditions of temperature, sodium flow, and loads are of primary interest. Methods of sampling the sodium for dissolved elements and monitoring the oxygen, carbon, temperature, and flow should be provided. Observations should be made on the surface conditions, for example evidence of corrosion, erosion, self-welding, galling, and fretting. Tests should be run at nominal and elevated temperatures and flows.

As recommended in E, a cermet fissile heater composed of UO_2-Fe fabricated in situ should be considered. Developmental efforts should be minimal. However, samples should be made and included in the operational prototype tests. In-pile test of the assembly could confirm the operating characteristics. Nickel soft gaskets or hollow molybdenum o-rings should be used in preference to aluminum or copper.

VIII. CONCLUSIONS AND RECOMMENDATIONS

At the present time there is considerable emphasis upon the safety of nuclear power plants (including the LMFBR) and requirements for a high degree of reliability for plant protection systems. Because of this, it is recommended that the advantages of a Self-Actuated Shutdown System (SASS), based upon an Inherent Shutdown Assembly (ISA), not be overlooked. In particular it is recommended that the development of an SASS based upon the ferromagnetic Curie point be continued.

Because the SASS is self-contained and does not require an external signal for operation, its design can be greatly simplified and made highly reliable. It is also virtually immune to malfunction due to accidental or deliberate human intervention.

Several conceptual designs of the SASS based upon the ferromagnetic Curie point have been presented. A variation of the proposed designs was constructed and tested in the laboratory including testing in static sodium at elevated temperatures (CRBR core exit temperature). The proof of principle of operation of the Curie point device was demonstrated and it was shown that the device will continue to operate quite satisfactorily after extended periods of time at elevated temperatures.

Methods have been developed and applied to designing and analyzing the selected SASS concept. Many of the technical areas in the development of an SASS, based upon the ferromagnetic Curie point, have been examined including magnetic, thermal, hydraulic, reactor physics, and materials. Design parameters such as size of assembly, required holding area, time of response, coolability, absorber worth, impact on core design, have been delineated.

The results of the testing and analysis of the proposed designs lead to the conclusion that the selected concept is feasible. An accident

analysis shows that the selected SASS can protect the reactor against severe accident transients.

It is recommended that the SASS development proceed along the following broad lines:

(1) Build additional assemblies based upon the more promising conceptual designs for testing under simulated reactor conditions of sodium flow, temperature and radiation.

(2) Analyze the results of the tests of the SASS.

(3) Improve the SASS design.

ACKNOWLEDGMENT

We would like to take this opportunity to thank Messrs. Wayne Mitchell, Charles M. Andrews, Frank S. Greenwald, and Howard F. Graff of the Arnold Engineering Company of Marengo, Illinois for their help in the magnet design, and for their assistance in expediting the procurement of the Alnico V magnets for the ANL testing program.

We would also like to thank Messrs. George Goldfuss, Raymond Roth, and Robert Hodges of the Reactor Analysis and Safety Division of ANL for their assistance in assembling, constructing, and operating the SASS test installation.

APPENDIX I: MAGNETIC CIRCUIT ANALYSIS

NOMENCLATURE

A. Introduction

B. Magnetic Units, Circuit Parameters, and Materials

1. Magnetic Units and Definitions
2. Magnetic Circuit Analysis
3. Magnetic Materials

C. Calculation of Magnetic Holding Power and Flux Density

1. Calculation of Magnet Holding Power
2. Calculation of Magnetic Flux Density and Holding Power at 1000°F Operating Temperature
3. Calculation of Magnetic Flux Density and Holding Power During Sodium Temperature Transient

D. Results

NOMENCLATURE

(APPENDIX I)

H	magnetic flux intensity-ampere/meter, oersteds.
B	magnetic flux density, magnetic induction - webers/meter^2, gauss
ϕ	magnetic flux - webers
M	magnetization - webers/meter^2, gauss
M_s	saturation magnetization
M_r	remanance magnetization
μ	absolute premeability of a material-henry/meter
μ_o	permeability of free space, = $4\pi \times 10^{-7}$ henry/meter (1 henry = 1 weber/amp)
μ_r	relative permeability of a material = μ/μ_o - nondimensional
χ	magnetic susceptibility of a material, - $M/\mu_o H$ - nondimensional
T	temperature
T_c	Curie temperature
i	current density - amperes/meter^2
I	current - amperes
N	number of current turns - nondimensional
a	nonmagnetic material gap
l	magnetic path length
A	areas
R	magnetic circuit reluctance - henrys^{-1}
MMF	magnetomotive force = NI - ampere - turns
P	magnetic pressure - newtons/meter^2, kg/cm^2, psi
F	magnetic force - newtons, kg, pounds
erf	error function

Subscripts

i	steel or iron
m	magnet
o	absolute zero or initial temperature of free space
g	demagnetization length
a	nonmagnetic material gap
r	relative or remanance
s	saturation
f	fringing

APPENDIX I: MAGNETIC CIRCUIT ANALYSIS

A. INTRODUCTION

A thermal and magnetic circuit analysis of the magnetic self-actuated shutdown system has been performed. A model has been synthesized which gives the interaction between the temperature of the magnetic circuit and the magnetic flux density through it. This determines the holding force.

An equivalent magnetic circuit of the system is shown in Figure I-1. This circuit is based upon the conceptual designs shown in Figures 2 through 5 in the body of the report. The circuit configuration is typical and applies to all of the proposed conceptual designs.

The principle upon which the system operates is that the reluctance of the magnetic circuit path designed into the system is increased by the approach of the soft magnetic material (low carbon steel, 0.05-0.2% C) in the circuit to its Curie point temperature. This increase would be brought about by a rise in the temperature of the sodium coolant flowing through the magnetic circuit due to an accident condition in the core. The increase in the reluctance reduces the magnetic flux through the circuit resulting in a rapid reduction of the holding power of the magnet at the parting plane. The reluctance is particularly increased when the magnetic material exceeds the Curie point.

The temperature increase could also be brought about by a fast reactivity insertion transient due to the presence of the fissile source.

The magnetic flux in this design is obtained from a powerful magnet or series of magnets of Alnico V. This material exhibits the very high coercive force and moderately high magnetic flux density characteristics of permanent magnet materials. In addition it is probably the most stable high temperature magnetic material available.

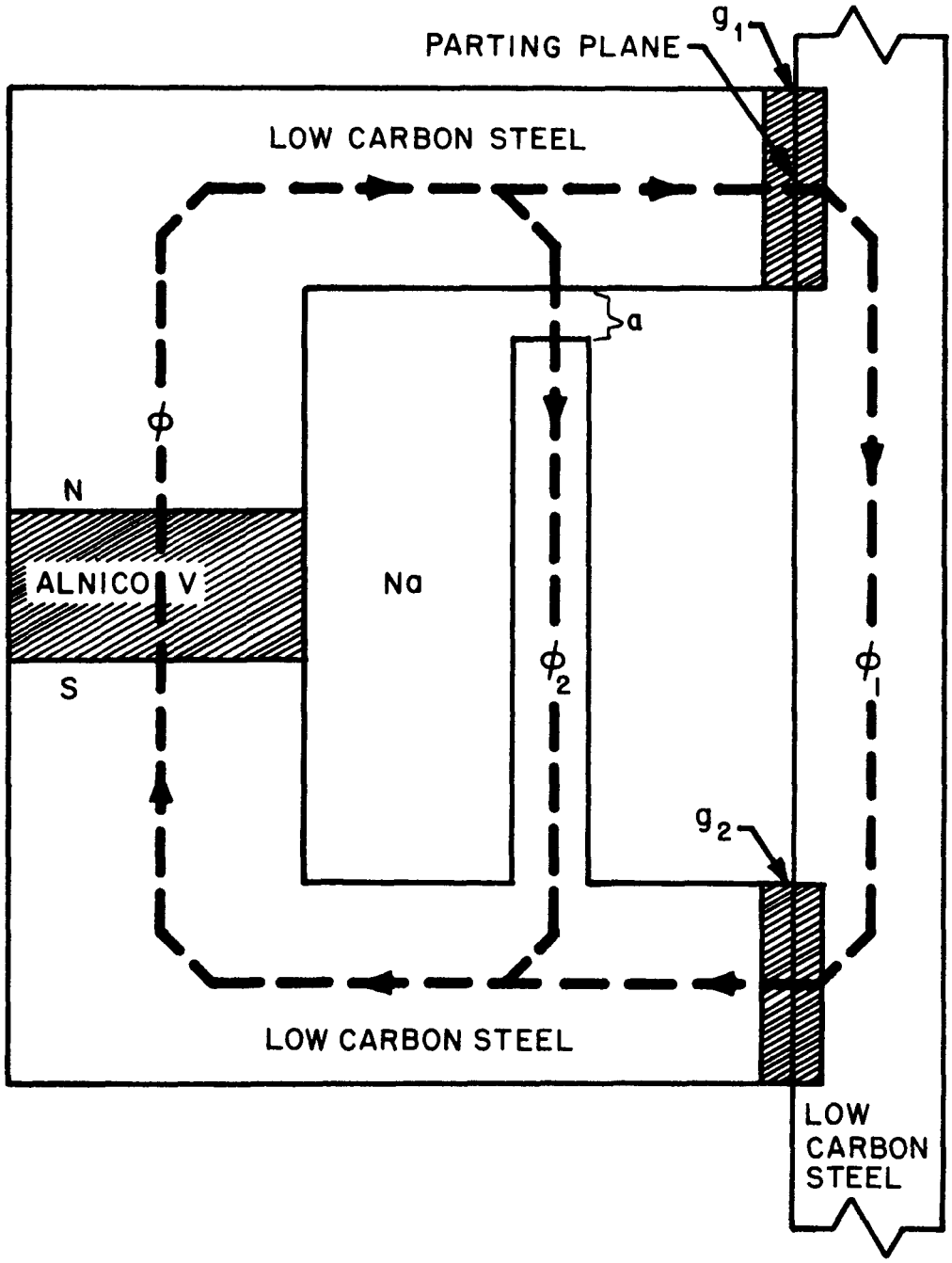

a - SHUNT GAP
$g_{1,2}$ - HIGH TEMPERATURE DEMAGNETIZED ZONES
ϕ - TOTAL MAGNETIC FLUX
ϕ_1 - HOLDING MAGNETIC FLUX
ϕ_2 - SHUNT MAGNETIC FLUX

FIGURE I-1. Equivalent Magnetic Circuit - Curie Point Holding Device

B. MAGNETIC UNITS, DEFINITIONS, AND CIRCUIT PARAMETERS

1. Magnetic Units and Definitions

A basic equation of magnetism states that the magnetic induction, that is the magnetic flux density, which provides the magnet holding force, is given by the sum of the applied magnetic field strength and the bulk magnetization of the material:

$$B = \mu_o H + M \tag{1}$$

For this way of defining the magnetization, the magnetic flux density, B, and the magnetization, M, are in units of webers/meter^2 in the MKS system of units. The magnetic flux intensity, H, is in units of amperes/meter (actually ampere-turns/meter). In addition, in the rationalized MKS system of units the magnetic permeability of free space, μ_o, is not unity, but is given by:

$$\mu_o = 4\pi \times 10^{-7} \frac{\text{henry}}{\text{meter}}$$

The calculations and discussion are based upon the rationalized MKS system of units. Note that the henry is the unit of inductance with the dimensions of webers/ampere.

The absolute permeability of a material, μ, is given by B, the magnetic flux density, divided by H, the magnetic field intensity. From equation (1):

$$\mu = \mu_o(1 + \frac{M}{\mu_o H})$$

In the MKS system of units the relative permeability is given by the permeability of the material divided by the permeability of free space:

$$\mu_r = \frac{\mu}{\mu_o} = 1 + \frac{M}{\mu_o H} = 1 + \chi \tag{2}$$

The non-dimensional quantity χ, given by $M/\mu_o H$, is called the magnetic susceptibility of the material. The magnetic susceptibility is a monotonically decreasing function of temperature and in a ferromagnetic material is practically zero above its ferromagnetic Curie point, a temperature characteristic of the material. (Above the Curie point the ferromagnetic material becomes paramagnetic exhibiting a slight positive paramagnetic susceptibility.)

Rewriting equation (2) to show its temperature dependence we have:

$$\mu_r = 1 + \frac{M_o}{\mu_o H} \frac{M_s}{M_o} = 1 + \chi_o(B) \frac{M_s}{M_o} \left(\frac{T}{T_c}\right) \tag{3}$$

χ_o is the susceptibility of the material at absolute zero temperature. M_s/M_o is the ratio of the saturation magnetization of the material at temperature T to its saturation magnetization at absolute zero. M_s/M_o is unity at $T = 0$ and goes to zero above the Curie point. The relative permeability at $T > T_c$ is then unity and the material is essentially nonmagnetic. The functional dependence of M_s/M_o is given in Figure I-2.

For carbon steel the Curie temperature is 1418°F. Therefore at room temperature $T/T_c = 0.28$, and from Figure I-2, M_s/M_o for carbon steel is practically unity. At 1000°F, M_s/M_o is 0.74 for carbon steel. Therefore in going from room temperature to 1000°F, carbon steel loses about 25% of its magnetization.

As is well known, the susceptibility and therefore the permeability of a ferromagnetic material is also a function of the magnetic flux density. The variation of the permeability with B for a typical low carbon steel is given in Figure I-3. The very high relative permeability, of a maximum of

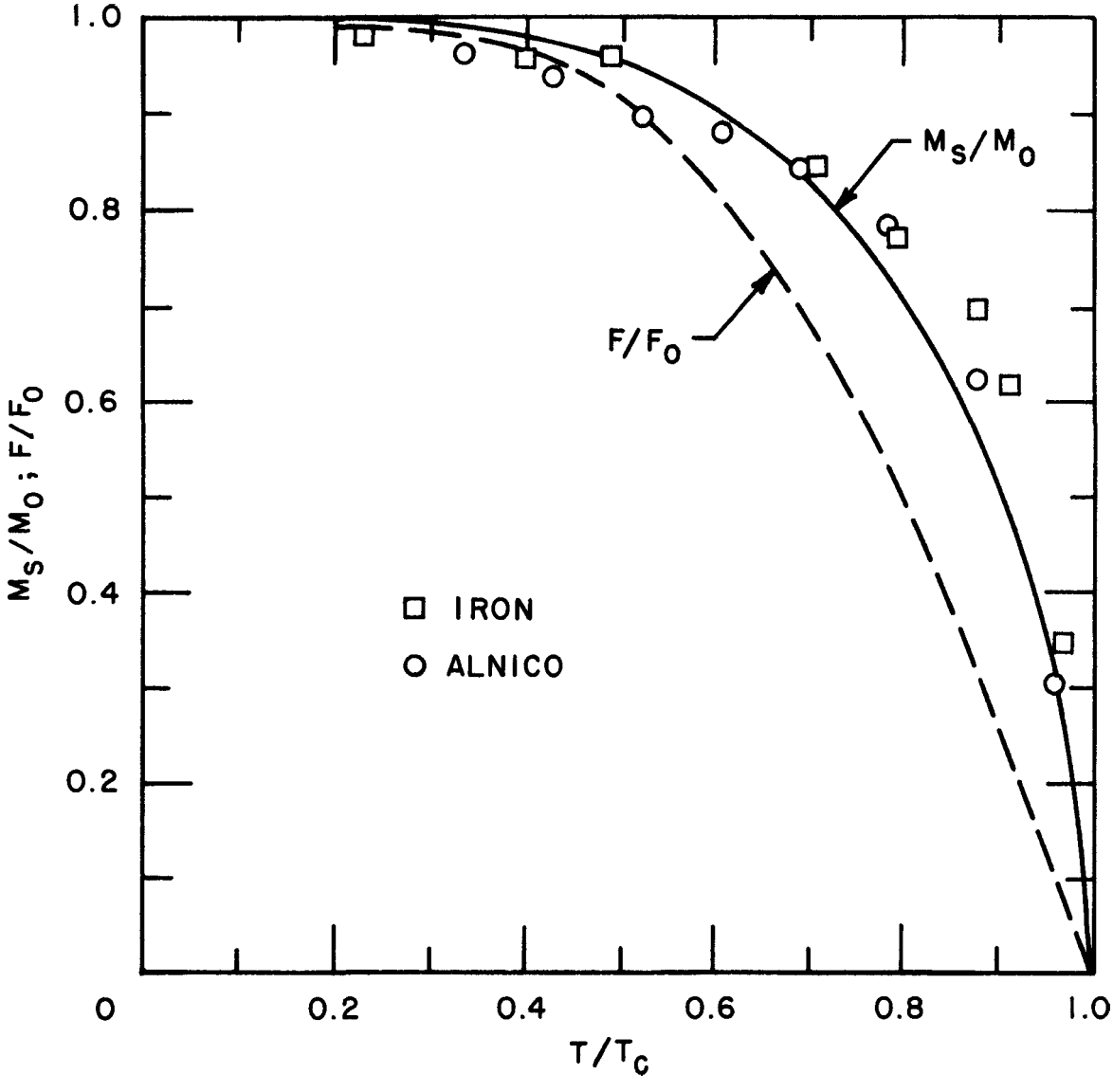

FIGURE I-2. Temperature Dependence of Magnetization (M_s/M_o) and Holding Power (F/F_o) Below the Curie Temperature (T_c)

(Data from Reference 20)

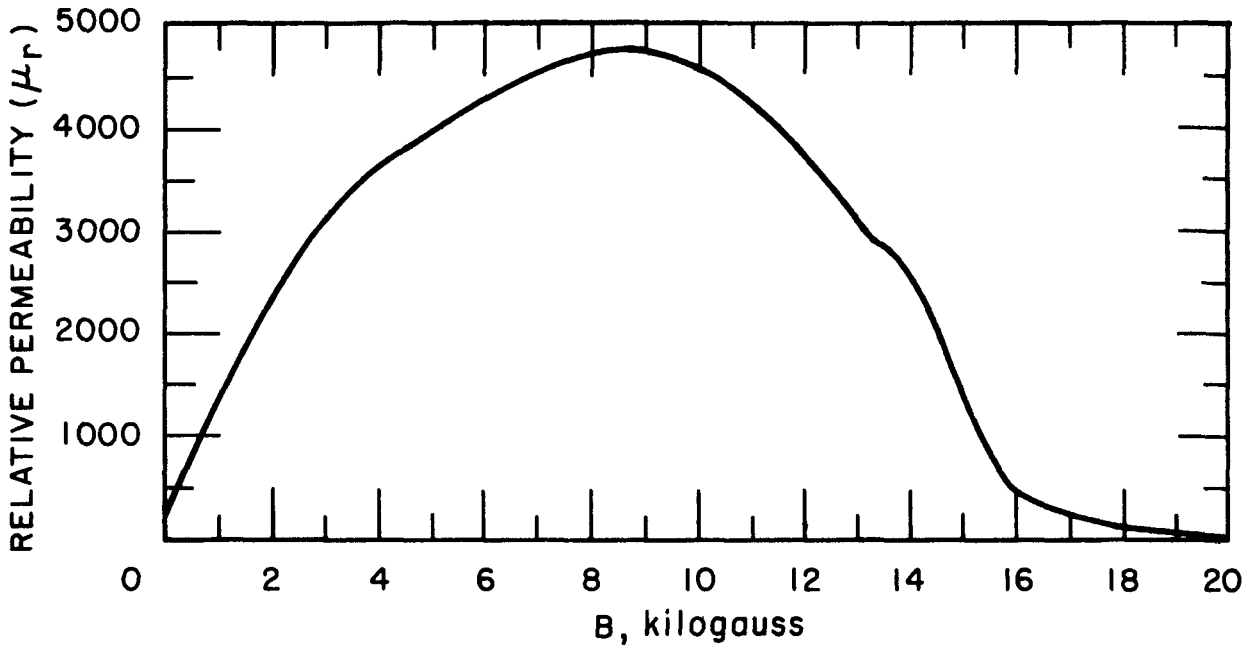

FIGURE I-3. Permeability of Low Carbon Steel at Room Temperature

(Data from Reference 17)

several thousand at room temperature, and attainable magnetic field densities, is characteristic of soft ferromagnetic materials.

Since the permeability of nonmagnetic materials is unity, even small gaps of nonmagnetic materials, e.g., air, copper, sodium, ferromagnetics above the Curie point, in general contribute almost all of the circuit reluctance. This is discussed in more detail below.

In addition, the complicated dependence of the permeability on the flux density results in the nonlinear characteristic of magnetic circuits. This makes their analysis more complicated than that of electric circuits. Generally, magnetic circuits must be solved by iteration procedures.

Because of their widespread application, the Gaussian units of the gauss and the oersted are also used here. The conversions to the MKS system are:

$$1 \text{ gauss} = 10^{-4} \text{ webers/meter}^2$$

$$1 \text{ oersted} = 79.58 \frac{\text{ampere}}{\text{meter}} = \frac{10^3}{4\pi}$$

It should also be noted that the permeability of free space is unity in the Gaussian units and that the relative permeability is given directly by the gausses divided by the oersteds.

2. Magnetic Circuit Analysis

The basic equation of magnetic circuits is obtained from Maxwell's field equation. There is no displacement current.

$$\nabla \times \bar{H} = \bar{i} \qquad \text{(rationalized MKS system of units)}$$

$\bar{H}$ is in amperes/meter and $\bar{i}$ in amperes/meter.[2]

Integrating over an area enclosing a field loop and perpendicular to the current we obtain:

$$\int \nabla \times \bar{H} \cdot \overline{dA} = \int \bar{H} \cdot \overline{d\ell} = NI \tag{4}$$

where NI represents the ampere-turns of the external circuit.

From Figure I-1, ignoring the shunt path for the time being, equation (4) becomes:

$$H_m \ell_m + H_i \ell_i + H_g \ell_g = NI = 0 \tag{5}$$

Equation (5) states that the sum of the magnetic potential drop in the materials making up the magnetic circuit is equal to the external magnetomotive force (MMF) in ampere-turns. We have identified three material regions in the circuit--the alnico region of the circuit (subscript m), the steel region (subscript i) and the demagnetized zone represented by the subscript g also of steel but with a reduced permeability. Since there is no external current, NI is zero.

Equation (5) can be written:

$$\begin{aligned} -H_m \ell_m &= H_i \ell_i + H_g \ell_g \\ -H_m \ell_m &= B_i \frac{\ell_i}{\mu_i} + B_g \frac{\ell_g}{\mu_g} \end{aligned} \tag{6}$$

The magnetic flux is constant about a single loop of a magnetic circuit to first approximation, that is if fringing is ignored.

Equation (6) then becomes:

$$-H_m \ell_m = \left(\frac{\ell_i}{A_i \mu_i} + \frac{\ell_g}{A_g \mu_g}\right) \phi = R\phi = RMA_m \tag{7}$$

The left-hand side of equation (7) represents the effective magnetomotive force (MMF) of the permanent magnet material in the circuit. The quantity multiplying the flux in equation (7) is the sum of the reluctances of the two regions of the circuit. We rewrite equation (7) as follows:

$$(NI)_m = (R_i + R_g)\phi = R\phi$$

where:

$(NI)_m = -H_m \ell_m$ = magnet equivalent MMF in ampere-turns

$R = R_i + R_g$ = circuit reluctance in reciprocal henries

The reluctance of a portion of a magnetic circuit of length ℓ, area A, and absolute permeability μ is given by:

$$R = \frac{\ell}{\mu A} \qquad \text{henrys}^{-1} \tag{8}$$

The flux is then given by the magnetomotive force divided by the reluctance. This is the analog of Ohm's law for magnetic circuits:

$$\phi = \frac{NI}{R} \tag{9}$$

In the rationalized MKS system of units the flux ϕ is in webers, the magnetomotive force (MMF) NI in ampere-turns, and the reluctance R in units of reciprocal henrys.

When the magnetic shunt is included in the analysis, the reluctance presented to the magnet magnetomotive force is given by the usual electric circuit equation analog for resistances in parallel:

$$R = \frac{R_a R_g}{R_a + R_g} \tag{10}$$

The reluctance of the steel can often be ignored to good approximation since it will be very small compared to the shunt gap or the demagnetized zone. This can be seen from equation (8) since the permeability of the steel is of the order of a thousand times that of the nonmagnetic material.

Figure I-4 shows an equivalent magnetic circuit diagram of Figure I-1 including possible fringing reluctances.

3. Magnetic Materials

Some of the main characteristic parameters of permanent magnetic materials are the coercive force H_c, the remanence flux density M_r, and the saturation flux density M_s. The coercive force and remanence flux density are obtained in the following way.

The nonmagnetized magnetic material is magnetized by means of a magnetic field set up by an external current to saturation as shown by the dotted curve in Figure I-5 . The current is then decreased. However, the material demagnetizes along the alternate solid path forming the hysteresis loop also shown in Figure I-5 . At zero current there is considerable magnetic induction given by the remanance flux M_r. The magnetic induction is brought to zero by reversing the current. The field necessary to completely demagnetize the material is the coercive force H_c.

The portion of the hysteresis loop between zero external field and the coercive force is the demagnetization curve of the permanent magnet material. This is the region of the hysteresis loop in which permanent magnets operate.

A typical demagnetization curve for Alnico V is shown in Figure I-6. In order to make calcuations, the demagnetization curve for Alnico V has been approximated by Watson's hyperbola (Ref. 18 and 20):

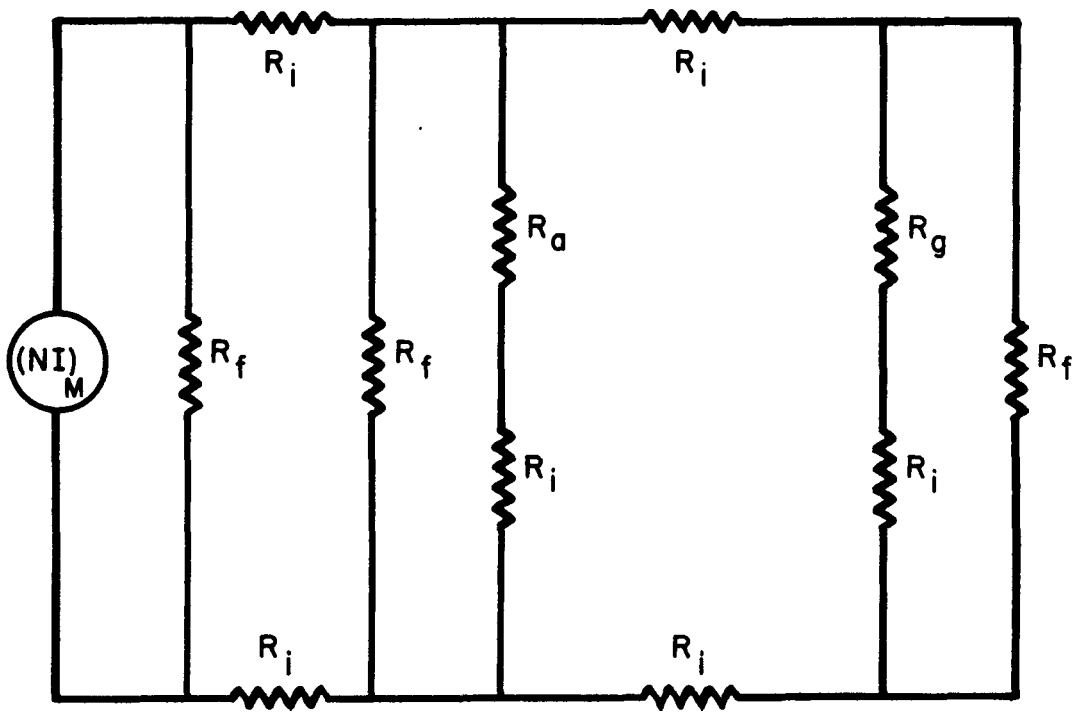

FIGURE I-4. Equivalent Magnetic Circuit Diagram

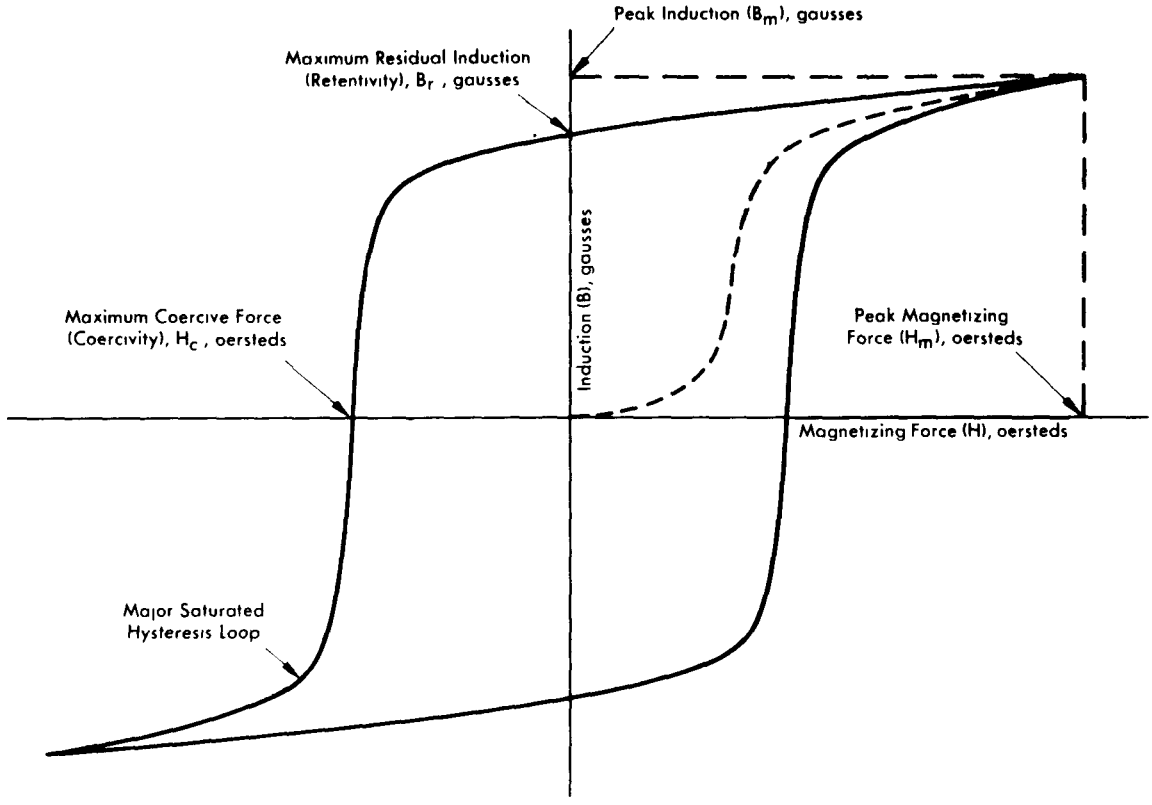

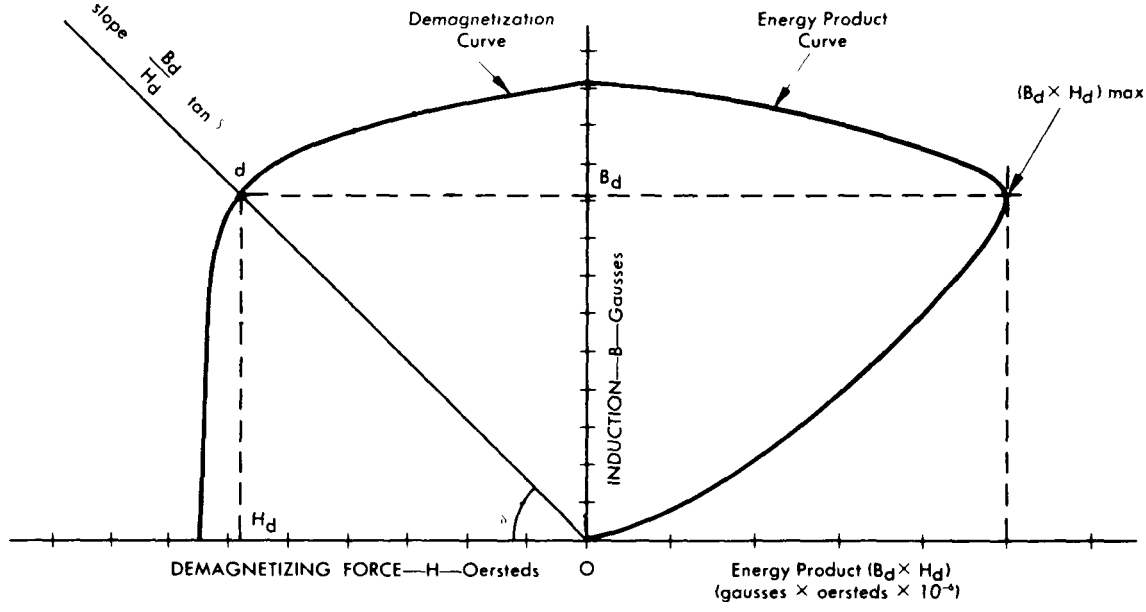

FIGURE I-5. Demagnetization Curve and Hysteresis Loop of a Permanent Magnet Material

(After Reference 17)

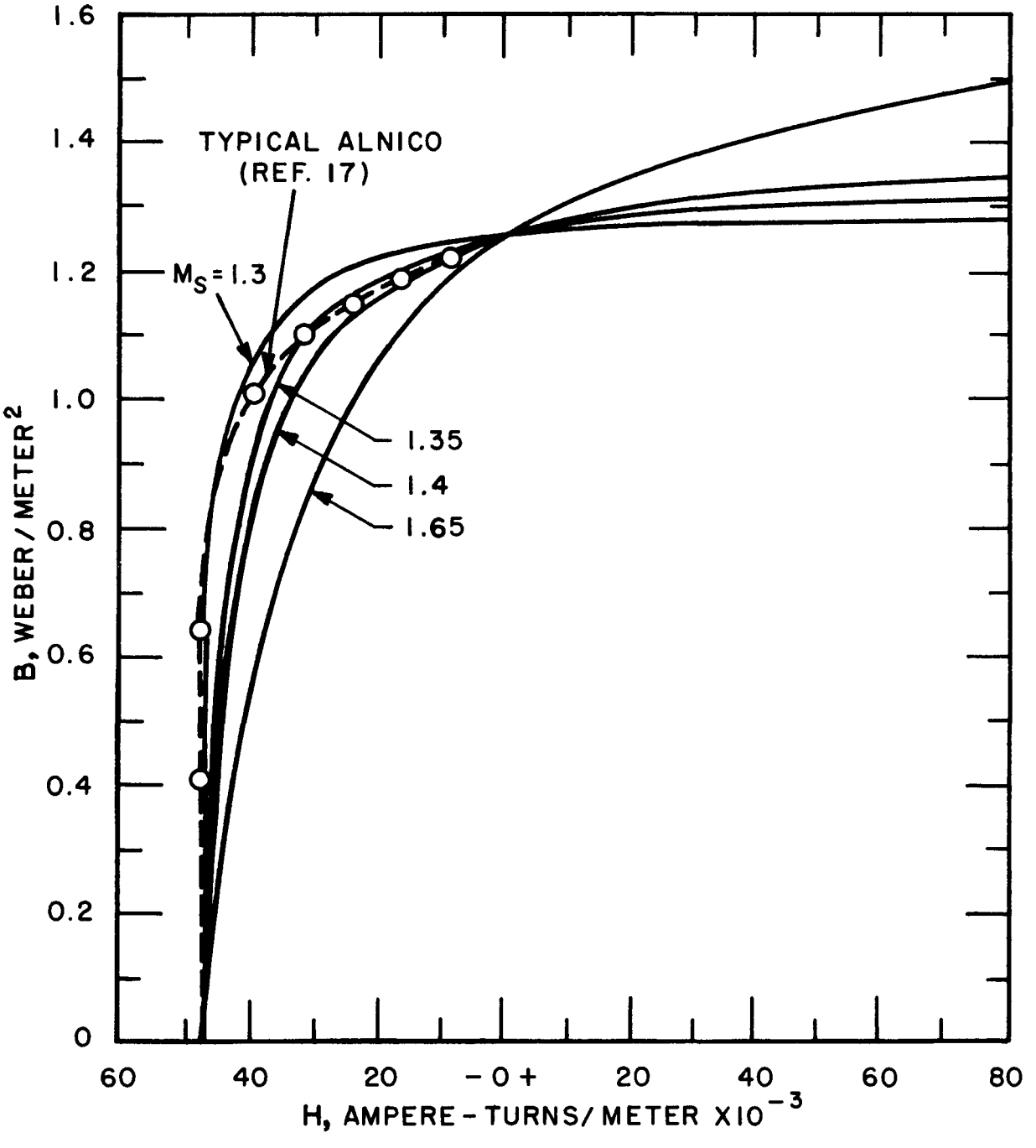

FIGURE I-6. Alnico V Demagnetization Curve

$$M = M_s \frac{H + H_c}{H + \frac{M_s}{M_r} H_c} \tag{11}$$

$M_s = 1.35 \frac{\text{webers}}{\text{meter}^2}$ $\quad M_r = 1.25 \frac{\text{webers}}{\text{meter}^2}$ $\quad H_c = 48{,}542 \frac{\text{ampere-turns}}{\text{meter}}$

The values of these parameters are for conditions at room temperature.

The maximum equivalent MMF of the one-inch Alnico magnet can be computed as follows:

$$\text{MMF} = H_c \ell_m = 610 \text{ oersteds} \times 1 \text{ in.} = 48{,}542 \frac{\text{amperes}}{\text{meter}} \times .0254 \text{ meter} = 1233 \text{ ampere-turns}$$

The composition and properties of Alnico V are given in Table I-1.

The demagnetization curves of carbon steels are shown in Figure I-7. For 1.2% carbon steel the coercive force is about 47 oersteds compared to 610 oersteds for Alnico V. For low carbon steel, about 0.06% C, the coercive force is 9 oersteds. It is less than 1 oersted for relay iron. The curve of Figure I-3 of relative permeability versus magnetic flux density is typical for low carbon steel or relay iron.

C. CALCULATION OF MAGNETIC HOLDING POWER AND FLUX DENSITY

The purpose of the analysis is to compute the magnetic flux density in the magnetic circuit and its variation with temperature. Once the magnetic flux density is known, the holding force of the magnet can be computed directly.

As pointed out above, somewhat of an iterative process must be used to compute magnetic circuits. One proceeds by assuming parameters for the circuit external to the magnet, thereby obtaining its reluctance. The magnetic field

TABLE I-1. Properties of Alnico V

ALNICO V

COMPOSITION	%	%
Aℓ	8.0	
NI	14.0	
CO	24.0	
CU	3.0	
TOTAL		49.0
BAL FE		51.0

H_C	(COERCIVE FORCE)	610 OERSTEDS
		48,500 $\frac{\text{AMPERE-TURNS}}{\text{METER}}$
NI	(MAGNETOMOTIVE FORCE)	1233 AMPERE-TURNS (1 IN.)
B_R	(REMANANCE)	12,500 GAUSS
		1.25 WEBER /METER^2
B_S	(SATURATION FLUX DENSITY)	1.35 WEBER/METER^2
T_C	(CURIE TEMPERATURE)	860°C
		1580°F
		2040°R
μ_R	(RELATIVE PERMEABILITY)	20.5

REF. 17

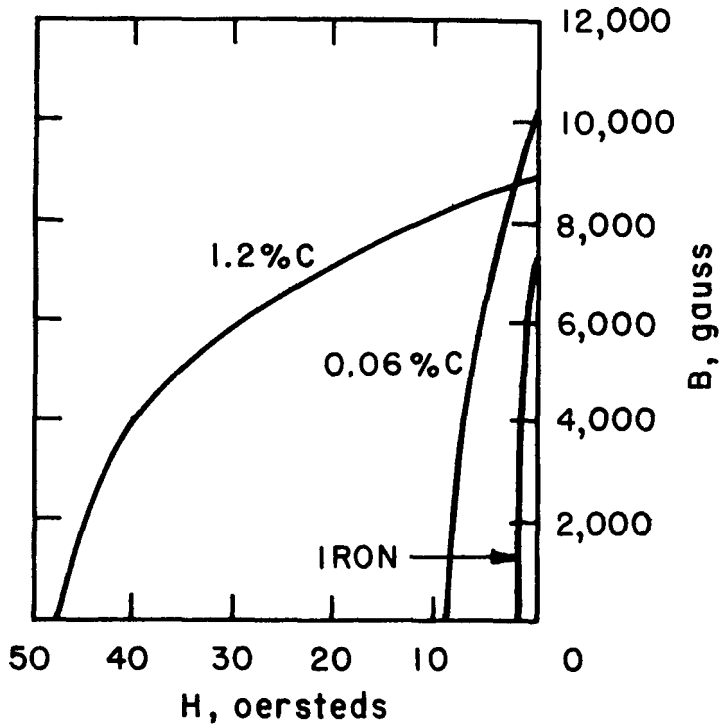

FIGURE I-7. Steel Demagnetization Curves

(Data from References 16 and 17)

intensity H in the magnet then adjusts to supply the needed MMF to drive the flux through the circuit based upon matching the magnetic field density at the magnet and external circuit interface. Once the magnetic flux densities in the circuit are known, the external circuit reluctances must be checked to assure that the proper permeabilities, which depend upon the magnetic flux densities have been used. If not, then an iteration must be performed.

Usually a very good guess can be made as to the expected flux densities. For example, if the reluctance of the external circuit is very low, not very much MMF is needed to drive a high magnetic flux through the circuit. In this case the magnet would be operating at a slightly negative demagnetizing magnetic flux intensity and therefore low MMF, but at a high flux density close to but just less than the remanence flux B_r. Therefore the permeabilities can be assumed at values in the vicinity of the remanence flux density.

For very high external circuit reluctances the magnet operates at a high MMF with a magnetic field intensity close to the coercive demagnetizing force and at very low magnetic flux densities (see Figures I-5 and I-6).

1. Calculation of Magnet Holding Power

In the MKS system of units the energy density of the magnetic field in a material of absolute permeability μ is given by:

$$P = \frac{B^2}{2\mu} \tag{12}$$

where B is in webers/meter^2, μ the absolute permeability in henrys/meter, and P in joules/cu. meter. The energy density is also the pressure in newtons/meter^2.

If we consider a magnetic circuit containing ferromagnetic material with an air gap, it is apparent from equation (12) that the energy of the system is reduced considerably by replacing the gap with ferromagnetic material. This

occurs because μ for ferromagnetics can be many times, often several thousand times, greater than for air or a nonferromagnetic. Therefore a ferromagnetic material near a magnetic pole experiences a force pulling it toward the pole, since the tendency of magnetic systems, like mechanical systems, is to the state of least energy.

The potential energy of a small gap is given by:

$$-dV = \frac{B^2 A}{2\mu_o} dx$$

therefore:

$$F = PA = -\frac{dV}{dx} = \frac{B^2 A}{2\mu_o}$$

The holding force of the pole is given by equation (12) times the area of the pole. For example, for 10,000 gauss (1.0 weber/m^2)

$$P = \frac{B^2}{2\mu_o} = \frac{1}{2 \times 4\pi \times 10^{-7}} = 3.98 \times 10^5 \frac{\text{newton}}{\text{meter}^2}$$

$$P = 57.6 \frac{\text{lb}}{\text{in}^2} = 4.06 \frac{\text{kg}}{\text{cm}^2}$$

The holding power of a single alnico magnet module, at 10,000 gauss field density (1 weber/$meter^2$) and a holding area of about 2 $in.^2$ per hex is:

$$F = 57.6 \times 2 \times 2 = 230.4 \text{ lb} = 104.7 \text{ kg}$$

At 5000 gauss:

$$F = 26.2 \text{ kg}$$

The mass of the assemblies is about 15 kg. (See Table 1.)

For the two-sided holding device, at 10,000 gauss, Figure 3 of the body of the report, the holding power of a single module would be approximately:

$$F = \frac{104.7}{3} = 35 \text{ kg}$$

The results of more detailed calculations of holding power are given below.

2. Calculation of Magnetic Flux Density and Holding Power at 1000°F Operating Temperature

The magnetic flux density is first computed for the circuit of a single module containing a one-inch Alnico V magnet.

For this first calculation we assume two regions in the circuit, alnico and steel at a constant, uniform temperature.

We also initially assume that the shunt path in Figure I-1 can be ignored. The sum of the potentials around the loop are then zero (Kirchoff's law for magnetic circuits, which was derived above).

$$H_m \ell_m + H_i \ell_i = 0$$

Therefore the circuit condition is, from the above or equation (7):

$$M = -\frac{H_m \ell_m}{RA_m} = -\mu_i \frac{\ell_m}{\ell_i} \frac{A_i}{A_m} H_m$$

where again the subscript m refers to the magnet and i to the steel.

Substituting into equation (11), the condition on the magnet, we find that the following quadratic must be solved to obtain the field conditions in the magnet.

It is apparent that the magnet to steel contact area $A_i = A_m$.

$$\frac{\mu_i \ell_m}{\ell_i} H^2 + \left(\frac{\mu_i \ell_m}{\ell_i} \frac{M_s}{M_r} H_c + M_s\right) H + M_s H_c = 0 \qquad (13)$$

The values of the parameters M_s, M_r, H_c in equation (11) and Figure I-6 are for room temperature. At 1000°F, using Figure I-2 the values of these parameters must be reduced by about 20%. We have therefore used for 1000°F:

$$M_s = 1.0935 \frac{\text{weber}}{\text{meter}^2}, \quad M_r = 1.0125 \frac{\text{weber}}{\text{meter}^2}, \quad H_c = 39{,}319.3 \frac{\text{ampere}}{\text{meter}}$$

From Figure 2 of the body of the report:

$$\ell_m = 1 \text{ in.}, \quad \ell_i = 4.17 \text{ in.}$$

From Figure I-3, at about $1.1 \frac{\text{weber}}{\text{meter}^2}$ (11 kilogauss)

$$\mu_i = 4000\ \mu_o$$

Since the flux density is above its value for the peak permeability, the steel in the circuit is above saturation. Solving equation (13) we obtain:

$$H = -839 \frac{\text{ampere}}{\text{meter}} \qquad M = 1.0109 \frac{\text{webers}}{\text{meter}^2} \ (\sim 10.1 \text{ kilogauss})$$

M gives the flux density at the alnico-steel interface. Therefore the flux is given by:

$$\phi = MA_m = 1.0109 \times 2.71 \times (.0254)^2$$

$$\phi = 0.001795 \text{ webers}$$

where $A_m = 2.71 \text{ in.}^2$

However, the holding area of the hex is $A_H = 2.67$ in.^{2} Therefore,

$$M(\text{holding}) = \frac{\phi}{A_H} = 1.026 \frac{\text{webers}}{\text{meter}^2} = 10{,}260 \text{ gauss}$$

Substituting into the holding equation, the holding force per magnet module at 1000°F is:

$$F = \frac{B^2 A}{2\mu_o} = \frac{(1.0260)^2}{2 \times 4\pi \times 10^{-7}} \times 2 \times 2.67 \times (.0254)^2$$

$$F = 1442.99 \text{ newton} = 147.1 \text{ kg}$$

3. <u>Calculation of Magnetic Flux Density and Holding Power During Sodium Temperature Transient</u>

The temperature response of the magnetic circuit steel at the parting plane, following a 500°F step increase in the sodium is shown in Figure I-8. The responses shown are based upon the thermal diffusion of heat into the carbon steel, that is, they are the solutions to the heat equation:

$$\frac{\partial T}{\partial t} = \alpha \frac{\partial^2 T}{\partial x^2}$$

where α is the thermal diffusivity of carbon steel. The solution of the equation above is:

$$\frac{T_{Na} - T}{T_{Na} - T_1} = \text{erf } \xi, \ \xi = \frac{x}{2\sqrt{\alpha t}}$$

Although this thermal model is extremely oversimplified, the response times are of the same order as those obtained from more detailed models. (See Appendix II-B.)

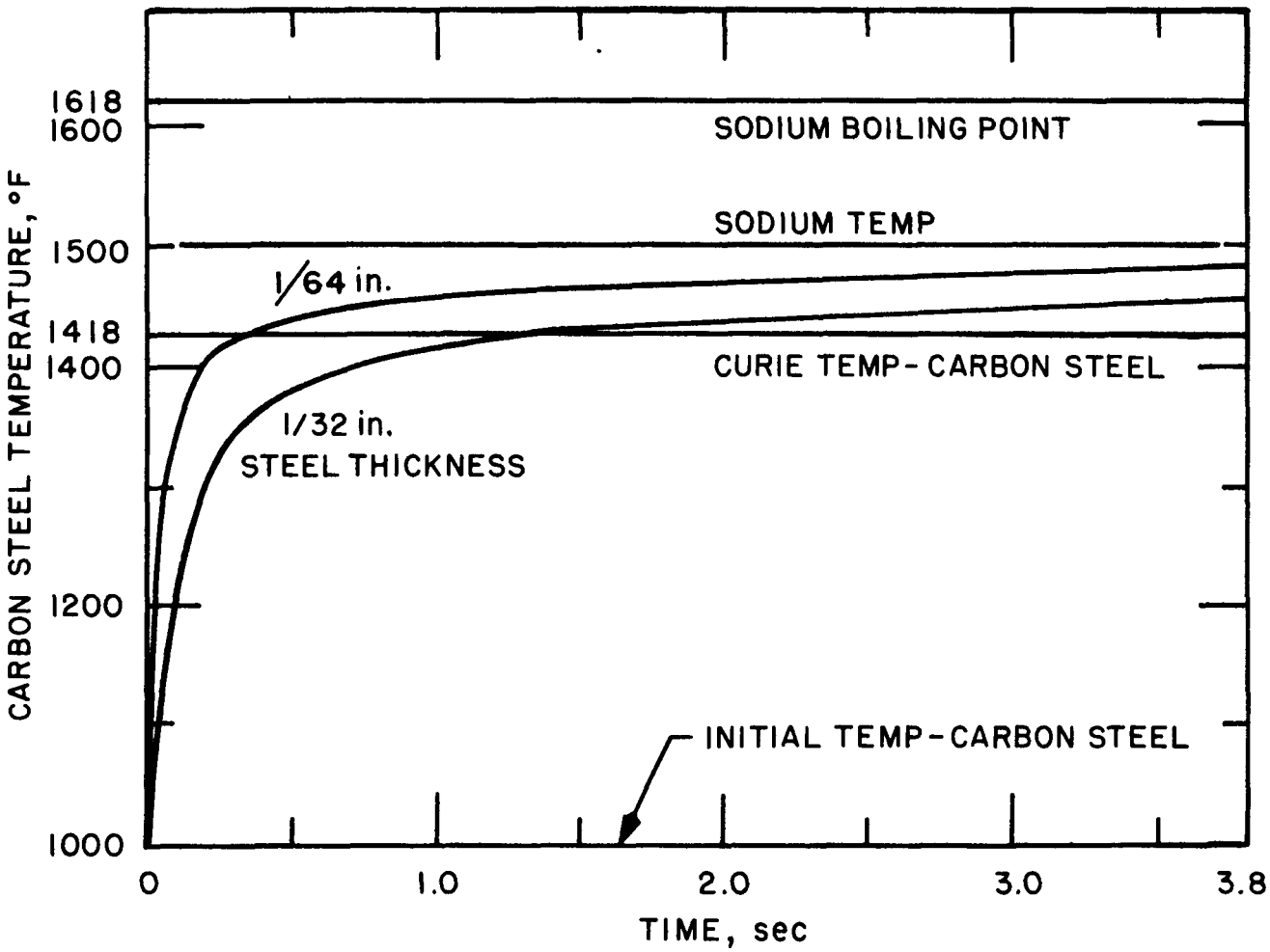

FIGURE I-8. Temperature Response in Carbon Steel at Parting Plane to Increase in Sodium Temperature

This thermal analysis would apply in particular to the two-face SASS conceptual design configuration for an increase in the temperature of the sodium in the fuel pin annulus.

From Figure I-8 it is seen that in 0.15 sec., 1/64 in. of the carbon steel is above the Curie temperature, that is, it has been completely demagnetized. This means that a gap of 1/64 in. has been introduced into the magnetic circuit. The reluctance of this gap is:

$$R_g = \frac{\ell}{\mu A} = \frac{1/64 \times 2}{\mu_o \times 2.67 \times .0254}$$

$$R_g = 0.367 \times 10^6 \text{ henrys}^{-1}$$

The next 1/64 in. zone, from Figure I-8, is seen to be at an average temperature of 1384°F; $T/T_c = 0.982$. Assuming a relative permeability of at least 1000, from Figure 4 it is apparent that the relative permeability of this second 1/64 in. zone is $\geq$ 200 since $M_s/M_o \cong 0.2$. Therefore, the reluctance of this second zone contributes less than 0.5% of the reluctance of the first zone.

The shunt reluctance is given by the reluctance of the gap "a" (Figure I-1) which because of swelling problems must be not less than 0.25 in.

$$R_a = \frac{0.25}{\mu_o \times 1.363 \times .0254}$$

$$R_a = 5.75 \times 10^6 \text{ henrys}^{-1}$$

Therefore the total reluctance seen by the magnet MMF is:

$$R = \frac{R_a R_g}{R_a + R_g} = \frac{5.746 \times .367}{5.746 + .367} \times 10^6$$

$$R = 0.345 \times 10^6 \text{ henrys}^{-1}$$

The circuit condition is now:

$$-H_m \ell_m = R\phi = RA_m M$$

$$M = -\frac{H_m \ell_m}{RA_m} = -\frac{.0254 \quad H_m}{.345 \times 10^6 \times .1748 \times 10^{-2}}$$

$$M = -0.421 \times 10^{-4} H_m$$

Substituting into equation (11):

$$.421 \times 10^{-4} H^2 + (.421 \times 10^{-4} \frac{M_s}{M_r} H_c + M_s)H + M_s H_c = 0$$

$$0.421 \times 10^{-4} H^2 + 2.8935 H + 42,995.7 = 0$$

$$H = -22,285.5 \frac{\text{ampere}}{\text{meter}} \qquad M_{tot.} = 9230.5 \text{ gauss}$$

$$M_g = \frac{R_a}{R_g + R_a} \times M_{tot.} = 9230.5 \times \frac{5.746}{6.113}$$

$$M_g = 8676.3 \text{ gauss}$$

At 1.2 sec. the gap is 1/32 in.

$$R_g = .734 \times 10^6 \text{ henrys}^{-1}$$

$$R = \frac{5.746 \times .734}{5.746 + .734} \times 10^6 = .651 \times 10^6 \text{ henrys}^{-1}$$

$$M = -.223 \times 10^{-4} H_m$$

$$.223 \times 10^{-4} H^2 + 2.041 H + 42,995.7 = 0$$

$$M_g = 6443.2 \text{ gauss}$$

Using these calculations and taking area ratios, the holding power of a single magnet module can be computed.

The computations were also made for a magnet with internal cooling channels reducing the magnet surface area by 20% thereby decreasing the holding power.

D. RESULTS

The results of these calculations are summarized in Table I-2. As can be seen in the table, the holding power will be decreased by about 38% in 0.15 sec. according to this model.

The effect of the shunt is also shown in the table. A higher percentage of the flux is shifted into the shunt as the temperature change demagnetizes the steel in the holding path.

For a reference design, the mass of a single assembly, including one magnet module, is about 15 kg. Therefore, one magnet module would be sufficient to hold a boron carbide absorber assembly.

According to the results of Table I-2, a 15 kg assembly would not be released out to 1.2 sec. However, it should be realized that the computed holding powers are certainly above that which would be attained in an actual device.

The following items all act to reduce the holding power:

1. Additional cooling channels in the magnet. The magnet material should be maintained at not more than about 1000°F steady state. This is required in order to maintain stability and to preserve magnetic force and flux of the alnico, which decreases as its Curie point is approached.

The effect of a 20% reduction in magnet material for cooling has already been calculated and summarized in Table I-2.

2. Fringing of the magnetic flux. The reluctance of paths other than the iron and alnico are not zero, so that there is some inevitable fringing of the

TABLE I-2. Flux and Holding Force Response to Step in Sodium Temperature from 1000°F to 1500°F

t(sec)	g(in)	$(A/A_m)_{nom}$	$H \frac{amp}{m}$	M_{tot}(gauss)	M_g(gauss)	M_H(gauss)	% Shunt Flux	Holding Force F(kg)	Holding Force F%
0	0	1	-839	10,109	10,109.0	10,260.0	-	147.1	100
0.15	1/64	1.0	-22,285.5	9,230.5	8,676.3	8,806.3	6.0	108.4	74
1.20	1/32	1.0	-33,089.4	7,266.3	6,443.2	6,539.7	11.3	59.8	41
0	0	0.8	-839	10,109	10,109.0	8,280.8	-	117.7	100
0.15	1/64	0.8	-18,848.3	9,478.5	8,909.4	7,234.3	6.0	73.2	62
1.20	1/32	0.8	-29,659.5	8,247.6	7,313.4	5,938.4	11.3	32.2	27

flux through these alternate paths reducing the holding flux. Fringing occurs particularly at discontinuities in the circuit such as at gaps.

Estimates can be made of the fringing for calculational purposes, but there are always some uncertainties as to the precise amount of fringing to expect. The experimental work will resolve this question.

3. The reluctance of contact gaps between materials, e.g., the iron-alnico interface.

4. Slight distortions of surfaces introducing additional reluctances.

5. Slight impurities at surfaces introducing additional reluctances.

6. Introduction of nonmagnetic fissionable material into the magnetic circuit.

7. The temperature increases throughout the circuit during the transient have been ignored. This applies in particular to the alnico which has substantial sodium cooling.

These calculations can undergo considerable refinement and a code could be written based upon the above for production calculations.

APPENDIX II: THERMAL-HYDRAULIC ANALYSIS

NOMENCLATURE

A. Hydraulic Analysis

1. ISA Flow Rate
2. Sample Calculation of Bypass Flow
3. Reduced Flow in ISA Bypass
4. Calculations of Various Geometry Related Factors for the Hydraulic Analysis

B. Thermal Transient Analysis and Thermal Time Constant of Magnetic Holding Circuit

1. Transient Response to Change in Coolant Temperature
2. Transient Response to Change in Neutron Flux

C. Cooling of Holding Magnet and Boron Carbide Assembly

1. Thermal-Hydraulic Analysis
2. Temperature Peaking in Magnet

NOMENCLATURE

(APPENDIX II)

w	mass flow rate, lb/hr
U	coolant velocity, ft/hr
A	coolant flow area, ft^2
ρ	density, lb/ft^3
μ	viscosity, lb/ft hr
D	hydraulic diameter, ft
Re or N_{Re}	Reynolds Number, $\rho UD/\mu$
r	radius, in.
d	diameter of fuel rod, in.
ℓ	width of region, in.
p	pitch of fuel rods in.
p_w	pitch of wire wrap, in.
L	flow length, ft.
f	friction factor - Mf_s
f_s	smooth friction factor
M	friction multiplication factor
P	wetted perimeter, ft.
V	volume, ft^3
g	acceleration of gravity, ft/sec^2
Δp	pressure differential, psi
T	temperature, °F
θ	temperature, °F
c_p	specific heat, Btu/lb/°F

k	thermal conductivity, Btu/hr/ft/°F
h	heat transfer coefficient, Btu/hr/ft^2/°F
Pr	Prandl No. = $\mu c_p/k$
P_e	Peclet No. = RePr = $\rho U D c_p/k$
B	Biot No. = hd/k (h of fluid, k of solid)
q	heat generation rate, Btu/hr
q_v	heat generation rate per unit volume, Btu/hr/ft^3
τ	time constant, sec.
τ_p	reactor period, sec.

Subscripts and superscripts

region or location (subscript)

- f fuel bundle
- a entrance to ISA
- b exit of lower pole
- c entrance to upper pole
- d exit to upper pole
- A lower armature
- B lower pole
- C between poles
- D upper pole
- E upper armature
- F annulus between inner duct and poison tube

flow regions (subscript)

- s main flow through ISA
- f flow through upper fuel bundle
- m flow through magnet assembly

type of flow coefficient (superscript)

- f friction
- c contraction (entrance)
- e expansion (exit)

material

- Na sodium
- s steel
- cs carbon steel
- m magnet

APPENDIX II: THERMAL-HYDRAULIC ANALYSIS

For the ISA to operate to protect the core under conditions of loss of flow, which results in an increased exit temperature in the fuel channels, a part of the flow from the fuel channels must pass through the magnetic circuit. The hot flow must heat the carbon steel adjacent to the parting surfaces, between the magnet pole pieces and the yokes, above the Curie temperature. The flow must also be sufficient to provide a convective heat transfer rate high enough to activate the device within the time required by the accident analysis. The flow through the triggering device is determined by the pressure drop across the length of fuel-blanket region spanned by the entrance and exit ports (holes), providing for the by-pass coolant (points a and f on Figure II-1).

Since the triggering device is located about one inch below the upper core-blanket interface, diverting 10 to 25% of the fuel element flow to the magnet, will not lead to overheating the fuel cladding. The return flow should be located as near the top of the device as practical, to minimize the difference in pressure and temperature between the two adjacent coolant streams. However, the bypass stream (which will be cooler) should not be introduced into the main stream if thermal stress due to poor mixing might be of concern.

A. Hydraulic Analysis

1. ISA Flow Rate

In the following analysis, it has been assumed that the flow per element in the ISA fuel channels is based upon that for an average element in the core (Table 2-5 CRBRP Reference Design Report, Volume 1)[5]

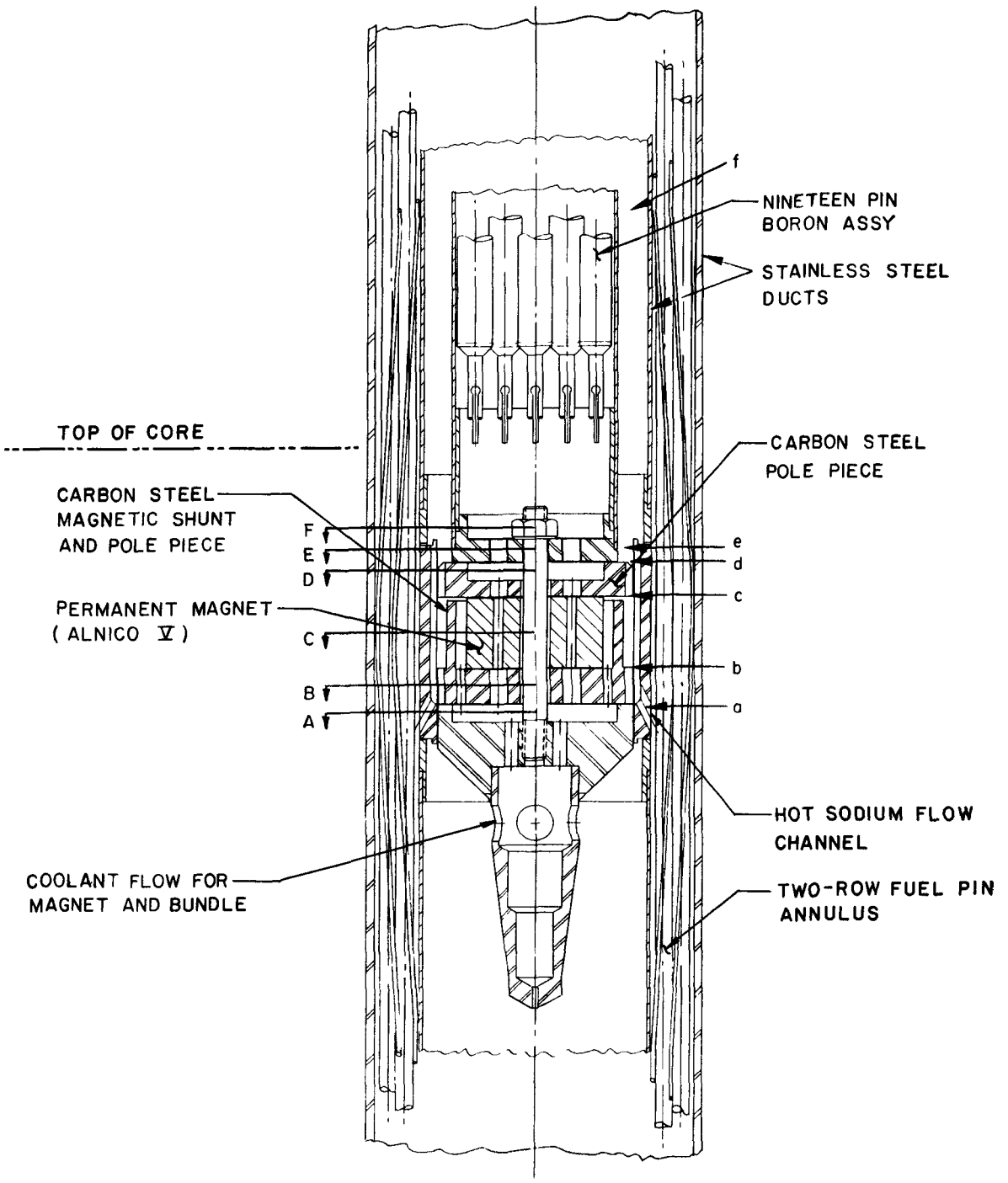

FIGURE II-1: Six-Face Horizontal Hold SASS Conceptual Design Showing Elevations for Hydraulic Analysis Calculations

$w = 33.2 \times 10^6$ lb/hr for 198 fuel assemblies of 217 elements each

$w' \cong 775$ lb/hr per element

There are 90 fuel elements in the ISA. Therefore the flow through the fuel annulus would be:

$w_s = 90 \times 775 = 69750$ lb/hr

This does not include the flow through the inner channel which cools the Alnico V magnet and B_4C rods. If the annulus flow is greater than or less than this, the bypass flow through the magnet will increase or decrease proportionally. As will be developed later, the margins of flow are sufficient for at least $\pm$ 15% of this nominal flow.

2. Sample Calculation of Bypass Flow

The calculations have been done for the six-faced horizontal hold design with side yokes (Figure II-1). However, as will be observed in the calculations, most of the pressure losses are in the entrance and exits of the channels. Therefore, the results of the analysis should be almost the same for the alternative designs.

Since it is likely that the design will continue to evolve, the calculations can be based on the configuration shown in Figure II-1 for an estimate of the feasibility of the hydraulic design. A step by step calculation procedure is presented so that a similar analysis could readily be made for a modified design. Symbols are defined in the nomenclature at the beginning of Appendix II. Values of parameters used in this section are also given, as well as calculations of flow areas, hydraulic diameters, volumes and pressure drop coefficients.

We assume as a starting point that 10% of the main flow is bypassed into the ISA magnet triggering channels. That is, $w_m = 6975$, $w_f = 62775$. For the first step we calculate velocities $U = \frac{w}{A\rho}$ in the various sections.

The subscripts give the elevations as shown in Figure II-1:

$$U_f = \frac{62775}{0.0287(50.51)} = 43334 \text{ ft/hr } (\sim 12 \text{ ft/sec})$$

$$U_{AB} = U_D = \frac{6975}{3.45\text{x}10^{-3}(50.51)} = 40010 \text{ ft/hr } (\sim 11.1 \text{ ft/sec})$$

$$U_C = U_E = \frac{6975}{0.0108(50.51)} = 12829 \text{ ft/hr } (\sim 3.6 \text{ ft/sec})$$

$$U_F = \frac{6975}{0.0185(50.51)} = 7450 \text{ ft/hr } (\sim 2.1 \text{ ft/sec})$$

Next we calculate the Reynolds numbers:

$$Re = \frac{\rho UD}{\mu}$$

and the friction coefficients:[6]

$$K = \frac{0.316}{Re^{1/4}} \quad \frac{L}{D} \quad M$$

where:

$M = 1$ for smooth channels

$$M = \left[\frac{1.034}{(p/d)^{.124}} + \frac{29.7\,(p/d)^{6.94}\,Re^{0.086}}{(p_w/d)^{2.239}}\right]^{0.885} \text{ for wire wrapped rods.}^{6}$$

a) $$Re_f = \frac{50.51(43334)(0.0127)}{0.508} = 54600$$

$$K_f = \frac{.316}{(54600)^{\frac{1}{4}}} \left[\frac{1.034}{(1.2565)^{0.124}} + \frac{29.7(1.2565)^{6.94}(54600)^{0.086}}{(51.739)^{2.239}}\right]^{0.885} \text{x } (118)$$

$$= .02067(1.052)(118) = 2.566$$

b) $Re_{AB} = Re_D = \frac{40010(50.51).0156}{.508} = 62059$

$K_{AB} = \frac{.316}{(62059)^{1/4}} (1)\ 5.3 = 0.0200(5.3) = 0.106$

$K_D = \frac{1}{2} K_{AB} = 0.053$

c) $Re_C = Re_E = \frac{12827(50.51).0234}{.508} = 29844$

$K_C = 2K_E = \frac{.316}{(29844)^{1/4}} (1)\ 3.6 = .0240(3.6) = .0866$

d) $Re_F = \frac{7450(50.51)(.05)}{.508} = 37037$

$K_F = \frac{.316}{(37037)^{1/4}} (1)\ (25) = 0.0228\ (25) = 0.569$

The pressure drop in the fluid through the fuel bundle from a to f should be the same as that bypassed through the magnet assembly since they are parallel paths:

$$\Delta P_f = K_f \frac{\rho U_f^2}{2g} = 2.566 \frac{(50.51)(43334)^2}{2(4.173\times10^8)144}$$

$$= 2.025 \text{ psi}$$

$$\Delta P_m = \Delta P_{ab} + \Delta P_{bc} + \Delta P_{cd} + \Delta P_{de} + \Delta P_{ef}$$

$$= (K_c^c + K^f_{AB} + K_b^e) \frac{\rho U_{AB}^2}{2g} + \frac{K_c^f \rho U_C^2}{2g} + (K_c^c + K_D^f + K_d^e) \frac{\rho U_C^2}{2g}$$

$$+ K_E^f \frac{\rho U_E^2}{2g} + K_F^f \frac{\rho U_F^2}{2g}$$

$$\Delta p_m = \frac{50.51}{2(4.173 \times 10^8)} (1.372 + .106 + .436)(40010)^2 + 0.0866(12829)^2$$

$$+ (1.128 + .053 + .436)(40010)^2 + (.0433)(12828)^2$$

$$+ (.569)(7450)^2$$

$$= 4.2028 \times 10^{-10} [3.064\text{x}10^9 + 1.425\text{x}10^7 + 2.588\text{x}10^9 + .713\text{x}10^7 + 3.158\text{x}10^7]$$

$$= 4.2028 [.5705) = 2.398 \text{ psi}$$

We note that if all the frictional terms (K^f_{AB}, K^f_C, K^f_D, K^f_E, K^f_F) were neglected we would have obtained:

$$\Delta p_m = 4.2088\text{x}10^{-10} [(1.372 + .436) + (1.128 + .436)](40010)^2$$

$$= 4.2088(3.372)(.1601) = 2.269 \text{ psi}$$

[about a five percent difference].

To summarize these calculations:

Region	U (ft/hr.)	Re	K	With Frictional Terms Δp (psi)	Neglecting Frictional Terms Δp (psi)
f	43334	54600	2.566	2.025	2.025 (Fuel)
a			1.372		
AB	40010	62059	.106	1.288	1.216
b			.436		
C	12829	29844	.087	.006	
c			1.128		
D	40010	62059	.053	1.088	1.052
d			.436		
E	12829	29844	.043	.003	
F	7450	37037	.569	.013	
m			3.564	2.398	2.269 (Magnet)

where:

$$K_m = \frac{\Delta p}{\frac{\rho U^2}{2g}}$$

If we assume that the friction factors don't change very much, with small changes in velocity, we are able to improve the estimates of the relative bypass flow as follows:

$$A_f U_f + A_m U_m = w_s/\rho$$

and

$$K_f U_f^2 \cong K_m U_m^2$$

or

$$U_f \cong \sqrt{\frac{K_m}{K_f}}\ U_m$$

and

$$A_f \sqrt{\frac{K_m}{K_f}} + A_m \quad U_m = w_s/\rho$$

where $K_m \approx (3.372 + .159) + (\frac{.1299}{.0108} + \frac{.569}{.0185}) \times .00345$

≈ 3.679

$K_f = 2.566 \quad \sqrt{\frac{K_m}{K_f}} = 1.197$

$$U_m = \frac{69750/50.51}{.0287(1.197) + .00345} = 36519\ \frac{ft}{hr}$$

$U_f = 43714$ ft/hr.

Using these values we find:

Region	U (ft/hr)	Re	K	Δp (psi)	
f	43714	55200	2.559	2.0553	(Fuel)
a, AB, b	36519	56644	1.372, .1086, .436	1.0742	
C	11666	27142	.0886	.0051	
c, D, d	36519	56644	1.128, .0543, .436	.9070	
E	11666	27142	.0443	.0025	
F	6810	33857	.982	.0114	
			∿ 3.569	2.0000	(Magnet)

Iterating again, we find for $K_m \approx 3.569$, $K_f = 2.559$:

$$\sqrt{\frac{K_m}{K_f}} = 1.181, \; U_m = 36978, \; U_f = 43671 \text{ ft/hr}$$

Region	U (ft/hr)	Re	K	Δp (psi)	
f	43671	59146	2.560	2.052	(Fuel)
a, AB, b	36978	57356	1.372, .1082, .436	1.101	
C	11812	27483	.088	.005	
c, D, d	36978		1.128, .0561, .436	.930	
E	11812		.044	.003	
F	6896	34283	.581	.012	
m			3.567	2.050	(Magnet)

The convergence is sufficiently close.

Therefore $w_m = \rho U_m A_m = 6444$ lb/hr

$w_m/w_s = 9.2\%$

3. Reduced Flow in ISA Bypass

If we assume the flow into the ISA is reduced by 15%, due to local flow blockage or general loss of flow conditions, we can find the heat capability from the flow rate through the magnet.

$$w_s = 0.85 \times 69750 = 59287 \text{ lb/hr}$$

Assume $w_f = 53359$ and $w_m = 5928.8$.

Region	U (ft/hr)	Re	K	Δp (psi)	
f	38800	47984	2.650	1.608	(Fuel)
a			1.372		
AB	34022	52772	.110	.933	
b			.436		
C	10868	25286	.090	.004	
c			1.128		
D	34022	52772	.055	.788	
d			.436		
E	10868	25286	.045	.002	
F	6345	31542	.593	.010	
m			3.567	1.735	(Magnet)

On iteration $\sqrt{\frac{K_m}{K_f}} = 1.160, U_m = 32850$ ft/hr. Therefore:

f	38135	48154	2.648	1.618	(Fuel)
a			1.372		
AB	32874	50991	.111	.872	
b			.436		
C	10501	24433	.091	.004	
c			1.128		
D	32874	50991	.056	.736	
d			.436		
E	10501	24433	.045	.002	
F	6131	30478	.598	.009	
m			3.574	1.623	(Magnet)

And so $U_m \cong 32850$ ft/hr $w_m \cong 5725$ lb/hr $w/w_s \cong 9.7\%$

The ratio of flow through the magnet for full versus 85% flow is $\frac{5725}{6444} \cong 89\%$.

4. Calculation of Various Geometry Related Factors for the Hydraulic Analysis

a. Area and Hydraulic Diameter of Fuel Channel

In the main channel below A (Figure II-1) we consider a 1/12 segment (Figure II-2):

$$\frac{1}{12}A_f = \left\{\left(\frac{1.251 + 0.915}{2} \times .592\right) - 7.5\left[\frac{.23^2}{4}\pi + \left(\frac{11.9 + 0.276\pi}{11.9}\right) \times .056^2 \frac{\pi}{4}\right]\right\}$$

$$= 0.30852 \text{ in}^2 =$$

$$\frac{1}{12}P_f = 1.251 + 0.916 + 7.5\left[.230\pi + \left(\frac{11.9 + 0.276\pi}{11.9}\right) \times .056\pi\right]$$

$$= 8.9969 \text{ in}$$

$$D_f = \frac{4A_f}{P_f} = 0.13724 \text{ in} = 0.0114 \text{ ft}$$

$$A_f = \frac{12(.30852 \text{ in}^2)}{144 \text{ in}^2/\text{ft}^2} = 3.702 \text{ in}^2 = 0.0257 \text{ ft}^2$$

In the channel adjacent to the magnet:

$$\frac{A_f^1}{12} = \frac{A_f}{12} + .06(0.594) = .344 \text{ in}^2$$

$$\frac{P_f^1}{12} = \frac{P_f}{12} + .06 = 9.0569 \text{ in}$$

$$D_f^1 = 0.152 \text{ in} = 0.0127 \text{ ft}$$

$$A_f^1 = 4.1275 \text{ in}^2 = 0.0287 \text{ ft}^2$$

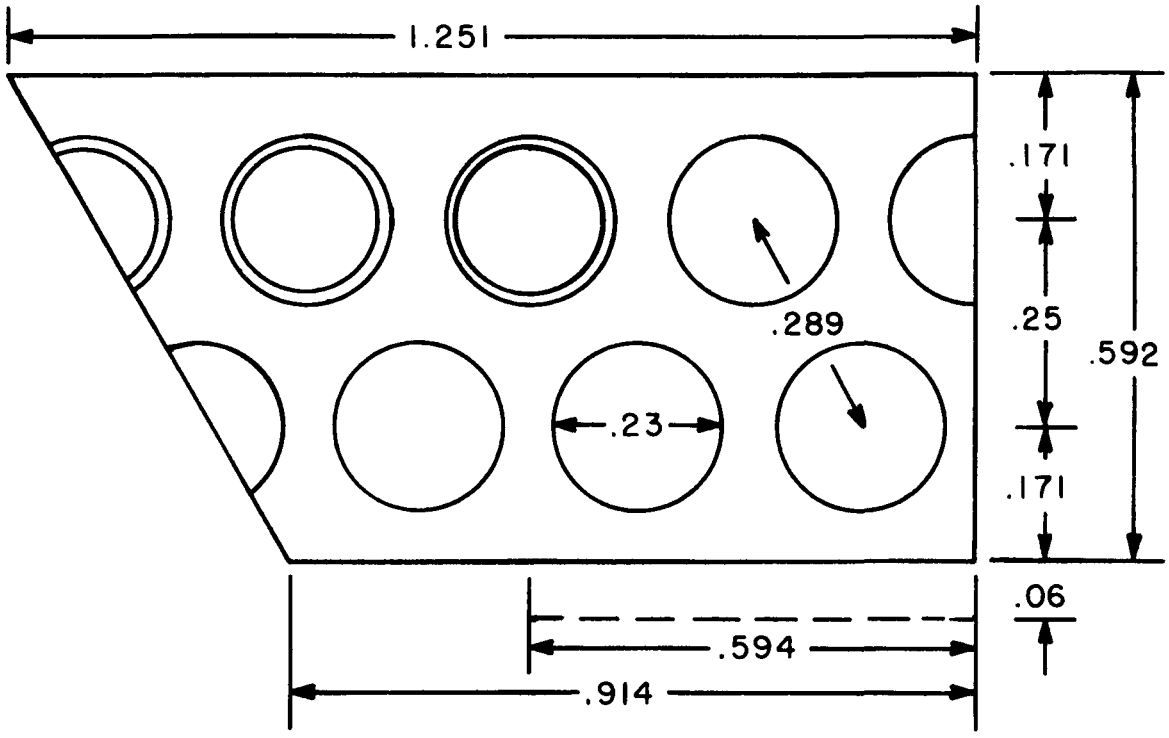

FIGURE II-2. One-Twelfth Segment of Fuel Channel of ISA

b. Areas and Hydraulic Diameters Along By-pass Channels Through ISA Magnet

Refer to Figure II-1 for section dimensions.

At section AB (entrance and lower pole piece) and Section D (upper pole piece) there are eighteen 3/16 in. diameter holes

$$A_{AB} = A_D = 18\left(\frac{3}{16}\right)^2 \frac{\pi}{4} = 0.497 \text{ in}^2 = 3.45 \times 10^{-3} \text{ft}^2$$

$$P_{AB} = P_D = 18\left(\frac{3}{16}\right)\pi = 10.603 \text{ in} = .884 \text{ ft}$$

$$D_{AB} = D_D = 0.1875 \text{ in} = 0.156 \text{ ft}$$

At section C and E:

$$A_C = A_E = 6\left(\frac{1.3125^2}{2 \cos 30}\right) - (1.219)^2 \pi + 9(.188)^2 \frac{\pi}{4}$$

$$= 1.550 \text{ in}^2 = 0.0108 \text{ ft}^2$$

$$P_C = P_E = \frac{(1.3125)(6)}{\cos 30} + (1.219)2\pi + (18)(.1875)\frac{\pi}{2}$$

$$= 22.052 \text{ in} = 1.838 \text{ ft}$$

$$D_C = D_E = 0.281 \text{ in} = .0234 \text{ ft}$$

At section F:

$$A_F = \left(\frac{(1.455)^2}{2 \cos 30}\right) 6 - (1.219)^2 \pi = 2.667 \text{ in}^2 = 0.0185 \text{ ft}^2$$

$$P_F = \frac{(1.455)6}{\cos 30} + 2(1.219)\pi = 17.738 \text{ in} = 1.478 \text{ ft}$$

$$D_F = 0.601 \text{ in} = 0.050 \text{ ft}$$

c. Entrance and Exit Coefficients for Flow

The contraction (entrance) coefficient can be represented based on conservation of momentum by $K_m^c \simeq 2(1 - \frac{a_1}{a_o})$ or on conservation of energy by $K_{en}^c \simeq [1 - (\frac{a_1}{a_o})^2]$. The former over-estimates, while the latter under-estimates, the measured value. The exit (expansion) coefficient is reasonably represented by the momentum expression:

$$K_m^e = 2\left[1 - \frac{a_o}{a_1}\right]\left(\frac{a_o}{a_1}\right)$$

The contraction coefficient at a is given by:

$$K_a^c = \frac{1}{2}\left\{2\left[1 - \frac{0.497}{4.128}\right] + \left[1 - \frac{.497}{4.128}\right]^2\right\}$$

$$= 1.372$$

The expansion coefficient at b and d is given by:

$$K_b^e = K_d^e = 2\left(1 - \frac{.497}{1.55}\right)\frac{.497}{1.55} = 0.436$$

The contraction coefficient at c is given by:

$$K_c^c = \frac{1}{2}\left\{2\left[1 - \frac{.497}{1.55}\right] + \left[1 - \frac{.497}{1.55}\right]^2\right\}$$

$$= 1.128$$

No correction has been made for the turn from the main stream into the by-pass holes, or the bend in the entrance, since all lengths are short and no developed flow down-stream is realized.

TABLE II-1. Summary of Geometric Parameters

	L(ft)	A(ft^2)	D(ft)	K	L/D
Normal fuel channel		0.0257	0.0114		
Bypass fuel channel	1.5	0.0287	0.0127	2.566*	118
Entrance A				1.372	
Pole face B	0.083	3.45×60^{-3}	0.0156	.106*	5.3
Exit B				0.436	
Section C	0.083	0.0108	0.0234	.0866*	3.6
Entrance C				1.128	
Pole face D	0.042	3.45×10^{-3}	0.0156	0.053*	2.7
Exit d				0.436	
Section E	0.042	0.0108	0.0234	0.0433*	1.8
Section F	1.25	0.0185	0.050	0.569*	25

*calculated in text.

B. Thermal Transient Analysis and Thermal Time Constant of Magnetic Holding Circuit

Several transient analyses have been carried out to estimate the temperature transient response in triggering the device. This has been done both for an increase in the sodium coolant temperature flowing through and around the device, as would occur for a loss of coolant accident, and for a fast reactivity insertion which depends upon the presence of the fissile source.

1. Transient Response to Change in Coolant Temperature

a. Three-Node Model

First a conservative multi-node thermal transient analysis was carried out, to determine the temperature transient response at the magnetic parting plane due to a change in the temperature of the sodium coolant flowing through and around the device. It is shown that a simple single node model gives almost the same time constant.

In order to make the calculation, one side of the hexagonal geometry of Figure 2 in the body of the report is mocked up as shown in Figure II-3. Sodium flows in the three channels, and on the outside of the floating panel, as indicated in Figure II-3.

We wish to compute the change in the temperature, T_2 of node 2 containing the parting plane, due to an increase in the temperature of the flowing sodium. As an added conservativism, it is assumed that the temperature of the root of the device T_4 remains constant at the initial ambient temperature.

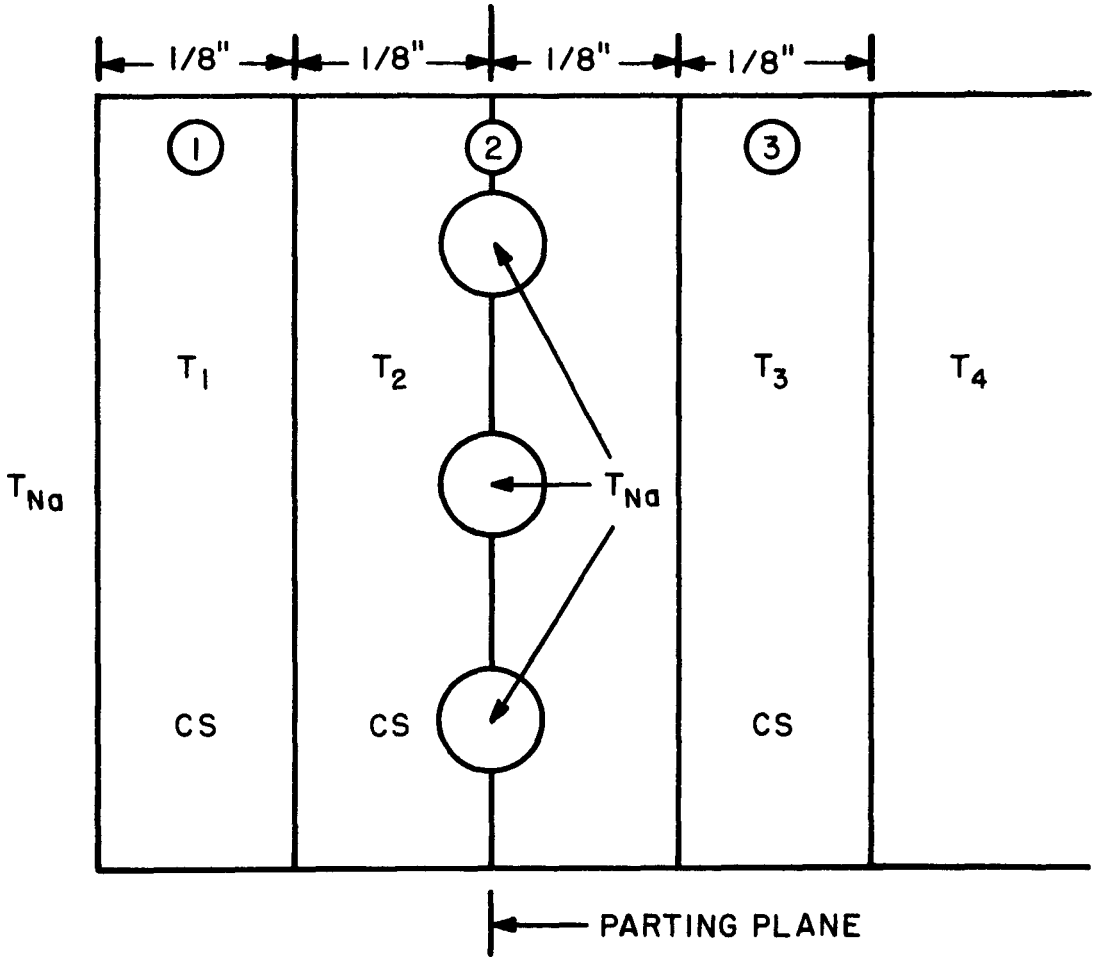

FIGURE II-3. Nodal Mockup of Magnet Assembly

The transient equations of the three nodes are written as shown below:

$$\rho C_p V_1 \frac{dT_1}{dt} = h A_1 (T_{Na} - T_1) - \frac{kA_1}{\ell_1} (T_1 - T_2) \tag{1}$$

$$\rho C_p V_2 \frac{dT_2}{dt} = h A_2 (T_{Na} - T_2) - \frac{kA_1}{\ell_2} (T_2 - T_1) - \frac{kA_1}{\ell_2} (T_2 - T_3) \tag{2}$$

$$\rho C_p V_3 \frac{dT_3}{dt} = - \frac{kA_1}{\ell_2} (T_3 - T_2) - \frac{kA_1}{\ell_3} (T_3 - T_4) \tag{3}$$

Taking the Laplace transform of equations (1), (2), and (3) above and solving for the temperature in node 2 we obtain:

$$\begin{aligned} T_2(s) = {} & \frac{0.960\ (.142s + 1)(.565s + 1)}{s(.136s + 1)(.182s + 1)(.585s + 1)}\ T_{Na} \\ & + \frac{0.00688(.575s + 1)}{(.136s + 1)(.182s + 1)(.585s + 1)}\ T_1(0) \\ & + \frac{0.182(.138s + 1)(.575s + 1)}{(.136s + 1)(.182s + 1)(.585s + 1)}\ T_2(0) \\ & + \frac{0.0286(.138s + 1)}{(.136s + 1)(.182s + 1)(.585s + 1)}\ T_3(0) \\ & + \frac{0.04(.138s + 1)}{s(.136s + 1)(.182s + 1)(.585s + 1)}\ T_4 \end{aligned} \tag{4}$$

s is the Laplace transform variable.

From the first term of Eq. (4) we see that the temperature in node 2 approaches that of 96% of the sodium temperature with a time constant of about 0.2 sec. This is apparent since the two lead modes in the numerator practically cancel two of the lag modes in the denominator.

Applying the final value theorem to Eq. (4), the steady state temperature in node 2 containing the parting plane is given by

$$T_{2ss} = 0.96\ T_{Na} + 0.04\ T_4 \tag{5}$$

Assuming step changes in sodium temperature, it is seen in Table II-2 that the steady state temperature at the parting plane in node 2 approaches within about 1% of the sodium temperature. We have assumed that the temperature in the root, T_4, remains at the colder initial ambient.

b. Single Node Model

If the three nodes in Figure II-4 are treated as a single node, the resulting equation is:

$$\rho c_p V \frac{dT}{dt} = h\ A(T_{Na} - T) \tag{6}$$

The time constant is:

$$\tau = \frac{\rho c_p V}{hA} \tag{7}$$

Using material properties for carbon steel:

$$\rho = 490\ \text{lb/ft}^3$$

$$c_p = 0.16\ \text{btu/lb/°F}$$

and a heat transfer coefficient of 20,000 btu/hr/ft^2/°F, the time constant of Eq. (7) is computed to be:

$$\tau = 0.24\ \text{sec.}$$

This is very close to the result obtained for the dominant time constant of the three node case. It is indicative of the large Biot number in

TABLE II-2. Three Node Model Steady-State Temperatures

T_{Na} (°F)	T_4 (°F)	T_{2ss} (°F)	ΔT (°F)	ΔT (%)
1200	1000	1192	8	0.67
1300	1000	1288	12	0.92
1400	1000	1384	16	1.14
1500	1000	1480	20	1.33

that the rate of heat transfer into the solid from the liquid is great compared to the rate at which it is conducted away.

c. Results and Conclusions

The calculations above indicate that a thermal time constant of about 0.25 sec. is attainable with the present design of the magnetic Curie point device. This is one of the main time constants which controls the response of the ISA during accident conditions. In order to be conservative, a minimum time delay of 0.5 sec. instead of 0.25 sec. has been used in performing the accident analyses (see Section V).

2. Transient Response to Change in Neutron Flux

The single node model will be used in this analysis. In order to compute the response of the assembly to a change in neutron flux due to a fast reactivity insertion, a source term must be added to equation (6) of the previous section.

Equation (6) then becomes:

$$\rho c_p V \frac{dT}{dt} = hA(T_{Na} - T) + q \qquad (8)$$

where q is the total heat source in the carbon steel treated as a single node. q is the total fissile source in the node, which is proportional to the neutron flux at the assembly. The assembly is placed at the top of the core.

Because of the presence of the fissile source, the carbon steel of the assembly will run at a steady state temperature substantially above that of the sodium ambient.

From equation (8) this temperature is given by:

$$\theta_o = T_{cs} - T_{Na} = \frac{q}{hA}$$

For a cermet, 35% UO_2 by volume, using fully enriched uranium, θ_o is about 200°F; for 50% enriched uranium it is about 100°F. This is based upon the fissile source heating rates given in the reactor physics section of this report for the CRBR at 100% power (Section VI). The optimum temperature would be determined in the final design by adjusting the uranium enrichment and cermet UO_2 volume percent.

If θ is the temperature of the carbon steel above the sodium ambient, equation (8) becomes:

$$\tau \frac{d\theta}{dt} + \theta = q(t) \tag{9}$$

τ is given by equation (7).

For an accident resulting in a neutron flux ramp, the response of the carbon steel temperature is obtained from equation (9):

$$\theta(t) = \frac{Q}{hA} [t - \tau(1 - e^{-t/\tau})] \tag{10}$$

where Q is the source ramp rate.

It is apparent from equation (10) that, after a delay time τ, the temperature ramp in the carbon steel, which eventually triggers the assembly, lags the flux by the time constant τ. (τ was shown to be about 0.25 sec. for the device.) The addition of the fissile source has the effect of removing the dependence of the device upon the thermal time constant of the core.

The response of the device to an exponential flux rise is also obtained from equation (9):

$$\theta(t) = \frac{q_o}{hA(1 + \frac{\tau}{\tau_p})} [\frac{\tau}{\tau_p} e^{-t/\tau} + e^{t/\tau_p}] \tag{11}$$

where τ is again the dominant time constant of the ISA, and τ_p is the reactor period. This response has been plotted in Figure II-4 for a reactor period of 3 sec. and a conservative time delay of 1 sec. The exponential flux rise is also shown on Figure II-4. Again we have the result that the temperature of the magnetic circuit is delayed with respect to the neutron flux response at the top of the core by the time constant of the device.

These simple model calculations have been performed to bring out the characteristics of the response of the assembly based upon the presence of the fissile source, and to present some of its pertinent design parameters. The effectiveness of this magnetic hold device in protecting the core is brought out in the accident analysis of Section V.

C. Cooling of Holding Magnet and Boron Carbide Assembly

1. Thermal-Hydraulic Analysis

A nominal flow of sodium is required to cool the permanent magnet assembly, to maintain it at about 1000°F, well below the Curie temperature of Alnico V of about 1580°F. Coolant must also flow through the poison column of clad B_4C rods located above the magnetic trigger. Simple calculations indicate that a flow of 3.9 ft/sec of sodium in the poison column is adequate for cooling the poison in the cocked condition at power, or in the released position at decay heat power. It is assumed that the poison column is an array of 19 stainless steel clad B_4C rods. The outer cladding diameter is 0.472 in., the triangular pitch is 0.482 in. The bundle is contained in a hexagonal tube and is 72 inches long. The pressure drop through the poison column is about 2 psi.

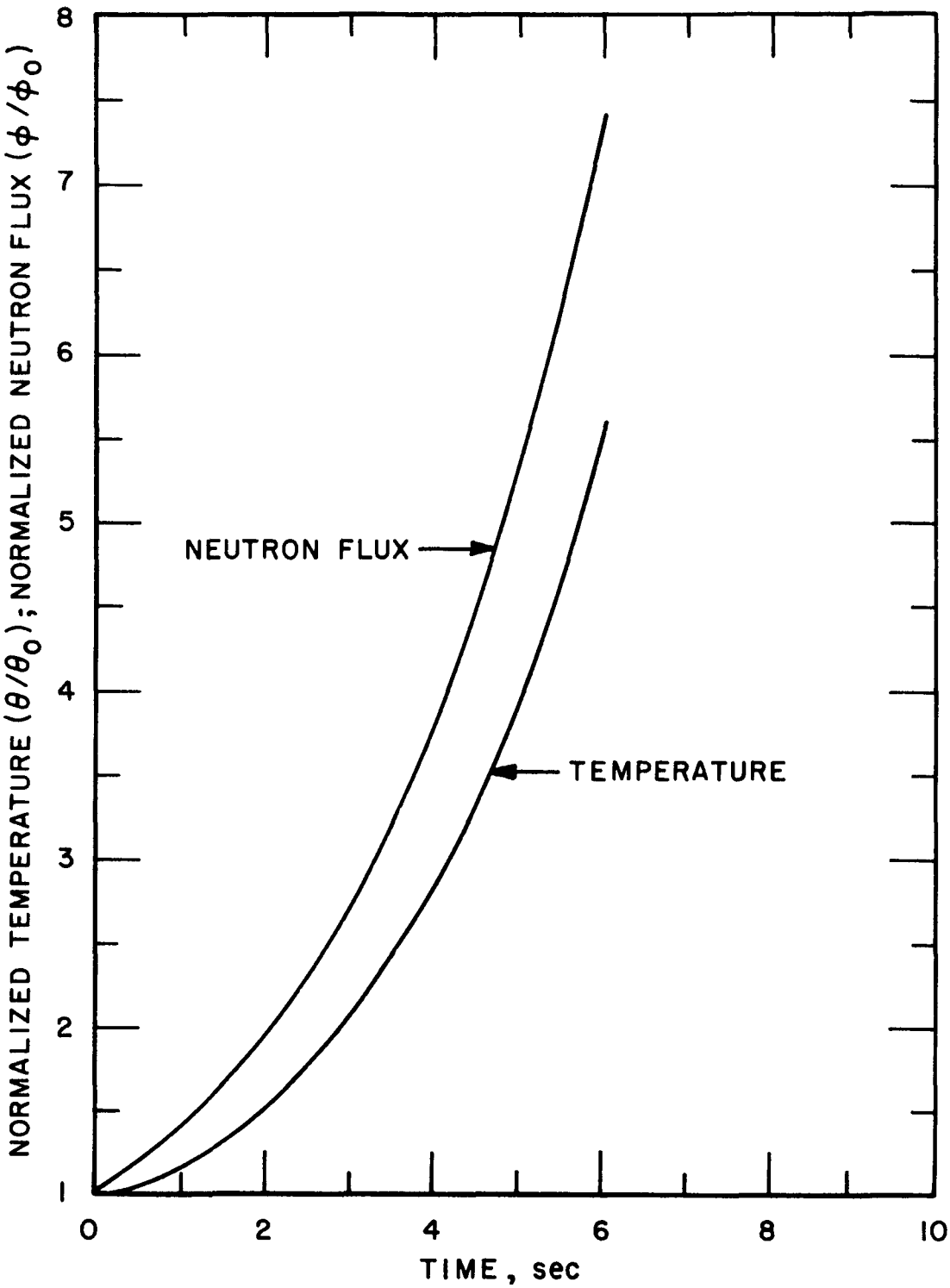

FIGURE II-4. Response of ISA to Exponential Flux Rise

The flow through the magnet assembly is via a channel through the nose piece to the lower pole face ($\Delta p \simeq 2.15$ psi), and via twelve 3/16 in. holes in the Alnico V magnet and six 3/32 in. holes. The flow then proceeds into the annular region between the Alnico V and shunt pole (1.05 psi), and from the magnet through the upper assembly (1.55 psi) for a total loss of about 4.75 psi.

The total pressure loss through the magnet and poison column is about 7 psi at this low flow. The rest of the pressure drop between the lower orifice area and the top of the fuel element must be provided by orifices below the core region. In order to reduce pressure differentials as much as possible, two orifices are provided, one six inches long at the lower end (partly to provide shielding), and a second, one inch long located just below the poison assembly snubber.
The fuel assembly nominal pressure drop is 17 psi between the orifice area and upper plenum. Therefore,about 64 psi must be lost in these two orifices. By assuming an entrance loss coefficient of 1, exit loss of 0.5 and frictional losses of about 3.5, one calculates a flow velocity through the orifices of about 60 ft/sec and an orifice size of about one-quarter inch.

A heat transfer coefficient of about 20,000 Btu/hr/ft^2/°F is calculated in the magnet assembly, and a time constant for heat flow of about 0.2 sec. is realized as noted above. A heat rate of 4 watts/gm in the magnetic materials due to gamma and neutron heating will produce a heat load of about 37000 Btu/hr. At the nominal flow rate there will be a temperature rise of about 35°F through the magnet, which is reasonable. There will be no danger of overheating even for flow rates reduced by a factor of five, especially since the coolant will be only nominally above the inlet temperature.

2. Temperature Peaking in Magnet

Calculations have also been performed to estimate the temperature peaking to be expected inside the Alnico magnet stack due to internal heating.

The internal heat generation is due to deposition of high energy gamma and neutron radiation produced directly or indirectly by the fission process. For fast reactors about 14% of the power generation is produced in this way. The computation has been carried out for a conservative deposition rate of 10 w/gm and for a best estimate deposition rate of 4 w/gm based upon CRBR full power operation. The computation of this deposition rate by the Applied Physics Division is discussed in Section V of this report. Assuming a density roughly that of steel for the magnet stack, the volumetric power density is conservatively about:

$$q_v = 75 \frac{\text{watts}}{\text{cm}^3} = 7.25 \times 10^6 \frac{\text{Btu}}{\text{hr ft}^3}$$

and $q_v = 30 \frac{\text{watts}}{\text{cm}^3} = 2.9 \times 10^6 \frac{\text{Btu}}{\text{hr ft}^3}$ as a best estimate. The geometry assumed for the calculation is that of a hollow circular cylinder of internal radius r_1 and external radius r_2. It has been assumed that both the internal and external surface of the cylinder are cooled by sodium with a heat transfer coefficient of from 10,000 to 20,000 Btu/hr/ft^2/°F. The temperature within the cylinder is given by:

$$T = T_1 - \frac{q_v}{4k} (r^2 - r_1^2) + E \ln \frac{r}{r_1}$$

The constant E in the equation has the value:

$$E = \frac{q_v r_1 r_2}{2k} \frac{[\frac{B_1}{2} + 1]}{[B_2 + 1]}$$

where B_1 and B_2 are characteristic Biot numbers:

$$B_1 = \frac{h(r_2 - r_1)}{k}$$

$$B_2 = \frac{h}{k} \left(\frac{r_1 r_2}{r_1 + r_2}\right) \ln \frac{r_2}{r_1}$$

The internal and external temperatures of the cylinder are given by:

$$T_1 = T_o - \frac{q_v r_1}{2h} + \frac{E}{B_3}$$

$$T_2 = T_o + \frac{q_v r_2}{2h} - \frac{E}{B_4}$$

where T_o is the sodium ambient temperature and B_3 and B_4 are additional Biot numbers as follows:

$$B_3 = \frac{hr_1}{k}$$

$$B_4 = \frac{hr_2}{k}$$

Using the following parameters for the magnet with an internal cooling channel (see Figure II-5):

$r_1' = 0.55$ in.

$r_2 = 0.95$ in.

$k = 20$ Btu/hr/ft/°F

$h = 20{,}000$ Btu/hr/ft^2/°F

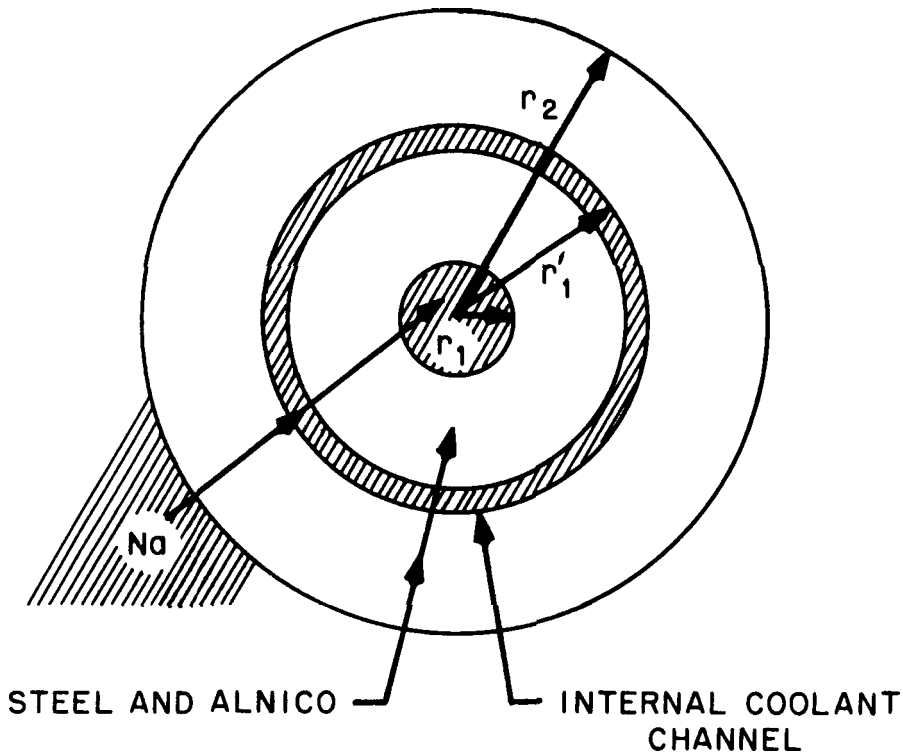

FIGURE II-5. Split Magnet Cooling Arrangement for Holding Magnet

The values of the Biot numbers are:

$B_1 = 33.3$ $\qquad$ $B_3 = 45.8$

$B_2 = 15.9$ $\qquad$ $B_4 = 79.2$

and the constant E in equations (1) and (4) has the value:

$$E = 275.1°F$$

on a best estimate basis.

The internal and external film temperatures are obtained from equation (4):

$T_1 - T_o = 2.7°F$ (Internal)

$T_2 - T_o = 2.3°F$ (External)

The maximum temperature in the stack occurs at a radius of:

$$r = \sqrt{\frac{E}{q_v/2k}} = 0.739 \text{ in.}$$

and the maximum internal temperature for these conditions, using equation (1) is:

$$T_{max} = T_o + 22.7°F$$

The calculations above were performed for a heat transfer coefficient of 20,000 internally and externally. They were repeated for a heat transfer coefficient of 10,000 Btu/hr/ft^2/°F.

The same calculations were also performed for solid cylinders without the additional internal cooling channel for 10,000 and 20,000 Btu/hr/ft^2/°F. This calculation was also done assuming an internal radius $r_1 = 0.15$ and the same external radius of 0.95 in. and for a larger size magnet, all on the conservative heat deposition basis. The results are shown in Table II-3.

TABLE II-3. Temperature Rise in Magnet Due to Internal Heating

Inner Radius	Outer Radius		Heat Transfer Coeff.	Temp. Across Film Internal	Temp. Across Film External	Maximum Temperature Rise in Magnet	
r_1 in.	r_2 in.	q_v $\frac{w}{cm^3}$	h $\frac{Btu}{hr\ ft^2\ °F}$	T_1-T_o °F	T_2-T_o °F	$T_{max} - T_o$ °F	
.15	.95	75	10,000	41.8	21.4	248.0	6.3%
.15	.95	75	20,000	21.3	10.6	232.4	
.55	.95	75	10,000	13.3	11.4	62.7	9.3%
.55	.95	75	20,000	6.7	5.7	56.9	
.825	1.5	75	10,000	23.0	19.0	159.5	6.6%
.825	1.5	75	20,000	11.5	9.5	148.9	
.825	1.5	75	-	0	0	144.8	
.55	.95	30	10,000	5.3	4.5	25.1	9.6%
.55	.95	30	20,000	2.7	2.3	22.7	

It is apparent from Table II-3 that, without additional internal cooling for the hollow cylinder magnet stack, the temperature rise due to internal heating would not be acceptable.

However, with internal cooling, the maximum internal temperature rise can be reduced to less than 25°F. Since we wish the alnico to run at about 1000°F, the internal cooling makes the temperature rise manageable. Because of the high Biot numbers, doubling the heat transfer results in a maximum temperature decrease of from 5 to 10%, the higher heat transfer being more effective in reducing the maximum temperature for the internally cooled case, as would be expected.

APPENDIX III: REACTOR PHYSICS ANALYSIS

A. Description of CRBR First Core and Equilibrium Core Models

B. Assembly Worths and Impact on Core Performance

C. Fissile Source Heating Rates

APPENDIX III: REACTOR PHYSICS ANALYSIS

A. Description of CRBR First Core and Equilibrium Core Models

A general description of the first core and equilibrium core models is given in Table III-1. The beginning of cycle first core is representative of the initial load; the beginning of cycle equilibrium core is representative of an equilibrium cycle with a two year core and axial blanket residence time, and a three year radial blanket residence time. Figure III-1 is a CRBR R-Z map showing region detail and physical dimensions. Each radial region corresponds to one ring of assemblies, and control regions are centered within their appropriate rings. Figure III-2 is a CRBR layout showing individual control assembly placements.

B. Assembly Worths and Impact on Core Performance

Assembly worths were calculated for both a first core and an equilibrium core using ISA and CRBR type control assemblies. A description of masses and enrichments used for CRBR rod worths is given in Table III-2. CRBR primary and secondary control assembly positions in hex geometry are shown in Figure III-3, and the corresponding first core and equilibrium core rod worths are given in Table III-3. Calculated values show a 2-5% upward bias when compared with CRBR reported worths.[14] These differences are attributed to different prescriptions for developing self-shielding control cross sections, and to a lesser extent on modeling differences. Relative comparisons between ISA and CRBR control assemblies are not affected by these differences.

TABLE III-1. Summary of CRBR Heavy Metal* Masses (kg)

First Core, Beginning of Cycle

	Inner Core	Outer Core	Radial Blanket	Axial Blanket
^{235}U	20.36	15.24	32.12	10.61
^{238}U	2924.76	2189.14	16233.4	5361.76
^{239}Pu	463.25	563.37		
^{240}Pu	132.78	161.47		
^{241}Pu	70.10	85.25		
^{242}Pu	16.77	20.		

Equilibrium Core, Beginning of Cycle

^{235}U	17.37	13.61	29.50	10.63
^{238}U	2832.62	2120.96	16069.55	5331.00
^{239}Pu	470.84	564.26	143.20	28.49
^{240}Pu	147.71	174.81	3.00	0.453
^{241}Pu	64.60	81.43	0.0388	0.004
^{242}Pu	18.67	22.22	0.0004	0.00002

*Heavy metal excludes oxygen

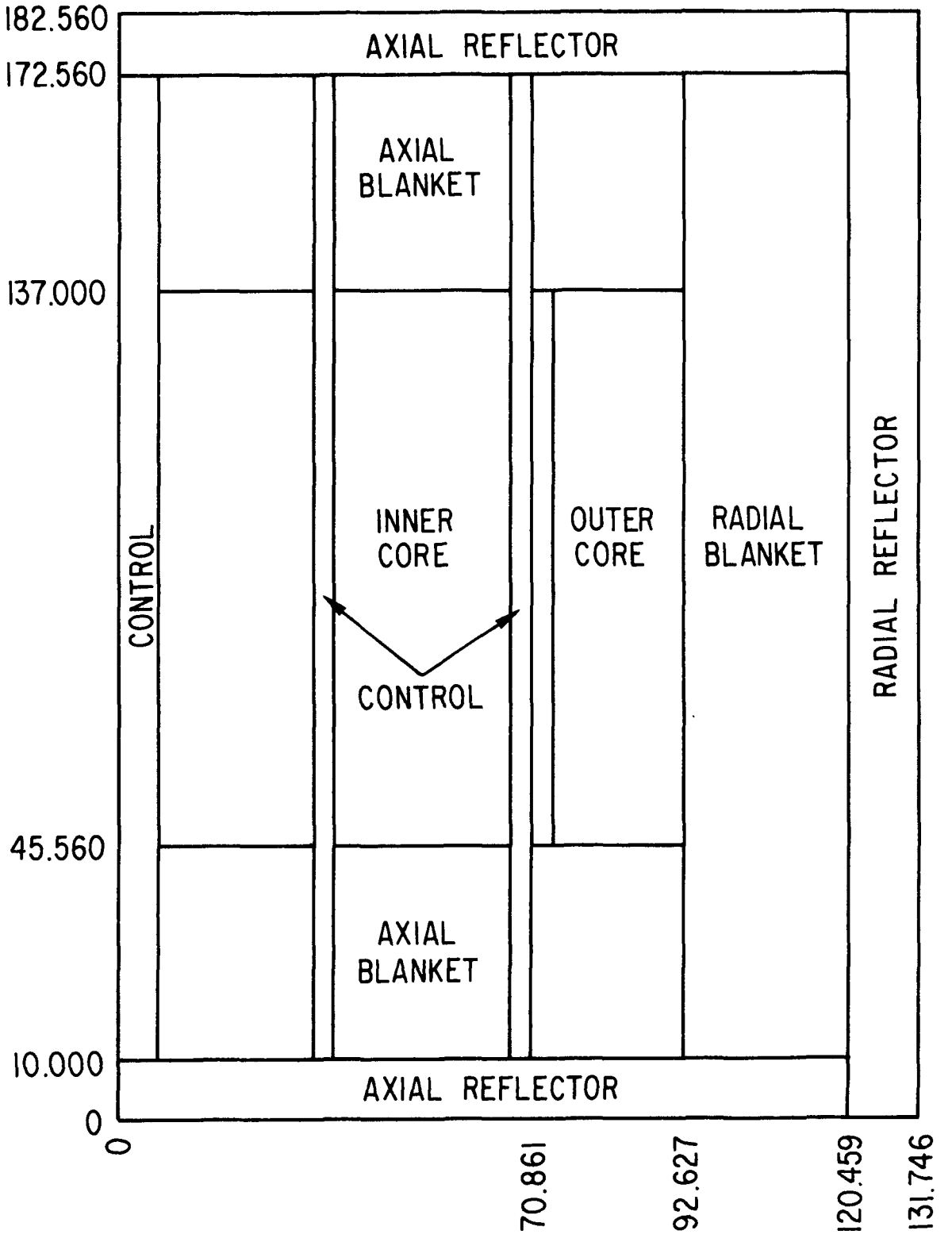

FIGURE III-1: CRBR Model

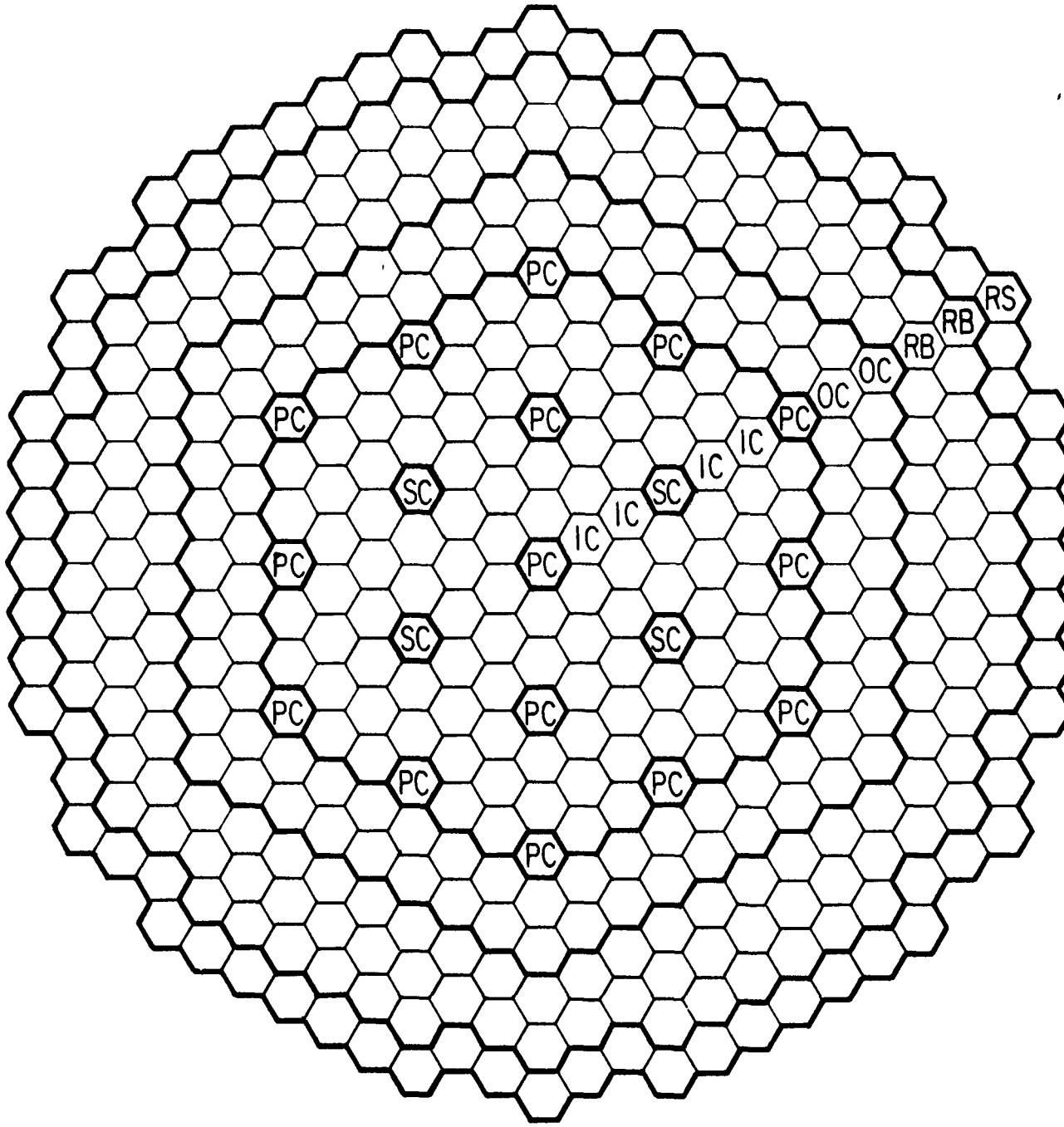

		QUANTITY
IC	INNER ZONE FUEL ASSEMBLY	108
OC	OUTER ZONE FUEL ASSEMBLY	90
RB	RADIAL BLANKET ASSEMBLY	150
RS	RADIAL SHIELD ASSEMBLY	72
PC	PRIMARY SYSTEM CONTROL ASSEMBLY	15
SC	SECONDARY SYSTEM CONTROL ASSEMBLY	4

FIGURE III-2: CRBR Cross Section

TABLE III-2. CRBR Control Rod B-10 Masses Per Assembly

	Central Rod	2-Row 4 Startup Rods	4-Row 4 Safety Rods	12-Row 7 Burnup and Load
First Core	1.21 kg[1]	1.21 kg	3.07 kg[2]	1.21 kg
Equilibrium Core	1.21 kg	3.07 kg	3.07 kg	3.07 kg

[1] 1.21 kg B-10 is natural enriched B_4C

[2] 3.07 kg B-10 is equivalent to 50% enriched B_4C

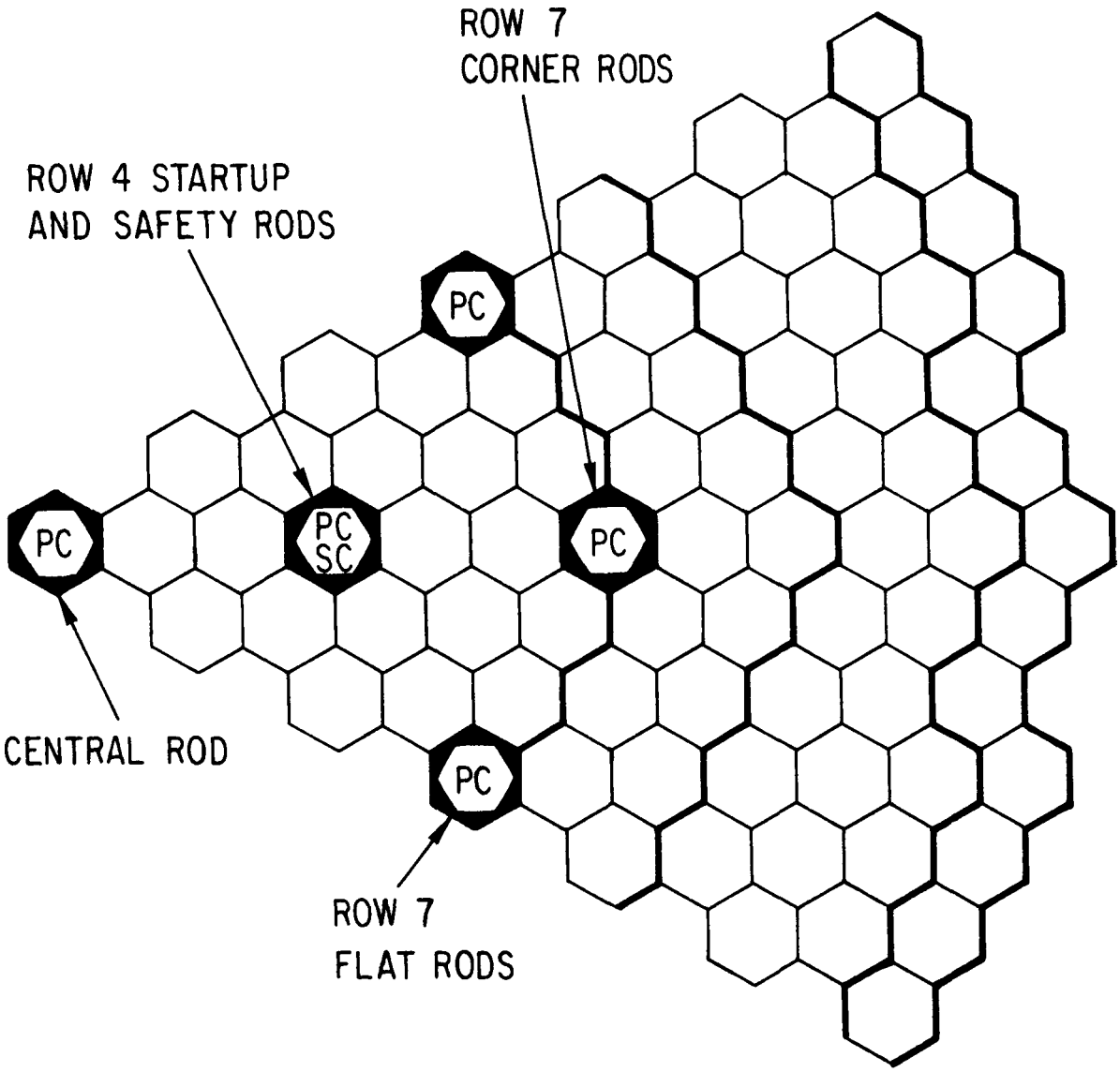

PC PRIMARY SYSTEM CONTROL ASSEMBLY

SC SECONDARY SYSTEM CONTROL ASSEMBLY

FIGURE III-3: CRBR Control Assembly Positions

TABLE III-3. CRBR Control Rod Worths

Reactivity Worth ($)

Primary System	First Core *	Equilibrium Core *
2 Row 4 Startup Rods	4.82	6.47
6 Row 7 Corner Rods	8.41	12.54
Center and 6 Row 7 Flat Rods	14.42	19.65
Secondary System		
4 Row 4 Safety Rods	13.62	12.93

*Adjustments for energy or spatial self-shielding have not been applied to the computation of these worths. Including these effects would reduce the worths by about 15%.

An optimum B-10 enrichment is determined by fully inserting an ISA into the CRBR central rod and varying the boron enrichment. The worth in dollars ($) per kg B-10 as a function of mass of B-10 per assembly is shown in Figure 22. The worth in dollars ($) as a function of the mass of B-10 per ISA is given in Figure 23. Both figures show that the relative increase in worth for an increase in B-10 enrichment increases but at a decreasing rate for increasing enrichments. Increases in B-10 enrichment past 75% are marginal since they provide little additional worth for the increase in cost. A maximum enrichment of 75% is picked for use with ISA assemblies. This enrichment corresponds to a mass of approximately 3 kg of B-10.

In order to determine the optimum ISA position, assemblies with 75% enriched B-10 were placed at all inner core positions, see Figure 24. The corresponding rod worths for both a first core and an equilibrium core are given in Table 8. The maximum rod worth positions occur in row five positions (5,1) and (5,3). Position (5,3) is the more desirable since it combines a high worth position with a minimum coupling with row 4 safety rods.

C. Fissile Source Heating Rates

The heating rates for a UO_2-iron cermet placed near the core-axial blanket interface were determined as a function of uranium enrichment, and radial and axial position. These rates were determined by calculating the fission and capture reaction rates for 1 gm of UO_2. Figure 26 shows the fissile heating rate in watts/gm of UO_2 for uranium enrichments

from 0.7% to 100% U-235. The axial position was varied from 36.0 to 55.0 cm above the core centerline. The heating rate was calculated as the sum of the individual contributions due to fission and (n,γ) capture. The following fission energy conversion factors were used:

U-235	3.08×10^{-11} watt-sec/fission
	1.04×10^{-12} watt-sec/capture
U-238	3.09×10^{-11} watt-sec/fission
	9.09×10^{-13} watt-sec/capture

Almost all of the power generation is contributed by the fission rates of U-235 and U-238. Prompt fission gammas and fission product delayed gammas are included in the energy conversion factors which assume a uniform gamma transport. The flux distributions were generated using a half-core r-z model with the assumption that the UO_2 cermet imposes only a small perturbation on the flux.

APPENDIX IV: PRELIMINARY SYSTEM DESIGN DESCRIPTION (SDD) OF A SELF-ACTUATED SHUTDOWN SYSTEM (SASS) FOR USE IN LMFBRs

Summary

1.0 Functions and Design Requirements

- 1.1 Functions
- 1.2 Design Requirements
- 1.3 Surveillance and Inservice Instrumentation
- 1.4 Instrumentation and Control
- 1.5 Interfacing Systems
- 1.6 Quality Assurance
- 1.7 Applicable Standards

2.0 Design Description

- 2.1 Summary Description
- 2.2 Drop Assembly
- 2.3 Fueled Region

Drawing List

APPENDIX IV: PRELIMINARY SYSTEM DESIGN DESCRIPTION (SDD) OF A SELF-ACTUATED SHUTDOWN SYSTEM (SASS) FOR USE IN LMFBRs

A preliminary System Design Description (SDD) has been prepared based upon the six-face conceptual design of the ISA of Section III of this report. Much of this description applies to the other conceptual designs discussed in the body of the report, and could be readily revised to apply to any one of them.

SUMMARY

The Self-Actuated Shutdown System is a totally self-contained reactor protection system operating on natural phenomena which is triggered by an accident condition in the reactor. The present system has been designed to insert a neutron absorber into the reactor core effecting a safe shutdown if the primary shutdown systems fail to operate. The system is independent of other systems. Its operation requires no external mechanical or electrical connections, or human intervention. The ISA fits within the envelope of a reactor fuel assembly; therefore, no changes are necessary at the core fuel assembly interface. In the application to the Clinch River Breeder Reactor, the fuel is removed from all but the two outer rows of a standard fuel assembly and an inner duct provided. A magnetic holding assembly and a B_4C neutron absorber within the inner duct is positioned just above the core. When heated by a power or flow transient above a set temperature, the magnetic holding assembly releases the B_4C bundle which is inserted into the core by gravity.

1.0 Functions and Design Requirements

1.1 Functions

1.1.1 The function of the Self-Actuated Shutdown System is to provide a backup system to insure safe reliable shutdown of the reactor due to an overpower or under-flow transient after failure or ineffective performance of the normal plant control and protection systems.

1.1.2 The system shall be wholly contained within the reactor. No subcomponents, subsystems or instrument lines, essential to the performance of the shutdown function, shall penetrate the reactor vessel.

1.1.3 The actuation of the system (which includes one or more ISAs) shall result in the insertion of sufficient negative reactivity to control the most severe reactor transient specified. Less severe transients are to be terminated with less or no damage occurring.

1.1.4 Actuation shall be initiated by a temperature increase in the coolant or heating produced by high neutron flux in a fissile source.

1.1.5 The time response of the ISA and the rate of negative reactivity inserted shall be sufficient to control all transients such that there is no eventual release of reactivity from the containment building.

1.1.6 The margin between the trip setting for the ISA and the conventional shutdown system shall be large enough to avoid spurious trips of the SASS.

1.2 Design Requirements

1.2.1 Configuration

The absorber and its actuation components shall fit into the space available upon removal of all but the two outer rows of fuel elements from a fuel assembly,such as a CRBR assembly. The neutron absorber bundle shall be positioned at the top of the core in the axial blanket. Each unit is composed of a neutron absorber bundle containing B_4C enriched with B-10, a magnetic support assembly, and design features providing for trip and actuation on coolant overtemperature or high neutron flux.

1.2.2 General Requirements

1.2.2.1 The ISA shall be completely interchangeable with a fuel assembly and require no electrical leads or mechanical extensions. (An in-vessel handling machine may be employed to reset the device after a trip.)

1.2.2.2 No subcomponent shall release fission products or delayed neutrons to the primary coolant.

1.2.2.3 The fuel provided shall be the standard fuel elements used in the reactor fuel assemblies.

1.2.2.4 The quantity of fuel in the ISA shall be equal to 30% or more of the fuel in a regular fuel assembly.

1.2.2.5 Fuel performance such as burnup, and peak cladding temperature shall conform to the standard requirements for fuel assemblies in comparable core locations.

1.2.2.6 The triggering sensors shall be located at the top of the core.

1.2.2.7 During normal reactor operation, the absorber bundle shall be located 1 in. to 2 in. above the top of the core.

1.2.2.8 In the tripped position, the bottom of the absorber section shall be 1 in. to 2 in. below the bottom of the core and the top of the active section of the absorber shall be 1 in. to 2 in. above the top of the core.

1.2.2.9 The absorber release shall be triggered by a single mechanism sensitive to both high coolant temperature and high neutron flux.

1.2.2.10 The normal average outlet coolant temperature from the ISA shall not exceed that of the corresponding temperature from the hottest of six adjacent reactor fuel assemblies, and be not more than 150°F less.

1.2.2.11 The design shall satisfy the requirements of applicable sections of ASME Code Section III,* Class 1, Subsection NG, Subsection NB and applicable sections of the CRBR design specifications.

1.2.3 Specific Design Requirements

1.2.3.1 The neutron absorber material shall be B_4C enriched with ^{10}B.

1.2.3.2 The absorber bundle support assembly shall utilize permanent magnets to generate the necessary holding force. Triggering and release is accomplished by inserting a soft ferromagnetic material into the magnetic circuit with a Curie point selected to match the desired temperature at which the absorber bundle is to be dropped.

1.2.3.3 The magnet holding and release assembly shall provide for release of the absorber bundle when a specified temperature is reached in a selected part of the magnetic circuit (yoke).

---

*See Section 1.7

1.2.3.4 The release temperature range capability shall be from 1200°F to 1500°F measured in a sensitive section of the magnetic yoke.

1.2.3.5 The holding force shall be larger than the absorber bundle insertion force (gravity, plus spring force if provided) so that any temperature excursions to within 50°F of the trip temperature will result in negligible probability of accidental absorber insertion. Transient forces from vibration, hydraulic shock and ASME Section III upset conditions, if any, shall be included in the insertion forces.

1.2.3.6 The signal for absorber insertion shall be derived from overtemperature in coolant flowing around the two outer rows of fuel elements and/or from high neutron flux.

1.2.3.7 Design life, corresponding to that of surrounding fuel assemblies.

1.2.3.8 Gravity, supplemented by spring force, if necessary, shall be the absorber insertion force.

1.2.3.9 Total insertion time measured from the time the sensing element receives the trip signal to complete insertion of the absorber shall be not greater than three seconds.

1.2.4 Maintenance

The shutdown assembly will be removed for refueling and maintenance inspection at intervals coinciding with replacement of adjoining fuel assemblies as a minimum. More frequent maintenance inspections may be scheduled and removal effected with the invessel handling machine.

1.2.5 Structural Requirements

1.2.5.1 The shutdown assembly shall satisfy the design requirements imposed on the core and core support structure for the CRBR.

1.3 Surveillance and Inservice Inspection

The SASS is designed so that no surveillance and inservice inspection is required except for the possibility of providing testability and rapid identification of a spuriously tripped ISA.

1.4 Instrumentation and Control

The shutdown system is totally self-contained and self-actuating. No external instrumentation or control equipment is employed. All calibration and testing is completed before installation.

1.5 Interfacing Systems

1.5.1 The ISA interfaces with the core supports for standard fuel assemblies in the CRBR.

1.5.2 For installation and removal, the assembly interfaces with the invessel handling machine.

1.5.3 The neutron absorber bundle interfaces with a retrieval tool and the invessel handling machine to lift the bundle and reset the magnetic holding device.

1.5.4 An interface exists with the sodium coolant flow orifices to establish proper parallel cooling flows over the fuel region, magnet holding assembly, soft magnetic yoke containing neutron and thermal trigger and boron carbide absorber bundle.

1.6 Quality Assurance

[The quality assurance requirements will be specified in a Quality Assurance Plan for the Self-Actuated Shutdown System].

1.7 Applicable Standards

ASME Boiler and Pressure Vessel Code, Section III.

E15-2T	Requirements for Nuclear Components (Supplement to the ASME Boiler and Pressure Vessel Code)
E6-13T	Core Support Structure for Sodium Cooled Reactors
E6-17T	Core Restraint Mechanisms for Sodium Reactors
E6-20T	Austentic Stainless Steel Hexagonal Duct Tubes for Core Components and Assemblies
F2-2T	Quality Assurance Requirements
F5-1T	Cleaning and Cleanliness Requirements for Nuclear Components

2.0 Design Description

2.1 Summary Description

The Inherent Shutdown Assembly performs its function by releasing a B_4C neutron absorbing bundle inserted by gravity into the reactor core when triggered by an overtemperature condition in the reactor coolant or a high neutron flux condition.

The self-contained system as shown in Drawing T0037-0016-DE-00 consists of:

a. A drop assembly comprised of a hexagonal duct containing 19 boron carbide pins, and a magnet holding assembly.

b. A hexagonal tube separating the drop assembly from 90 fuel pins in a concentric hexagonal array.

c. 90 fuel pins

d. An outer hexagonal container duct with nozzle, upper end fittings and handling socket.

The exterior configuration of the ISA is identical with the fuel assembly for the CRBR allowing a 1 for 1 replacement.

The drop assembly containing the neutron absorbing material housed in a hexagonal duct is supported just above the top of the core by a permanent magnet assembly. The permanent magnet and associated iron or carbon steel pole pieces are attached to the bottom of the hexagonal duct surrounding the absorber bundle. A soft iron yoke which completes the low reluctance path for the magnet is confined to a support cage in a second annular hexagonal duct. When the drop assembly is pulled to the "up stop" position, the pole pieces of the magnet align with the yoke pieces and are clamped together by the magnetic flux.

Sodium heated by flowing along the double row of fuel pins in the hexagonal annular space is passed through 13 holes parallel to the interface between each of the six pole pieces faces and each of the six yoke faces. An overtemperature in the coolant heats the yoke-pole piece interface decreasing the magnetic permeability until, at a preselected temperature, the holding force is reduced to less than the break away force and the absorber is propelled into the core.

After the power excursion is controlled and the magnet pole pieces have cooled, the system may be reset by lifting the drop assembly to the up stop. The magnet pole pieces and the yoke will reengage and resume the standby protective function.

2.2 Drop Assembly

The drop assembly shown on Drawing No. T-0037-0017-DE-00 consists of a magnet assembly, boron rod assembly, a hexagonal tube, grid assembly, and top end piece. The nineteen boron absorber rods are housed in a 0.050 in. thick hexagonal tube, 2.250 in. across the flats OD, and

72 and 15/16 in. long. The grid assembly provides support and alignment for the boron absorber rods.

2.2.1 Magnet and Yoke Assembly

The function of the magnet and yoke assembly is to support the drop assembly through long periods of normal operation but provide a highly reliable release and insertion mechanism when a transient occurs. The magnet assembly is physically a part of the drop assembly. The yoke assembly is constrained to less than 0.05 in. lateral motion in the support structure in the hexagonal tube separating the drop assembly from the fuel region. Drawing T0037-0022-DD-00 shows the arrangement of the inner support hex duct, yoke assembly and magnet assembly.

2.2.1.1 Magnet and Pole Pieces

The magnetomotive force for the magnet assembly is provided by an Alnico V magnet in the form of a right circular cylinder 1.906 in. in diameter x 1.000 inch high. The magnet is clamped between two magnetically soft carbon steel pole pieces by a 5/16 in. steel bolt to which is attached a steel cone on the lower side, and the end piece of the absorber bundle on the top side. This arrangement is shown in Drawing No. T0037-0021-DC. (See appended drawing list.)

A cone shaped piece below the magnet provides a streamlining effect during the free fall through the sodium and acts as a snubber to decelerate the drop assembly at the fully inserted position. The inside volume of the cone is machined out to reduce weight and radiation heating.

The pole piece, constructed of magnetically soft carbon steel, provide a low reluctance path for the magnetic flux from the permanent magnet to the yoke assembly. The drop assembly is supported by the magnetic attraction between the pole pieces and the yoke assembly confined to a cage in the inner duct.

The pole pieces provided structural and physical support for the magnet. The lower pole piece provides an alternate magnetic shunt path with an air gap of sufficient size to minimize parallel magnetic leakage when the yoke assembly is in place. However, when the reluctance in the primary magnetic path through the yoke assembly is increased to a specified level, the primary magnet flux will switch to the shunt path through the pole piece. Whenever the yoke is not across the pole pieces, the shunt will function as a partial keeper.

The pole pieces and magnet are pressed tightly together by a 5/16 in. steel bolt anchored in the cone piece at the lower end, and by the bottom plate of the boron carbide bundle at the top. All pieces in the magnet assembly are precisely located by machined shoulders. Assembly consists of placing each component on the retaining bolt in the proper sequence, fitting each piece in the machined shoulder or aligning pin, and torquing the retaining nut to produce proper tension in the bolt.

2.2.1.2 Cooling of the Magnet Assembly

The magnet assembly located about 2 in. above the top of the core, is subjected to intense gamma and neutron heating. To minimize heating, the maximum amount of material has been machined from the snubber-cone piece. The magnet is cooled by sodium flowing in twelve 1/8 in. holes and six 3/32 in. holes located in a symmetrical

array. Sodium at 730°F from the lower plenum flows up through the inner hex can entering the magnet assembly through four holes in the snubber-cone. The coolant flow is distributed to all 18 cooling holes in the magnet by a short cylindrical volume just below the lower pole piece. After passing through and cooling the magnet, the sodium stream with less than 40°F temperature rise (< 790°F) passes through the B_4C bundle. The flow rate will be fixed in a later design phase by proper sizing of the orifice above the lower plenum exit. Calculated pressure drop across the magnet assembly will range from 5 to 7.5 psi for sodium flow rates from 3500 to 4300 lb/hr.

2.2.1.3 Yoke Assembly

The yoke assembly is not actually a part of the drop assembly but interfaces closely with the magnet assembly. Therefore, it will be described in this section. Figure 2, Sections AA and BB, show how the six carbon steel yokes are positioned around the magnet assembly. The yoke is a piece of carbon steel approximately 2 3/4 in. long, 1 3/8 in. wide and 3/16 in. thick. Each of the six yokes are contained in a cage assembly welded in the inner duct. The yokes are allowed approximately 0.055 in. of movement perpendicular to the magnet face by machined shoulders and welded tabs. The outside surface of the yoke facing the fuel rods is recessed to prevent contact with the fuel rods when the yoke is retracted.

Three 11/64 in. holes through the lower end of each of the six yokes admit sodium from the annular space containing the fuel elements. The center of the three cylindrical flow channels is located at the parting plane between the yoke and the pole piece.

A semi-circular section of the flow channel is milled in the face of the pole piece and a matching section is milled in the yoke. When the magnet assembly is in the up and latched position with the yoke clamped to the pole piece by the magnetic force, the matching milled sections produce the required flow path.

The flow channels are located at the parting plane because this is the most effective location for applying heat to increase the magnetic resistance and effect a release of the absorber bundle. At 15 ft/sec. the eighteen flow channels in the yoke will pass 6450 lb/hr at an approximate pressure drop of 2 psi. Although the coolant flow will depend on core location, a representative number for the fuel bundle below the top of the core is approximately 69,750 lb/hr.

At the bottom of the magnet assembly, 6450 lb/hr is diverted through the yoke-flow channels, and flows between the inner hex duct and the drop assembly hex can, maintaining separate identity until it mixes in the upper plenum. The two parallel flows are balanced by orificing the smaller 6450 lb/hr flow until pressure drop matches the pressure drop in the flow around the fuel elements from the top of the core to the upper plenum. A preliminary estimate of this pressure drop is about 5 psi.

Each yoke contains pellets of fissionable material so sized that at normal neutron flux levels, the design cooling flow rate will keep the yoke at design operating temperature. However, a rapid increase in neutron flux density will cause the fissionable material to heat the yoke above or near the Curie temperature

reducing the magnet flux below that required to support the drop assembly. Gravity will propel the assembly into the core.

The second way the drop assembly can be released is through an increase in sodium coolant temperature from the fueled region. When the coolant temperature approaches or exceeds the Curie temperature of the yoke material, the drop assembly will be released.

2.2.2 Boron Carbide Bundle

The boron carbide is contained in a hexagonal tube 2.250 in. across the flats and with a wall thickness of 0.048 in. Nineteen pins set on 0.482 in. triangular pitch fill the interior volume. Each pin, 0.472 in. in diameter, is spaced from its neighbors by a 0.01 in. diameter wire wrap. Boron carbide pellets are contained in stainless steel tubes of 0.025 in. wall thickness. The boron carbide bundle is cooled by the same sodium flow which cools the magnet. This sodium flow maintains its identity until it exits the (control) assembly and mixes in the upper plenum.

2.2.3 Retrieval Tool

If the system is required to have the capability for testing in the reactor, a method of retrieving the drop assembly must be provided. A handling socket has been provided at the top of the drop assembly to accept a retrieval tool. The method of manipulating the retrieval tool has not been developed, but one possibility might be to utilize the invessel handling machine.

The mechanical design of the retrieval tool is shown in Drawing No. T0037-0057-DD-00.

For normal operation, the retrieval tool must be removed from the control assembly because the coolant flow from the magnet assembly and the boron carbide bundle must exit through the handling socket. Storage for the retrieval tool must be provided for outside the core area in the fuel storage rack.

In addition, a current-carrying coil would have to be provided for testing to buck out the magnetic holding flux causing the assembly to drop.

2.3 Fueled Region

Between the inner hexagonal tube and the outer hexagonal tube are two rows of fuel elements providing the control assembly with 90 fuel elements compared with 217 for the standard CRBR fuel assembly. The fuel elements are standard CRBR design (#1182E26) with the following dimensions:

Fuel rod outer diameter, in.	0.23
Cladding thickness, mils	15
Pitch to diameter ratio	1.25
Total length, in.	114.6
Wire wrap diameter, mils	56

DRAWING LIST*

T0037-0016-DE	Inherent Shutdown Assy.
T0037-0016-PL	Parts List for 0016-DE
T0037-0017-DE	Boron Drop Assy.
T0037-0017-PL	Parts List for 0017-DE
T0037-0018-DC	Double-faced Magnet Assy.
T0037-0018-PL	Parts List for 0018-DC
T0037-0019-DC	Grid Subassy.
T0037-0019-PL	Parts List for 0019-DC
T0037-0020-DE	Boron Rod Assy.
T0037-0020-PL	Parts List for 0020-DE
T0037-0021-DC	Magnet Assy.
T0037-0021-PL	Parts List for 0021-DC
T0037-0022-DD	Yoke Magnet Assy.
T0037-0022-PL	Parts List for 0022-DD
T0037-0023-DC	Hex Tube-Upper
T0037-0024-DD	Handling Socket
T0037-0025-DC	Spoked Hex
T0037-0026-DC	Compression Spring
T0037-0027-DC	Hex Tube-Outer
T0037-0028-DC	Grid-Fuel Rod
T0037-0029-DC	Stop-Down
T0037-0030-DD	Shield
T0037-0031-DB	Orifice Plate
T0037-0032-DD	Nozzle
T0037-0033-DC	Stop-Up
T0037-0034-DC	Hex Tube-Lower
T0037-0035-DB	Seal Ring
T0037-0036-DB	Hex Tube
T0037-0037-DC	Top End Piece
T0037-0038-DB	Cone
T0037-0039-DB	Pole Piece #1

*These drawings have been prepared but are not part of this report.

T0037-0040-DB	Pole Piece #2
T0037-0041-DB	Pole Piece #3
T0037-0042-DB	Magnet
T0037-0043-DB	Cap
T0037-0044-DB	Grid Bar
T0037-0045-DB	Boron Slug
T0037-0046-DB	Tip-Grid End
T0037-0047-DB	Plug-Top End
T0037-0048-DB	Tube
T0037-0049-DB	Compression Spring
T0037-0050-DB	Cone
T0037-0051-DB	Pole Piece #1
T0037-0052-DB	Pole Piece #2
T0037-0053-DB	Pole Piece #3
T0037-0054-DC	Cage Yoke
T0037-0055-DB	Yoke
T0037-0056-DB	Clip Spring
T0037-0057-DD	Retrieving Tool Assy.
T0037-0057-PL	Parts List for 0057-DD
T0037-0058-DB	Jaw-Retriever
T0037-0059-DC	Inner Rod
T0037-0060-DC	Outer Tube

REFERENCES

1. ANL Staff, Argonne National Laboratory, unpublished information (1974).
2. ANL Staff, Argonne National Laboratory, unpublished information (1974).
3. P. R. Huebotter, et al, "Self-Actuated Shutdown Systems for LMFBR Plants," ANS, 1975 Annual Meeting, June 8-13, 1975, New Orleans, La.
4. Technical Report on Anticipated Transients Without Scram for Water-Cooled Power Reactors, Regulatory Staff USAEC, WASH-1270 (September, 1973).
5. "Clinch River Breeder Reactor Plant Reference Design Report," Westinghouse Electric Corp., Advanced Reactor Div. (WARD), Vols. 1 and 2, June 1974.
6. W. T. Sha and R. C. Schmitt, Argonne National Laboratory, unpublished information (1974).
7. A. C. Raptis, "Survey of Permanent Magnet Materials for Flowmeters in Sodium Above 1000°F", ANL-CT-75-10 (Sept. 1974).
8. V. M. Stefanovic and N. L. Milasin, "Correlation Between the Mechanical Properties and Microstructure of Irradiated Iron and Low Carbon Steel", Irradiation Effects on Structural Alloys for Nuclear Reactor Applications, ASTM STP 484, 521 (1970).
9. C. O. J. Foust, (Ed.) Sodium-Nak Engineering Handbook, Vol. I, Gordon and Breach, New York (1972).
10. G. Arthur & J. A. Coulson, "Physical Properties of UO_2-SS Cermets", Journal of Nuclear Materials 13-2 242 (1964).
11. Magnetically Soft Materials, Metals Handbook, ASM, Vol. I, 8th ed.

12. George A. Forster, "Long Term Stability of Alnico V and VIII Magnets at 700° to 1200°F," ANL-CT-73-16.

13. J. D. B. Lambert, "Irradiation Study of UO_2 - Stainless Steel and $(Pu,U)O_2$ - Stainless Steel Cermet Fuels in Rod and Plate Geometry," AIME, The Metallurgical Society, High Temperature Nuclear Fuels, Vol. 12, Gordon and Breach, New York (1968).

14. "Clinch River Breeder Reactor (CRBR), Configurations and Basic Design Input," Attachment 1, WARD-LRA-73-498 (1973).

15. F. Bitter, Magnets, Doubleday & Co., Inc., Garden City, N. Y. (1959).

16. F. G. Spreadbury, Permanent Magnets, Sir Issac Pitman & Sons, Ltd., London (1949).

17. Electrical Materials Handbook, Allegheny Ludlum Steel Corporation, Pittsburgh 22, Pa. (1961).

18. S. S. Attwood, Electric and Magnetic Fields, John Wiley and Sons, Inc. New York (1945).

19. R. J. Parker and R. J. Studders, Permanent Magnets and Their Application, John Wiley and Sons, Inc., New York, London (1962).

20. R. M. Bozorth, Ferromagnetism, Van Nostrand Co. Inc., New York (1951).

21. D. Hadfield, Permanent Magnets and Magnetism, John Wiley and Sons, Inc., New York (1962).